Department: Physical Sciences

3.4.5

Research papers per teacher in the Journals notified on UGC website

Supporting Documents

IOP Publishing Mater. Res. Express 7 (2020) 095003 https://doi.org/10.1088/2053-1591/abb2cd

399

Materials Research Express

PAPER

Lattice thermal conductivity of pure and doped (B, N) Graphene

Sarita Mann[1], Isha Mudahar[2], Hitesh Sharma[3], V K Jindal[1], Girija S Dubey[4,5,6], Godfrey Gumbs[6] and Vassilios Fessatidis[5]

[1] Department of Physics, Panjab University, Chandigarh-160014, India
[2] Department of Basic and Applied Sciences, Punjabi University, Patiala-147002, India
[3] Department of Physical Sciences, IK Gujral Punjab Technical University, Kapurthala, Punjab-146003, India
[4] Department of Earth and Physical Sciences, York College of CUNY, Jamaica, 11451, United States of America
[5] Department of Physics and Engineering Physics, Fordham University, Bronx, New York, NY 10458, United States of America
[6] Department of Physics and Astronomy, Hunter College, CUNY 695 Park Anvenue, New York, NY 10065, United States of America

E-mail: dr.hitesh.phys@gmail.com

Keywords: thermal conductivity, graphene, density functional theory

OPEN ACCESS

RECEIVED
21 May 2020

REVISED
19 August 2020

ACCEPTED FOR PUBLICATION
26 August 2020

PUBLISHED
4 September 2020

Original content from this work may be used under the terms of the Creative Commons Attribution 4.0 licence.

Any further distribution of this work must maintain attribution to the author(s) and the title of the work, journal citation and DOI.

Abstract

In this paper, the effect of B and N doping on the phonon induced thermal conductivity of graphene has been investigated. This study is important when one has to evaluate the usefulness of electronic properties of B and N doped graphene. We have performed the calculations by employing density functional perturbation theory(DFPT) to calculate the inter-atomic forces/force constants of pristine/doped graphene. Thermal conductivity calculations have been carried out by making use of linearized Boltzmann transport equations (LBTE) under single-mode relaxation time approximation(RTA). The thermal conductivity of pristine graphene has been found to be of the order of 4000 W/mK at 100 K, which decreases gradually with an increase in temperature. The thermal conductivity decreases drastically by 96% to 190 W/mK when doped with 12.5% B and reduces by 99% to 30 W/mK with 25% B doping. When graphene is doped with N, the thermal conductivity decreases to 4 W/mK and 55 W/mK for 12.5% and 25% doping concentration, respectively. We have found that the thermal conductivity of doped graphene show less sensitivity to change in temperature. It has also been shown that the thermal conductivity of graphene can be tuned with doping and has a strong dependence on doping concentration.

1. Introduction

From a technological point of view, heat removal from devices plays a key role in producing ultra-small and energy-efficient electronic, optoelectronic, and photovoltaic devices and systems [1–3]. In recent years, one of the key issues for making further progress has been performance enhancement in energy conversion and thermal management technologies, which can be implemented into engineering applications [4]. The choice of thermal interface materials (TIM) between the emitter and receiver is critical to determine the effectiveness of any potential device. In addition, the 'green' revolution in a photovoltaic cell has also highlighted the need for novel thermally efficient materials based on graphene [4]. In low-dimensional structures, thermal conduction has disclosed many fascinating characteristics. When the dimension of a material is reduced to the nano dimension in electronic devices, there is a significant reduction in the thermal conductivity as a result of the enhanced boundary scattering, which is lower than the bulk value [5]. The wide range of thermal properties of carbon nanomaterials has highlighted the possibility of their usage in thermal management,heat dissipation and thermoelectric conversion[6, 7].

In the last decade, different theoretical methods and experimental techniques have been used for investigating thermal transport in carbon nanosystems [8]. At room temperature (RT), thermal conductivity of carbon nanomaterials have been found to vary from 0.01W/mK in amorphous carbons, 600 W/mK in supported graphene[9], 2300 W/mK in carbon nanotubes to more than 4000 W/mK in graphene [10, 11]. Isolated studies have even reported higher thermal conductivity of 5300 W/mK at room temperature of perfect

© 2020 The Author(s). Published by IOP Publishing Ltd

Department of Physical Sciences
I.K. Gujral Punjab Technical University
Main Campus

Effect of Twist Angle on Structural, Electronic and Magnetic Properties of Carbon Nano Hybrids: A DFT Study

Amrish Sharma[1], Sandeep Kaur[1], Hitesh Sharma[2], Neha Kapila[3], V. K. Jindal[3], Vladimir Bubanja[4,5] and Isha Mudahar[6*]

[1]Department of Physics, Punjabi University, Patiala.
[2]Department of Physics, IKG Punjab Technical University, Kapurthala.
[3]Department of Physics, Panjab University, Chandigarh.
[4]Measurement Standards Laboratory of New Zealand, Callaghan Innovation, PO Box 31310, Lower Hutt, 5040, Wellington, New Zealand.
[5]The Dodd-Walls Centre for Photonic and Quantum Technologies, University of Otago, 730 Cumberland Street, Dunedin, 9016, New Zealand.
[6]Department of Basic and Applied Sciences, Punjabi University, Patiala.
*dr.ishamudahar@gmail.com

Abstract: - Density functional calculations of hybrids consisting of a single wall carbon nanotube and a graphene nanoribbon have been performed. We consider the dependence of the structural, electronic and magnetic properties of the hybrids on the twist angle between their subunits. We calculated the binding energies, pyramidalization angles, Mulliken charge, and HOMO-LUMO gaps as functions of the twist angle. We find that, owing to the asymmetrical spin density distributions of their subunits, the hybrids have finite magnetic moments.

Introduction

Varying the twist angle between low dimensional nanomaterials has recently emerged as a fundamentally new direction in device engineering. This new approach is in a stark contrast to the conventional methods where the variability of electronic properties of materials is attained by changing their chemical composition. Current intense research in this field is in large part due to the surprising discovery of superconductivity in twisted bilayer graphene (TBG) at magic angles (for which Fermi velocity vanishes) [1]. One of the guiding ideas of twistronics has been to create different crystal cell sizes and symmetries by introducing Moiré patterns [2]. The consequences of such symmetries have been investigated within the continuum model for TBG, parametrized by interlayer coupling for AA and AB stacking [3]. It was shown that in the limit of vanishing coupling for AA stacking, the Hamiltonian of the system acquires chiral symmetry (a unitary particle-hole

Head
Department of Physical Sciences
I.K. Gujral Punjab Technical University
Main Campus

Physica E: Low-dimensional Systems and Nanostructures 111 (2019) 1–12

Contents lists available at ScienceDirect

Physica E: Low-dimensional Systems and Nanostructures

journal homepage: www.elsevier.com/locate/physe

Graphene nanoribbons under axial compressive and point tensile stresses

Sandeep Kaur[a], Hitesh Sharma[b], V.K. Jindal[c], Vladimir Bubanja[d,e], Isha Mudahar[f,*]

[a] Department of Physics, Punjabi University, Patiala, Punjab, India
[b] Department of Applied Sciences, IKG Punjab Technical University, Amritsar, Punjab, India
[c] Department of Physics, Panjab University, Chandigarh, Punjab, India
[d] Measurement Standards Laboratory of New Zealand, Callaghan Innovation, PO Box 31310, Lower Hutt, 5040, Wellington, New Zealand
[e] The Dodd-Walls Centre for Photonic and Quantum Technologies, University of Otago, 730 Cumberland Street, Dunedin, 9016, New Zealand
[f] Department of Basic and Applied Sciences, Punjabi University, Patiala, Punjab, India

ABSTRACT

The geometric, electronic and magnetic properties of strained graphene nanoribbons were investigated using spin polarized calculations within the framework of density functional theory. Cases of compressive stress along the longer axis of a nanoribbon and tensile stress at the midpoint and perpendicular to the plane of the nanoribbon were considered. Significant structural changes were observed including the formation of nanoripples. The calculated electronic and magnetic properties strongly depend on the size and shape of nanoribbons. The tunable magnetic properties of strained nanoribbons can be employed for designing magnetic nano-switches.

1. Introduction

Graphene nanoribbons (GNRs) are quasi-one-dimensional nanostructures with unique electronic, optical and transport properties [1–3]. Therefore, they have been the subject of numerous studies considering their potential applications as field effect transistors, optoelectronic, spintronic and other devices [4–6]. Of particular interest has been the possibility to tune the GNR properties by using the externally applied electric and magnetic fields, doping, defects, edge-modification and width-variation of nanoribbons [7–11]. GNRs have also been incorporated in hybrid materials, such as vanadium dioxide-graphene architectures [12], exhibiting extraordinary electrochemical performance, and therefore showing promise for electrode material in high-power lithium batteries. After the original discovery of graphene [13], a plethora of other two-dimensional materials have been synthesised [14] and have shown promise in a variety of fields, from photonics [15] to nanomedicine [16]. Calculations within the density functional theory framework have been carried out to investigate the electronic and magnetic properties of graphene-counterpart nanoribbons, such as those based on silicene [17,18], stenene [19], phosphorene [20], and germanene [21,22], as well as to make first-principles predictions of new monolayer materials [23].

A range of top-down methods has been used to successfully fabricate GNRs. They include graphene etching [24], chemical vapour deposition [25], scanning probe lithography [26] and unzipping of single- [27] and multi-walled carbon nanotubes [28]. However, these techniques lack the synthetic reproducibility and atomically precise control required for predetermined electronic structure of GNRs. Instead, bottom-up approach can be used for this purpose. A pioneering work [29], utilizing surface assisted coupling, has inspired a number of approaches based on appropriately designed precursor molecules to react in a selective way that ends up forming GNRs [30,31]. This approach has been followed in solution [32], as well as supported on solid surfaces [33].

Graphene has a remarkable stress-strain behaviour, including the highest stiffness and strength ever measured [34–36]. It can be easily bent to get complex folded structures [37] and can withstand elastic deformations of up to 25% [34], that are much larger than in any other known material. Owing to these outstanding mechanical properties, graphene is an ideal candidate for nanomechanical systems [38] and flexible electronic devices [39]. Measurements of the elastic response of graphene demonstrated that it is highly nonlinear for strains above 10% [34]. Subsequently, these experiments were interpreted within a generalized nonlinear stress-strain relation that incorporates cubic terms in strain, and nonlinear elastic coefficients have been estimated from

* Corresponding author.
E-mail addresses: sandeep_rs16@pbi.ac.in (S. Kaur), hitesh@ptu.ac.in (H. Sharma), vkjindal06@gmail.com (V.K. Jindal), vladimir.bubanja@yahoo.co.nz (V. Bubanja), dr.ishamudahar@gmail.com (I. Mudahar).

https://doi.org/10.1016/j.physe.2019.02.018
Received 20 December 2018; Accepted 15 February 2019
Available online 25 February 2019
1386-9477/ © 2019 Elsevier B.V. All rights reserved.

Head
Department of Physical Sciences
I.K. Gujral Punjab Technical University
Main Campus

403

Listen

Substitutional Doping of Asymmetrical Small Fullerene Dimers

Buy Article:
$105.00 plus tax
(Refund Policy)
ADD TO CART
BUY NOW

Authors: Kaur, Sandeep[1]; Sharma, Hitesh[2]; Mudahar, Isha[3]
Source: Advanced Science Letters, Volume 24, Number 2, February 2018, pp. 888-892(5)
Publisher: American Scientific Publishers
DOI: https://doi.org/10.1166/asl.2018.10867

< previous article view table of contents next article > ADD TO FAVOURITES

Abstract | References | Citations | Supplementary Data | Article Media | Metrics | Suggestions

We have employed spin polarized density functional theory for the investigation of small fullerene asymmetrical dimers C_n-C_m, where $n, m \leq 50$. Our study proposes that the dimer structures are energetically favorable. Variation in bond lengths and diameters of the cages has been found due to distortions in the cage structures. The HOMO-LUMO band gaps and electronic density of states are studied to explore the electronic properties of these dimers. The spin up band gap pattern of asymmetrical dimers is almost same as single fullerene cages, but the spin down band gap show somewhat oscillatory behavior. To study the effect of doping, the connecting bonds of fullerene dimers are substituted by N (nitrogen) and B (boron) atoms. There is decrease in the band gaps after substitution and hence there is increase in the conductivity of new complexes. Muliken charge analysis show a significant charge transfer from nitrogen to boron at the connecting bond of the dimer and this behavior can further be exploited for developing the molecular devices.

Keywords: Dimers; Fullerenes; Substitutional Doping

Document Type: Research Article

Affiliations: 1: Department of Physics, Punjabi University, Patiala 147002, Punjab, India 2: Department of Applied Sciences, IKG Punjab Technical University, Kapurthala 144603, Punjab, India 3: Department of Basic and Applied Sciences, Punjabi University, Patiala 147002, Punjab, India

Publication date: 01 February 2018

Head
Department of Physical Sciences
I.K. Gujral Punjab Technical University
Main Campus

403

Received: 22 December 2018 | Revised: 10 June 2019 | Accepted: 17 June 2019
DOI: 10.1002/qua.26019

FULL PAPER

QUANTUM CHEMISTRY WILEY

Substitutional doping of symmetrical small fullerene dimers

Sandeep Kaur[1] | Amrish Sharma[1] | Hitesh Sharma[2] | Shobhna Dhiman[3] | Isha Mudahar[4]

[1]Department of Physics, Punjabi University, Patiala, Punjab, India
[2]Department of Applied Sciences, IKG Punjab Technical University, Amritsar, Punjab, India
[3]Department of Applied Sciences, Punjab Engineering College, Chandigarh, India
[4]Department of Basic and Applied Sciences, Punjabi University, Patiala, Punjab, India

Correspondence
Isha Mudahar, Department of Basic and Applied Sciences, Punjabi University, Patiala, Punjab, India.
Email: dr.ishamudahar@gmail.com

Funding information
University Grants Commission, Grant/Award Number: MANF-2017-18-HAR-73650

Abstract

Magnetic carbon nano-structures have potential applications in the field of spintronics as they exhibit valuable magnetic properties. Symmetrically sized small fullerene dimers are substitutional doped with nitrogen (electron rich) and boron (electron deficient) atoms to visualize the effect on their magnetic properties. Interaction energies suggests that the resultant dimer structures are energetically favorable and hence can be formed experimentally. There is significant change in the total magnetic moment of dimers of the order of 0.5 μ_B after the substitution of C atoms with N and B, which can also be seen in the change of density of states. The HOMO-LUMO gaps of spin up and spin down electronic states have finite energy difference which confirm their magnetic behaviour, whereas for non-magnetic doped dimers, the HOMO-LUMO gaps for spin up and down states are degenerate. The optical properties show that the dimers behave as optical semiconductors and are useful in optoelectronic devices. The induced magnetism in these dimers makes them fascinating nanocarbon magnetic materials.

KEYWORDS
magnetism, small fullerenes, substitutional doping

1 | INTRODUCTION

The discovery of C_{60}, among fullerene family, has triggered an interest in the field of carbon nanostructured materials due to their fascinating physical and electronic properties.[1–3] An intensive research has been initiated for large and small fullerene derivatives after the large-scale synthesis of C_{60}.[1,3,4] Small fullerenes have possible usage in the field of nano-electronics, spin-electronics, molecular devices, superconducting devices, drug delivery, and energy storage owing to their unique physical and chemical properties.[2,5–8] C_{20} is the smallest fullerene cage that was synthesized using gas-phase debromination[9] and was found to be less stable kinetically than higher fullerenes such as C_{36} or C_{60} due to its strong curvature.[10,11] The carbon cages such as C_{32}, C_{44}, and C_{50} are important because of their large ionization potentials and band gaps.[12] The spectrum of 11.2 μm unidentified infrared band (UIR) indicates that C_{24} fullerene cage can be used as a carrier that acts as a useful probe for astrophysical environment.[13]

The surface of the fullerenes, depending on its inter- and intra-curvature, determines their stability and electronic properties. The ability of the surface to react with other objects strongly depends on its ability to form chemical bonds. In carbon networks, the substitution of N and B is strongly favorable as they bracket carbon in periodic table. The substitutional doping of N and B in fullerene cage structures leads to increase in their static polarizabilities.[14] The first N doped derivatives of C_{60} and C_{70} were synthesized using contact-arc vaporization of graphite in the vicinity of gaseous N_2 and NH_3.[15] The isolation of series of N-doped derivatives stimulated their theoretical studies further.[16,17] The modification in chemical composition of small fullerenes can increase their stability.[18] The substitutional doping of C_{20} with transition metals, B and N atoms alters the charge distribution of cage, stability, polarity, and electronic structure of small fullerenes.[19,20] Substitution of N atoms at hetero-position in C_{20} cage induce Stone-Wales defect that further depend on number and relative position of N atoms in C_{20} cage.[21] Though C_{36} cage like C_{60} can donate or gain maximum of six electrons but it has different properties.[22] The substitution of N and B in C_{36} cage alters the

Head
Department of Physical Sciences
I.K. Gujral Punjab Technical University
Main Campus

© 2019 Wiley Periodicals, Inc.

5

404

Listen

A First Principle Study on C_{20} and C_{40} Carbon Nanobuds

Buy Article:
$105.00 plus tax
(Refund Policy)
ADD TO CART
BUY NOW

Authors: Sharma, Amrish[1]; Sharma, Hitesh[2]; Mudahar, Isha[3]
Source: Advanced Science Letters, Volume 24, Number 2, February 2018, pp. 790-795(6)
Publisher: American Scientific Publishers
DOI: https://doi.org/10.1166/asl.2018.10845

< previous article view table of contents next article > ♥ ADD TO FAVOURITES

Abstract | References | Citations | Supplementary Data | Article Media | Metrics | Suggestions

The study of hybrid carbon nanostructure, carbon nanobuds (CNBs) has been done using first principle calculations based on density functional theory. In our present work, we have taken C_{20} and C_{40} fullerenes which are being attached to the sidewalls of armchair (5,5) and zigzag (5,0) single wall carbon nanotubes (SWCNT). The structural and electronic properties of these CNBs has been investigated. We have considered all possible configurations by placing the fullerenes onto the sidewalls of both armchair and zigzag SWCNT. The most stable geometries in all the cases come out to be different. The average C–C bond distances between fullerenes and SWCNT around the attachment region increase significantly from the original bond distances. To study the interaction strength, the interaction energy of the most stable configurations is calculated and is found to be negative which points toward the stability of the complex formed. Our results show that the interaction energy for C_{40} CNBs formation is almost twice that of C_{20} CNBs. The calculated HOMO–LUMO gap of these most stable CNBs lies in the range of 0.13 eV to 0.42 eV, which indicates the increase in gap as compared to pure SWCNT. The Mulliken charge analysis shows the redistribution of charge around the connecting and neighbouring carbon atoms of these CNBs. Furthermore, based on EDOS plots we observe that these CNBs show semi conducting behaviour irrespective of the nature SWCNT.

Keywords: Carbon Nanobud; Carbon Nanotube; Fullerene

Document Type: Research Article

Affiliations: 1: Department of Physics, Punjabi University, Patiala 147002, India 2: Department of Physics, IKG Punjab Technical University, Kapurthala 144603, India 3: Department of Basic and Applied Sciences, Punjabi University, Patiala 147002, India

Head
Department of Physical Sciences
I.K. Gujral Punjab Technical University
Main Campus

IOP Publishing Mater. Res. Express 5 (2018) 016105 https://doi.org/10.1088/2053-1591/aaa567

Materials Research Express

PAPER

Structural and magnetic properties of small symmetrical and asymmetrical sized fullerene dimers

Sandeep Kaur[1], Amrish Sharma[1], Hitesh Sharma[2] and Isha Mudahar[3,4]

[1] Department of Physics, Punjabi University, Patiala, India
[2] Department of Applied Sciences, IKG Punjab Technical University, Kapurthala, India
[3] Department of Basic and Applied Sciences, Punjabi University, Patiala, India
[4] Author to whom any correspondence should be addressed.

E-mail: sandeep_rs16@pbi.ac.in, amrish99@gmail.com, hitesh@ptu.ac.in and dr.ishamudahar@gmail.com

Keywords: carbon nanostructures, fullerenes, magnetism, density functional theory

RECEIVED
17 November 2017

REVISED
29 December 2017

ACCEPTED FOR PUBLICATION
5 January 2018

PUBLISHED
19 January 2018

Abstract

Magnetism in carbon nanostructures is of high scientific interest, which could lead to novel magnetic materials. The magnetic properties of symmetrical and asymmetrical sized small fullerene dimers (C_n for $n \leqslant 50$) have been investigated using spin polarized density functional theory. The interaction energies depict that small fullerene cages form stable dimer structures and symmetrical sized fullerene dimers are found more stable than asymmetrical sized dimers. The dimerization of fullerene cages in different modes leads to change in their magnetic properties. The non-magnetic fullerene cages become magnetic after formation of dimer (C_{20}–C_{20}, C_{24}–C_{24}, C_{32}–C_{32}, C_{40}–C_{40}, C_{20}–C_{24}, C_{40}–C_{44} and C_{44}–C_{50}), whereas the magnetism of magnetic fullerenes is enhanced or lowered after dimerization (C_{28}–C_{28} C_{36}–C_{36}, C_{24}–C_{28}, C_{28}–C_{32}, C_{32}–C_{36} and C_{36}–C_{40}). The individual cages of dimer structures show ferromagnetic interactions amongst them and resultant magnetic moment strongly depends on the type of inter-connecting bonds. The magnetism may also be explained based on distortion of carbon cages and change in the electron density of states in dimer configuration. The calculations presented show strong possibility of experimental synthesis of small fullerene based magnetic dimers.

1. Introduction

The non-IPR (isolated pentagon rule) fullerenes or small fullerenes (C_n, $n < 60$) are interesting to study as they exhibit significant structural, electronic and magnetic properties, owing to their high curvature and fused adjacent pentagons [1–5]. The fullerenes have been widely studied in recent years and they have been explored for emerging potential applications in various areas of research such as nano-electronics, molecular devices, spin-electronics etc [6–8]. The applications of these fullerenes in the field of chemical catalysis [9] and pharmaceutics [10] have also become important by virtue of their particular properties like high chemical reactivity and small diameter.

In past, carbon based systems have become increasingly interesting due to their significant magnetic properties and they can be considered as a possible magnetic materials [11]. The origin of carbon based ferromagnetism has been reported due to the dislocations, vacancies and impurity atoms [12]. Till date, various attempts have been made to study the magnetic properties of small and larger fullerene cages [13–15]. Synthesis of ferromagnetic polymerized fullerenes has been treated by photo assisted oxidation, which show magnetization of order 10^{-3} μ_B per C_{60} [16]. There is an introduction of strong magnetism in the fullerene cages when they are endohedrally doped [14, 15, 17]. When the transition metals are encapsulated inside small carbon cages, the magnetic behavior of small cages is altered, which furnish a novel possibility to control the magnetic properties of carbon systems [17]. A theoretical and experimental study on carbon clusters show that their magnetic moment can be significantly enhanced by appropriately choosing their size, geometry and composition [18].

Head
Department of Physical Sciences
I.K. Gujral Punjab Technical University
Main Campus

© 2018 IOP Publishing Ltd

406

Materials Research Express

ACCEPTED MANUSCRIPT

Adsorption of gas molecules on ultra-thin pristine and doped graphene nanoribbons

To cite this article before publication: Sandeep Kumar *et al* 2018 *Mater. Res. Express* in press https://doi.org/10.1088/2053-1591/aadaa8

Manuscript version: Accepted Manuscript

Accepted Manuscript is "the version of the article accepted for publication including all changes made as a result of the peer review process, and which may also include the addition to the article by IOP Publishing of a header, an article ID, a cover sheet and/or an 'Accepted Manuscript' watermark, but excluding any other editing, typesetting or other changes made by IOP Publishing and/or its licensors"

This Accepted Manuscript is **© 2018 IOP Publishing Ltd.**

During the embargo period (the 12 month period from the publication of the Version of Record of this article), the Accepted Manuscript is fully protected by copyright and cannot be reused or reposted elsewhere.
As the Version of Record of this article is going to be / has been published on a subscription basis, this Accepted Manuscript is available for reuse under a CC BY-NC-ND 3.0 licence after the 12 month embargo period.

After the embargo period, everyone is permitted to use copy and redistribute this article for non-commercial purposes only, provided that they adhere to all the terms of the licence https://creativecommons.org/licences/by-nc-nd/3.0

Although reasonable endeavours have been taken to obtain all necessary permissions from third parties to include their copyrighted content within this article, their full citation and copyright line may not be present in this Accepted Manuscript version. Before using any content from this article, please refer to the Version of Record on IOPscience once published for full citation and copyright details, as permissions will likely be required. All third party content is fully copyright protected, unless specifically stated otherwise in the figure caption in the Version of Record.

View the article online for updates and enhancements.

Head
Department of Physical Sciences
I.K. Gujral Punjab Technical University
Main Campus

This content was downloaded from IP address 128.163.2.206 on 29/08/2018 at 08:11

407

Nuclear Inst. and Methods in Physics Research B 416 (2018) 62–67

Contents lists available at ScienceDirect

Nuclear Inst. and Methods in Physics Research B

journal homepage: www.elsevier.com/locate/nimb

Chemical state analysis of Cl $K\alpha$ and $K\beta_{1,3}$ X-ray emission lines using polychromatic WDXRF spectrometer

Harpreet Singh Kainth[a,*], Arun Upmanyu[b], Hitesh Sharma[b], Tejbir Singh[c], Sanjeev Kumar[a,d]

[a] Department of Physics, Panjab University, Chandigarh 160014, India
[b] Department of Physics, IKG Punjab Technical University, Kapurthala 144601, India
[c] Department of CIL/SAIF, Panjab University, Chandigarh 160014, India
[d] Department of Physics, GGDSD College, Chandigarh 160030, India

ARTICLE INFO

Keywords:
WDXRF
Cl $K\alpha$ and $K\beta_{1,3}$
Emission lines
Effective charge
Relative intensity ratio and line-width

ABSTRACT

With the support of research projects focusing on sampling and data analysing of different varieties of chemical compounds, wavelength dispersive X-ray fluorescence (WDXRF) technique is commonly used in many research laboratories throughout the world wide to determine the elemental composition of various unknown samples. In the present study, first time we have employed polychromatic S8 TIGER WDXRF spectrometer to study the chemical state analysis in Cl $K\alpha$ and $K\beta_{1,3}$ X-ray emission lines. A Voigt function is used to determine the central peak position of the K shell emission lines in all samples. From the present measurements, it is seen that both positive and negative shifts have been observed in Cl $K\alpha$ (2.622 keV) and $K\beta_{1,3}$ (2.817 keV) emission peaks. It has been also seen that the effective charge, relative line-width and relative intensity ratio I($K\beta_{1,3}/K\alpha$) are found proportional with the chemical shift. Furthermore, a parabolic relation is also established between them.

1. Introduction

It is well known that X-ray emission lines originating from the different electronic transitions provide useful information on the electronic structures, the quantum states and the electron density of the various chemical compounds. Many researchers [1–12] discussed the $K\alpha$ and $K\beta$ X-ray emission spectra profiles of phosphorus, sulphur and chlorine compounds to study their chemical state behaviour using different analytic techniques. Woonglee et al. [6] successfully observed the chemical speciation of chlorine in atmospheric particulate matter (APM) using high resolution wavelength dispersive PIXE based spectrometer.

X-ray absorption spectroscopy (XAS) and X-ray emission spectroscopy (XES) are the most commonly used techniques to determine the chemical state analysis in various compounds. These types of spectrometers are mainly based on hard X-rays and usually performed at the synchrotron beamlines which are operated in air. To achieve high energy resolution, the target-detector distance is so large that the chemical speciation in low Z elements with energy ranges of (1–4) keV is not possible [13–16]. In recent years, the X-ray fluorescent peaks measured from particle induced X-ray emission (PIXE), X-ray emission (XRF), energy dispersive X-ray fluorescence (EDXRF) and electron probe microanalysis (EPMA) gave valuable information on the chemical state analysis in different variety of compounds [8,10]. However with limited resolution, poor data reliability and large number of uncertainty occurs in emission curves, these types of detectors are not well suited to detect low energy X-ray peaks more accurately and are not enough to observe the effects in chemical bonding.

Besides of this, wavelength dispersive X-ray fluorescence (WDXRF) spectroscopy is non-destructive, more effective and powerful technique used to identify the elemental composition of the different kinds of samples [17,18]. The major advantages of this technique are its high precision and accuracy, operated in vacuum, large linear scope, high energy resolution and automatic correct matrix effects. With recent advances in development of the detectors and optical instrumental parameters, these types of spectrometers can also be used to study the chemical speciation in different low Z compounds. There are many studies and theories [2–8] discussed on the Cl $K\alpha$ and $K\beta$ X-ray emission lines, but none of them provide sufficient and systematic information on the cause of chemical effects in these compounds.

In this paper, we attempt to implement the S8 TIGER WDXRF technique towards the chemical state analysis in low Z elements. The chemical effect combination and their relative theoretical explanation on these compounds have not been established completely. Various factors like line-width (FWHM), effective charge (q) and intensity ratio etc. are responsible for the chemical shift (ΔE) in various unknown compounds. In the present work, we develop a calibration curve between ΔE and

* Corresponding author.
E-mail address: harpreet.2january@gmail.com (H.S. Kainth).

https://doi.org/10.1016/j.nimb.2017.12.011
Received 24 August 2017; Received in revised form 6 December 2017; Accepted 8 December 2017
0168-583X/ © 2017 Elsevier B.V. All rights reserved.

Head
Department of Physical Sciences
I.K. Gujral Punjab Technical University
Main Campus

Scanned with CamScanner

IOP Publishing Mater. Res. Express 5 (2018) 065032 https://doi.org/10.1088/2053-1591/aacb18

Materials Research Express

PAPER

Electronic and magnetic properties of small fullerene carbon nanobuds: A DFT study

Amrish Sharma[1], Sandeep Kaur[1], Hitesh Sharma[2] and Isha Mudahar[3]

[1] Department of Physics, Punjabi University, Patiala, India
[2] Department of Physics, IKG Punjab Technical University, Kapurthala, India
[3] Department of Basic and Applied Sciences, Punjabi University, Patiala, India

E-mail: dr.ishamudahar@gmail.com

Keywords: carbon nanotubes, nanobuds, fullerenes

Supplementary material for this article is available online

RECEIVED 22 February 2018
REVISED 22 May 2018
ACCEPTED FOR PUBLICATION 7 June 2018
PUBLISHED 20 June 2018

Abstract

The electronic and magnetic properties of carbon nanobuds have been investigated using density functional theory. The carbon nanobuds are formed by attaching smaller fullerenes (C_{20}, C_{28}, C_{36} and C_{40}) of variable size with (5, 5) ACNT and (5, 0) ZCNT. Fullerenes interact strongly with CNT surface having binding energies within the range −0.93 eV to −4.06 eV. The C–C bond lengths near the attachment region increase from the original C–C bond lengths. The relative stabilities of the nanobuds are closely related to C–C bond lengths and bond angles in cycloaddition reaction. Nanobuds formed by bond cycloaddition are energetically most favorable amongst all cycloadditions. The electronic and magnetic properties of nanobuds depend strongly on electronic properties of its building blocks. The attachment of C_{20} and C_{40} on CNTs open up the HOMO-LUMO gaps of nanobuds whereas C_{28} and C_{36} results in addition of impurity states near the Fermi level. The total magnetic moment of nanobuds vary from $0.28\mu_B$ to $4.00\mu_B$ which depend on the nature of bonding between fullerene and CNTs. The results outline the potential of nanobuds as hybrid carbon nanostructures and how their properties can be tuned with the size and type of fullerene attached.

Introduction

Carbon nanobuds (CNBs) are new class of carbon nanostructures, which has attracted a lot of interest in recent years due to possibility of combining functionalities of its building blocks [1, 2]. The CNBs can be formed by combining nanostructures such as fullerenes, carbon nanotubes (CNTs) and graphene. Nanobud structure which can act as molecular anchors through fullerenes can modify electronic, magnetic and mechanical properties of CNTs [2–5].

CNBs have been synthesized during a process in which fullerenes (C_{60}) were formed on iron-catalyst particles together with CNTs during CO disproportionation [2]. The Raman spectroscopy of CNBs have confirmed the presence of fullerenes, CNTs, covalent bonding of fullerene with CNTs and predicted their lower thermal stability than pristine single walled carbon nanotube (SWCNT) [6, 7].

In addition to pristine CNBs, functionalized CNBs have also been synthesized using nucleophilic addition to CNB fullerenes where the most stable structure is formed when additions are at ortho position w.r.t a six membered ring of fullerene cage [8]. Field emission characteristics investigation of CNBs has revealed the current density of order of 10 A cm^{-2} predicting them for applications in high-current vacuum electronic devices [9]. The studies further predict high possibility of CNB formation with smaller fullerenes [2]. Therefore, combinations of chirality and size of CNTs with fullerenes of variable surface curvature offers a new class of carbon based hybrid structures which can be synthesized with tunable electronic properties.

CNTs have been investigated extensively in the literature which shows that they can be synthesized in the wide range of diameter. The smallest CNTs synthesized is with (3, 0) and (3, 3) chirality [10–12] and exhibit either metallic or semiconducting behavior depending on its helicity and chirality [12–14]. Similarly, fullerenes

Head
Department of Physical Sciences
I.K. Gujral Punjab Technical University
Main Campus

© 2018 IOP Publishing Ltd

408 11

Adsorption of Gas Molecules on ultra-thin pristine and doped graphene nanoribbons

Sandeep Kumar*, Meenakshi Malhotra and Hitesh Sharma

Department of Physical Sciences, I.K. Gujral Punjab Technical University Kapurthala,Punjab-144603, India

*skumar198712@gmail.com

Abstract: We have investigated the adsorption of CO, NO, CO_2, and NO_2 gas molecules on ultra-thin graphene nanoribbons (GNRs) using density functional theory-based calculations. In both armchair and zigzag GNR, the gas molecules stabilize at the center of hexagonal ring and interact weakly with GNR with adsorption energy in the range of -0.06 to -0.56 eV. The change in the electron density of states near fermi level on adsorption of gas molecules show that pristine GNR is more sensitive for NO_2 in comparison to CO, NO and CO_2. When dopant (B & N) and vacancy defect are introduced in the GNR surface, the adsorption of gas molecules is enhanced with higher interaction energy in the range -0.19 to -0.87 eV. The electronic properties of GNR shows strong dependence with width upto 5 layers and shows no change in the electronic properties with further increase in the width. The adsorption of gas molecules changes Electronic density of states (DOS) of GNRs near fermi level due to charge transfer and rearrangement. CO, CO_2, and NO_2 molecules behave as charge acceptor whereas NO molecule act as a charge donor. The result can be explained based on number of size dependent electronic properties of GNRs and nature of dopants/defects.

Keywords: Density Functional Theory; Ultra-thin Graphene Nanoribbons; Adsorption of gas molecules; Sensors.

1. Introduction

In recent times, there has been an immense focus for the development of accurate, faster, cost effective and portable gas sensors with high sensitivity for very low concentrations of gases [1-4]. Presently, most of the gas sensors are made up of metal wires, films, polycrystalline moss and semiconductors [5-10]. The limited accuracy of these gas sensors in detecting very low concentration of wide range of gases have necessitated the need for new generation of gas detectors with enhanced performance at a lower cost than their macro-counterparts [11,12].
Materials at nanosized dimension offers numerous opportunities to exploit its size dependent properties for development of gas detectors with ultrahigh resistivity at extremely low concentration, fast response and recovery, low power consumption and good reversibility [11-14]. Among various materials for designing next generation gas sensors, graphene has shown immense potential due to unique properties of ballistic transport, small gap semiconductor and physiochemical properties which depend on chirality of edges. So far only the usage of graphene has been demonstrated for gas sensing application, adsorption of gas molecules CO, CO_2, NO, NO_2 and NH_3 on graphene with defects have been studied theoretically and experimentally [15-21]. The studies have shown that there is very small amount of charge transfer take place with adsorbed gas molecules. However, the exact mechanism of adsorption of gas molecules and relative change in its electronic structure is yet to be understood. The thickness

Accepted Manuscript

Head
Department of Physical Sciences
I.K. Gujral Punjab Technical University
Main Campus

410

Materials Research Express

ACCEPTED MANUSCRIPT

Electronic and magnetic properties of small fullerene carbon nanobuds: A DFT study

To cite this article before publication: Amrish Sharma *et al* 2018 *Mater. Res. Express* in press https://doi.org/10.1088/2053-1591/aacb18

Manuscript version: Accepted Manuscript

Accepted Manuscript is "the version of the article accepted for publication including all changes made as a result of the peer review process, and which may also include the addition to the article by IOP Publishing of a header, an article ID, a cover sheet and/or an 'Accepted Manuscript' watermark, but excluding any other editing, typesetting or other changes made by IOP Publishing and/or its licensors"

This Accepted Manuscript is **© 2018 IOP Publishing Ltd**.

During the embargo period (the 12 month period from the publication of the Version of Record of this article), the Accepted Manuscript is fully protected by copyright and cannot be reused or reposted elsewhere.
As the Version of Record of this article is going to be / has been published on a subscription basis, this Accepted Manuscript is available for reuse under a CC BY-NC-ND 3.0 licence after the 12 month embargo period.

After the embargo period, everyone is permitted to use copy and redistribute this article for non-commercial purposes only, provided that they adhere to all the terms of the licence https://creativecommons.org/licences/by-nc-nd/3.0

Although reasonable endeavours have been taken to obtain all necessary permissions from third parties to include their copyrighted content within this article, their full citation and copyright line may not be present in this Accepted Manuscript version. Before using any content from this article, please refer to the Version of Record on IOPscience once published for full citation and copyright details, as permissions will likely be required. All third party content is fully copyright protected, unless specifically stated otherwise in the figure caption in the Version of Record.

View the article online for updates and enhancements.

Head
Department of Physical Science
I.K. Gujral Punjab Technical University
Main Campus

This content was downloaded from IP address 148.88.67.84 on 13/06/2018 at 12:07

411

Radiation Physics and Chemistry 135 (2017) 55–62

Contents lists available at ScienceDirect

Radiation Physics and Chemistry

journal homepage: www.elsevier.com/locate/radphyschem

Cross section measurements of radiative $KL_{2,3}$ RRS in $_{24}$Cr and $L_3M_{4,5}$ RRS in $_{59}$Pr for Mn $K_{\alpha 1,2}$ X-rays

Veena Sharma[a,b], Arun Upmanyu[b], Ranjit Singh[c], Gurjot Singh[a], Hitesh Sharma[b], Sanjeev Kumar[a,d,*], D. Mehta[a]

[a] Department of Physics, Panjab University, Chandigarh 160014, India
[b] Department of Physics, IKG Panjab Technical University, Kapurthala 144601, India
[c] Department of Radiotherapy, PGIMER, Chandigarh 160014, India
[d] Department of Physics, GGDSD College, Sector-32C, Chandigarh 160014, India

ARTICLE INFO

Keywords:
X-ray fluorescence
Resonant Raman scattering
Unpolarised radiations

ABSTRACT

The $KL_{2,3}$ and $L_3M_{4,5}$ radiative resonant Raman scattering (RRS) cross sections have been measured for the quasimonochromatic Mn $K_{\alpha 1,2}$ X-rays (5.895 keV) in $_{24}$Cr (K-shell level width (Γ_K) =1.08 eV) and $_{59}$ Pr (L_3-subshell level width (Γ_{L3}) =3.60 eV), respectively, using targets in metallic and various chemical forms. The incident Mn $K_{\alpha 1,2}$ X-ray energy is lower than the K-shell binding energy of $_{24}$Cr and L_3-subshell binding energy of $_{59}$Pr by ~94 Γ_K (Cr) and ~94 Γ_{L3} (Pr), respectively. The experimental measurements were performed with a low energy Ge detector (LEGe) and a radioactive ^{55}Fe annular source in conjunction with $_{24}$Cr absorber. The measured cross section values for the $_{24}$Cr and $_{59}$ Pr elements in their various oxidation states are found to be same within experimental errors. The measurements were further extended to investigate alignment of the intermediate L_3-subshell (J =3/2) virtual vacancy states in $_{59}$Pr through angular distribution measurements for RRS photon emission, which is found to be isotropic within experimental errors.

1. Introduction

The resonant Raman scattering (RRS) in X-ray energy region is an inelastic process and reminiscent of the red-shifted Stokes lines of normal optical Raman scattering. The contribution to normal Raman, elastic and Compton scattering are interpreted through A^2 term (A is the vector potential) in the photon-atom interaction Hamiltonian of the incident electromagnetic wave. On the other hand, $p.A$ (p is the electron momentum) term accounts for existence of RRS process. The RRS process occurs as the energy of incident photon (E_{in}) approaches from below the binding energy of the shell/subshell of the target element. The schematic representation of KL_2 and L_3M_4 RRS processes for any atom is shown in Fig. 1(a) and (b), respectively. In case of the KL_2 RRS, energy of the incident photon (E_{in}) is just below the K-shell threshold (B_K) of the target element. It proceeds by a virtual hole in the intermediate state to a final state in which there is a real hole (vacancy) in the L_2 subshell, an electron in the continuum and an emitted/scattered photon. The contribution comes only from tail of the K-shell Lorentzian electron distribution with lower binding energy. The scattered energy (E_s) spectrum consists of this tail and modulated with density of states. The maximum value of E_s is obtained from the energy conservation when the kinetic energy of the ejected electron is zero. As a result the measured RRS spectrum has a sharp edge at E_{in}-B_K, smeared by the experimental resolution function. Similar to the real vacancy produced in ionization process, the virtual vacancy produced in the RRS process is filled by an electron from higher shell through radiative (photon emission) as well as non-radiative (Auger and Coster–Kronig) transitions.

The resonant Raman scattering (RRS) process was firstly observed by Sparks (1974) and later on explained by Bannet and Freund (1975) on the basis of perturbation theory. The theoretical aspects of RRS have been given by Tulkki and Åberg (1975) within the framework of Kramers-Heisenberg formulation. Many aspects of the RRS process have been discussed by Sparks and Ice (1997) and Manninen (1997) in detail. Most of the radiative RRS measurements have been performed using wavelength-dispersive detectors (Szlachetko et al., 2005, 2007; Nakai et al., 2000) and synchrotron radiation (Sánchez et al., 2006). More information about the fine structure of radiative RRS (Nakai et al., 2000) can be obtained from high resolution Auger electron resonant Raman technique (Ichikawa et al., 1992; Baba et al., 1994). Recently, modest resolution energy dispersive X-ray fluorescence (EDXRF) setups involving radioisotope (Singh et al., 2004; Kumar

* Corresponding author at: Department of Physics, Panjab University, Chandigarh 160014, India.
E-mail address: sanjeevkchandel@gmail.com (S. Kumar).

http://dx.doi.org/10.1016/j.radphyschem.2017.02.049
Received 15 July 2016; Received in revised form 17 January 2017; Accepted 22 February 2017
Available online 24 February 2017
0969-806X/ © 2017 Elsevier Ltd. All rights reserved.

Head
Department of Physical Sciences
I.K. Gujral Punjab Technical University
Main Campus

13

412

Bull. Mater. Sci., Vol. 40, No. 7, December 2017, pp. 1397–1403
https://doi.org/10.1007/s12034-017-1490-1

© Indian Academy of Sciences

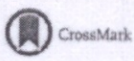

A first-principle investigation into effect of B- and BN-doped C_{60} in lowering dehydrogenation of MXH_4 (where M = Na, Li and X = Al, B)

MEENAKSHI[1], DEEPAK AGNIHOTRI[2], KIRAN JEET[3] and HITESH SHARMA[1,*]

[1]Department of Physics, I.K.G. Punjab Technical University, Kapurthala 144603, India
[2]Department of Applied Sciences, RBIEBT, Sahauran, Mohali 140104, India
[3]Electron Microscopy and Nanoscience Laboratory, Punjab Agricultural University, Ludhiana 141004, India
*Author for correspondence (hitesh@ptu.ac.in)

MS received 10 August 2016; accepted 14 March 2017; published online 23 November 2017

Abstract. The present paper reports the effect of B- and BN-doped C_{60} as catalysts for lowering the dehydrogenation energy in MXH_4 clusters (M = Na and Li, X = Al and B) using density functional calculations. MXH_4 interacts strongly with B-doped C_{60} and weakly with BN-doped C_{60} in comparison with pure C_{60} with binding energy 0.56–0.80 and 0.05–0.34 eV, respectively. The hydrogen release energy (E_{HRE}) of MXH_4 decreases sharply in the range of 38–49% when adsorbed on B-doped C_{60}; however, with BN-doped C_{60} the decrease in the E_{HRE} varies in the range of 6–20% as compared with pure MXH_4 clusters. The hydrogen release energy of second hydrogen atom in MXH_4 decreases sharply in the range of 1.7–41% for BN-doped C_{60} and decreases in the range of 0.2–11.3% for B-doped C_{60} as compared with pure MXH_4 clusters. The results can be explained on the basis of charge transfer within MXH_4 cluster and with the doped C_{60}.

Keywords. Density functional theory; complex metal hydride; C_{60} clusters.

1. Introduction

In the current scenario, harmful effects of pollution have highlighted the need for gradual transformations away from fossil fuel base, towards renewable, sustainable clean source of energy such as hydrogen [1]. Hydrogen has the highest energy density by mass and is therefore a potential future fuel option for on-board usage [2]. Among various scientific and technological challenges, search for hydrogen storage material that satisfies the commercial targets of gravimetric density and safety remains central for hydrogen economy [3,4].

Hydrogen storage in the solid state has advantages of safety and higher gravimetric density [5]. Among various solid-state storage options, the complex metal hydrides of lighter elements (Li, B, Na, Mg and Al) have high volumetric and gravimetric densities [6]. The usage of complex metal hydrides has been hindered due to their poor kinetics and higher temperature for hydrogen desorption [7].

In the last two decades, the use of various catalysts has been reported for improving dehydrogenation and re-hydrogenation behaviour of complex metal hydrides at ambient conditions [8–10]. When Ti, Sc and Ce as catalysts are introduced in $NaAlH_4$, the hydrogen desorption temperature is lowered with improved kinetics [11,12]. However, the low selectivity, poor durability and formation of undesirable bio-products have limited their success [7,12]. Therefore, the focus has shifted to other metal-free high-performance catalyst of nanocarbon [13].

Mixture of $NaAlH_4$ with carbon nanocomposite has affected the hydrogen desorption and re-hydrogenation favourably [14,15]. C_{60} when mixed with $NaAlH_4$ and $LiBH_4$ lowers the desorption temperature and improves the dehydrogenation kinetics [16–19]. C_{60}–$LiBH_4$ composite not only lowers the hydrogen desorption temperature but also provides conditions for re-hydrogenation at relatively low temperature of 350°C [15]. However, the role of fullerenes as catalyst in lowering the dehydrogenation is yet to be fully understood.

The paper describes the carbon nanostructures as catalysts for lowering dehydrogenation from complex metal hydrides. In the present paper, we have presented results on the effect of B- and BN-doped C_{60} as catalysts for lowering the dehydrogenation energy in MXH_4 clusters (M = Na and Li, X = Al and B) using density functional calculations. The hydrogen release energy of MXH_4 decreases sharply in the range of 38–49% for B-doped C_{60} and decreases in the range of 6–20% for BN-doped C_{60}. The hydrogen release energy of second hydrogen atom in MXH_4 decreases sharply in the

Electronic supplementary material: The online version of this article (https://doi.org/10.1007/s12034-017-1490-1) contains supplementary material, which is available to authorized users.

Head
Department of Physical Sciences
I.K. Gujral Punjab Technical University
Main Campus

14

413

Available online at www.sciencedirect.com

ScienceDirect

Materials Today: Proceedings 4 (2017) 10441–10445

materialstoday: PROCEEDINGS

www.materialstoday.com/proceedings

ICEMS 2016

Effect of Gas Adsorption on Graphene Nanoribbons: A Density Functional Theory

Sandeep Kumar[a*], Meenakshi[a], Hitesh Sharma[a]

[a]*Department of Applied Sciences, I.K Gujral PunjabTechnical University, Kapurthala, Punjab-144603, India*

Abstract

Using first principal calculations we have investigated the change in electronic and structural properties of CO, NO, CO_2, and NO_2 adsorbed on the ultra thin graphene nanoribbons (GNRs) with armchair and zigzag edges. Gas molecules interacts weakly with GNRs with adsorption energy of -0.07eV, -0.13eV, -0.56eV and -0.32eV for CO, NO, CO_2, and NO_2 respectively. The charge transfer take place from GNR to CO, CO_2 and NO_2 molecules while NO act as donor to GNR. Results show that armchair GNR is more sensitive to adsorption of NO_2 as compare to CO, NO and CO_2.

© 2017 Elsevier Ltd. All rights reserved.
Selection and Peer-review under responsibility of International Conference on Recent Trends in Engineering and Material Sciences (ICEMS-2016).

Keywords: Density Functional Theory; Graphene nanoribbons; Gas Adsorption.

1. Introduction

The development of sensors for detecting the gas molecules is a major challenge for pollution analysis, control of chemical species, public security, space, medical diagnosis and agricultural applications [1]. Carbon nanotubes (CNTs) and nanowires have been demonstrated as gas sensors from last few years [2-4]. Graphene nanoribbons (GNRs) are quasi one dimensional cuts of graphene with hexagonal two-dimensional carbon lattices which can be obtained from graphene by standard lithographic techniques [5-7]. GNRs due to their armchair and zigzag edge geometry have shown electronic properties variation from normal semiconductors to spin-polarized half metals. This has resulted in possibility of using GNRs as building block for electric devices [8,9]. All hydrogen terminated GNRs

*Corresponding author. Tel.: +09467274471, Email: skumar198712@gmail.com

2214-7853 © 2017 Elsevier Ltd. All rights reserved.
Selection and Peer-review under responsibility of International Conference on Recent Trends in Engineering and Material Sciences (ICEMS-2016).

Head
Department of Physical Sciences
I.K. Gujral Punjab Technical University
Main Campus

15

Journal of Magnetism and Magnetic Materials 405 (2016) 187–196

Contents lists available at ScienceDirect

Journal of Magnetism and Magnetic Materials

journal homepage: www.elsevier.com/locate/jmmm

Current Perspectives

Effect of nitrogen as co-dopant in carbon and boron-doped ZnO clusters

Neha Kapila [a,*], Gaurav Sharma [c], Isha Mudahar [d], Hitesh Sharma [b]

[a] Department of Physics, Center of Advanced Studies in Physics, Punjab University, Chandigarh 160014, India
[b] Department of Physics, Punjab Technical University, Jalandhar 144601, Punjab, India
[c] Electrical Department, ICGS VARAD, Indian Coast Guard, Port Blair, India
[d] Department of Basic and Applied Sciences, Punjabi University, Patiala 147002, India

ARTICLE INFO

Article history:
Received 9 October 2015
Received in revised form
23 November 2015
Accepted 2 December 2015
Available online 9 December 2015

ABSTRACT

The effect of N as co-dopant have been investigated on magnetic properties of C and B-doped $(ZnO)_n$ clusters ($n = 1 - 16$) using spin-polarized density functional theory. Total energy calculations show that C and N more stable when substituted at O site, whereas B is more stable at the Zn site. The B:N co-doping is energetically more stable than C:N which is more stable than N:N doping. C and N atoms do not show tendency to form clusters when doped separately. The magnetic moment (MM) of C-doped ZnO clusters is enhanced significantly with *N* co-doping. The MM of 2 μ_B, 1 μ_B and 1 μ_B per atom is induced due to C, N and B respectively. The MM of 3 μ_B or 5 μ_B and 2 μ_B or 4 μ_B are observed for co-doping of 2C:N and C:2N respectively. In contrary, the MM in 2B:N and B:2N co-doped $(ZnO)_n$ remains 1 μ_B for $n = 2 - 4$, 12 and 16. The results are in agreement with the available theoretical results.

© 2015 Elsevier B.V. All rights reserved.

1. Introduction

ZnO systems have acquired immense significance due to a wide band gap semiconductor with potential applications in optoelectronics, transparent electronics and spintronics. The room temperature ferromagnetism (FM) has been reported in *ZnO* system when injected with different magnetic (3d transition metals) and non-magnetic impurities [1,2].

Nitrogen is considered as most promising acceptor due to its similar ionic radius as compared to oxygen, for producing high quality p-type *ZnO*. However, N suffers from limitation of low solubility [3], high defect ionization energy (0.40 eV) [4] and compensating defects [5]. Further, experiments have reported *ZnO*:N as a weak ferromagnet. Recently, co-doping has been proposed to overcome some of these obstacles, by introducing acceptors and donors together in the system [6]. At the fundamental level, the co-doping is expected to increase the solubility of the dopants and enhance the ferromagnetism with appropriate choice of co-dopant.

Experimentally, the N doped *ZnO* synthesized using Pulsed laser deposition have shown FM [7]. C is doped unintentionally in N doped *ZnO* clusters by MOCVD method [8,9]. The p-type *ZnO* has been synthesized using NH_3 in Chemical Vapour Deposition (CVD) and an atomic N source in Molecular Beam Epitaxial (MBE) [5,10]. Literature survey suggests that very few co-doped ZnO systems have been synthesized and investigated theoretically [11,12]. Recently, B and N co-doped *ZnO* have shown improved electrical properties as compared to N doped *ZnO*. Ferromagnetism is greatly enhanced with Li co-doping in N doped *ZnO* [13]. p-type character have been reported in *ZnO* with the B-N doping in 1:3 ratio [14]. A co-doping enhances the N solubility and reduces the ionization energy of *ZnO*:N-based materials such as *ZnO*:N+Ga and *ZnO*:N+Be [15,16]. However, the effect of co-doping is still debated due to conflicting experimental results [17,18] as room temperature FM has also been reported in *ZnO* films deposited in N_2 environment without doping any other element [7]. Further, N co-doping in C and Cu-doped *ZnO* thin films have shown the enhancement of magnetic moment (MM). Therefore, to understand the effect of N as co-dopant in ZnO, it is of importance to investigate the effect at molecular level.

The *ZnO* nanoclusters sustain FM and are ideal for understanding the finite size effect on magnetic properties. The role of C, N and B as a dopant in *ZnO* have been discussed in our previous papers [19,20]. However, understanding of the effect of N as co-dopant in C and B doped $(ZnO)_n$ clusters e.g. (C-N, B-N) is essential for the understanding or tuning the magnetism in *ZnO* clusters. Therefore, in the present work we have explored the role of N as co-dopant in C and B doped $(ZnO)_n$ clusters for $n = 1 - 16$ using spin polarized density functional theory.

* Corresponding author.
E-mail address: kapilaneha5@gmail.com (N. Kapila).

http://dx.doi.org/10.1016/j.jmmm.2015.12.008
0304-8853/© 2015 Elsevier B.V. All rights reserved.

Head
Department of Physical Sciences
I.K. Gujral Punjab Technical University
Main Campus

415

Computational and Theoretical Chemistry 1097 (2016) 61–69

Contents lists available at ScienceDirect

Computational and Theoretical Chemistry

journal homepage: www.elsevier.com/locate/comptc

Carbon nanotubes for improving dehydrogenation from $NaAlH_4$

Meenakshi *, Deepak Agnihotri, Hitesh Sharma

Department of Physical Sciences, IKG Punjab Technical University, Kapurthala 144603, Punjab, India

ARTICLE INFO

Article history:
Received 30 July 2016
Received in revised form 3 October 2016
Accepted 13 October 2016
Available online 14 October 2016

Keywords:
Density functional theory
Complex metal hydrides
Carbon nanotubes

ABSTRACT

Carbon nanotubes (CNTs) improve the dehydrogenation kinetics of $NaAlH_4$. The present paper reports the effect of small diameter CNTs for lowering the dehydrogenation energy from $NaAlH_4$ cluster using Density functional theory. Pristine carbon nanotubes (P-CNTs) with Zig-Zag $(n,0)$ and Armchair (n,n) chirality with $n = 3, 4, 5$; chemically B/N doped CNTs (C-CNTs) and CNTs with vacancy defect (V-CNTs) are considered systematically to study the interaction with $NaAlH_4$ cluster. $NaAlH_4$ interacts with P-CNTs, C-CNTs and V-CNTs with binding energy of the order 0.77–0.98 eV, 0.60–1.01 eV and 0.81–1.74 eV respectively. The hydrogen release energy of $NaAlH_4$ decreases from 3.95 eV by 38%, 49% and 39% when interacting with P-CNTs, C-CNTs and V-CNTs respectively. Results can be explained on the basis of electronic charge transfer and redistribution between CNTs and $NaAlH_4$ which weaken the bonds involved in cluster and enhance easy removal of hydrogen. The results are in agreement with the available experimental data.

© 2016 Elsevier B.V. All rights reserved.

1. Introduction

Hydrogen has been considered as one of the possible alternate for clean and renewable energy in the recent past [1–6]. Enormous efforts have been made in finding appropriate hydrogen storage materials which meet the commercial storage target of 9.5 wt.% with fast kinetics and favorable thermodynamics at ambient conditions [7,8]. Among various hydrogen storage materials, $NaAlH_4$ has been explored most extensively due to its high hydrogen content at moderate temperature with stable thermodynamics [8–11].

The presence of strong ionic and covalent interactions in $NaAlH_4$ result in their poor kinetics and energetics behavior [6] which has hampered its practical application as hydrogen storage material [10]. To address this challenge, different strategies have been reported in the literature. In the last two decades, the use of transition metal based catalysts such as Ti, Sc and Ce have shown significant improvement in hydrogen adsorption/desorption behavior [12–19]. However, use of transition metals result in lower efficiency, formation of undesirable bye-products and high level of contamination [20].

Alternatively, the adsorption/desorption of complex metal hydrides have shown improvement when the size of their crystals is reduced to nanosize. $NaAlH_4$ nanoparticles of 10 nm size have shown adsorption/desorption at milder conditions (adsorption at 90 bar, 115 °C yielding 0.7 wt.%) [21,22]. In addition when $NaAlH_4$ is confined into 2–3 nm porous carbon structure, the hydrogen release temperature is lowered from 283 °C to 100–120 °C at under 1 bar of H_2 [22,23]. However, the role of complex metal hydrides nanoparticles of hydrides and use of transition metal based catalysts in lowering hydrogen desorption/adsorption is still debated.

In last few years, the focus has shifted to the use of carbon nanostructures as catalysts and co-catalysts [23,24]. Experiments have shown that C_{60}, Carbon nanotubes (CNTs), carbon nanofibers and graphene nanoribbons when mixed with $NaAlH_4/LiBH_4$, show sharp improvement in their energetics [23,25–29]. Single wall CNTs (SWCNTs) when admixed with $NaAlH_4$ have improved the dehydrogenation temperature up to 160 °C by the weakening of Al–H bond which has been confirmed by Fourier transform infrared spectroscopy (*FTIR*) [23]. Mechanically milled SWCNTs have shown improvement in the reversible dehydrogenation behavior of $LiBH_4$-MgH_2 two times higher than pure composite [30]. $LiBH_4$ when dispersed on multi wall CNTs (MWCNTs) the dehydrogenation temperature decreases from 400 °C up to 60 °C [31,32]. However, the exact mechanism for the observed behavior has not been fully understood. So far, to best of our knowledge, CNTs have not been investigated theoretically as a possible catalyst for improving dehydrogenation of $NaAlH_4$. Therefore, it is of immense significance to investigate and understand the role of CNTs in lowering the dehydrogenation of $NaAlH_4$.

* Corresponding author.
E-mail address: mmalhotra62@gmail.com (Meenakshi).

http://dx.doi.org/10.1016/j.comptc.2016.10.011
2210-271X/© 2016 Elsevier B.V. All rights reserved.

Head
Department of Physical Sciences
I.K. Gujral Punjab Technical University
Main Campus

Materials Research Express

PAPER

Improvement in dehydrogenation of MXH_4 where M = Na, Li and X = Al, B confined in CNTs: a DFT investigation

To cite this article: Meenakshi *et al* 2016 *Mater. Res. Express* **3** 115013

View the article online for updates and enhancements.

Related content

- First-principles study of hydrogen storage material NaBH4 and LiAlH4 compounds: electronic structure and optical properties
T Ghellab, Z Charifi, H Baaziz et al.
- Effects of electron doping on the stability of the metal hydride NaH
M A Olea-Amezcua, J F Rivas-Silva, O de la Peña-Seaman et al.
- Theoretical study of C60 as catalyst for dehydrogenation in LiBH4
Ralph H Scheicher, Sa Li, C Moyses Araujo et al.

Recent citations

- Effect of Dopants and Defect in Graphene Nanoribbons on Dehydrogenation of MXH4, where M=Na,Li and X=Al,B
Meenakshi *et al*
- A review on design strategies for metal hydrides with enhanced reaction thermodynamics for hydrogen storage applications
Ki Chul Kim

Head
Department of Physical Sciences
I.K. Gujral Punjab Technical University
Main Campus

This content was downloaded from IP address 157.39.21.26 on 25/06/2018 at 09:09

417

IOP Publishing Mater. Res. Express 3 (2016) 095007 doi:10.1088/2053-1591/3/9/095007

Materials Research Express

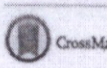

RECEIVED
22 July 2016

ACCEPTED FOR PUBLICATION
11 August 2016

PUBLISHED
2 September 2016

PAPER

Size dependent electronic and magnetic properties of ultra thin graphene nanoribbons

Sandeep Kumar, Meenakshi and Hitesh Sharma

Department of Physics, IKG Punjab Technical University, Kapurthala-144603, Punjab, India

E-mail: skumar198712@gmail.com

Keywords: density functional theory, ultra thin graphene nanoribbons, electronic and magnetic properties

Abstract

We present the results of systematic investigation into size dependent electronic and magnetic properties of ultra thin graphene nanoribbons (GNRs) of finite and infinite length using spin polarized density functional calculation. The rectangular GNRs with width up to 1.40 nm with finite (2.50 nm) and infinite length were investigated. The ultra thin GNRs are found less stable in comparison to larger GNRs with binding energy increasing with increase in the size. All GNRs have shown finite HOMO-LUMO gap which decreases oscillatory as a function of width. HOMO-LUMO gap in the Finite length armchair GNRs is in range of 0.01–0.36 eV, where as in infinite length GNR the energy gap is in the range of 0.30–1.41 eV. Zigzag GNRs have shown very small HOMO-LUMO gap in the range 50–80 meV. The zigzag GNR have shown opening of energy band gap. However, for $N = 8$ and 10 layers, GNRs with zigzag edges are found to be ferromagnetic. The edge C atom on zigzag edges contribute magnetic moment of 0.94 μ_B per C atom with total magnetic moment remaining constant with increase in the width. The energy difference between ferromagnetic and anti-ferromagnetic state decreases sharply with the increase in GNR width suggesting iso-energetic behavior in larger GNRs. The results are consistent with the reported experimental results.

1. Introduction

Graphene nanoribbons (GNRs) are quasi one dimensional cuts of graphene with hexagonal two-dimensional carbon lattices which have been studied extensively in the last decade due to their unique properties ranging from semiconducting to spin polarized half metallic [1–3, 31]. With recent advances in the bottom up experimental techniques, it has become possible to synthesize ultra thin GNRs with different width and doping [5, 6]. The GNR with zigzag edges has been predicted as the target material, for future electronics and spintronics based devices due to their long spin relaxation times and length [3, 7, 8].

The geometrical termination of the GNR edges in different shapes result in modification of electronic structure to be either semiconducting or metallic [8–10]. Their electronic and magnetic properties have shown strong edge dependence [11, 12]. Zigzag edge possesses localized edge states with energies close to the Fermi level inducing magnetic and metallic behavior [12, 13]. However, the exact measurement into the effect of GNR edges on electronic properties has remained a challenge owing to very limited control over the edge orientation of the GNRs and different results have been reported [14]. Theoretical calculations with tight binding approximation and density functional theory have predicted different electronic properties of GNRs as function of width, depending on the type of exchange correlation functionals [15, 16]. So far smallest GNR which have been synthesized consists of five layers of carbon atoms, highlighting the possibility of tailoring their electronic properties [5, 17].

Further, room temperature magnetic order in zigzag edges of narrow GNR have been reported for zigzag GNR narrower than 7 nm but larger than 2 nm width [18]. The magnetism in GNRs with zigzag edges have been attributed to the spin states of edge carbon atoms, the spin orientation of the electrons along the edge are still debated [18, 19]. Therefore, a systematic investigation into the electronic and magnetic properties of ultra thin

© 2016 IOP Publishing Ltd

Head
Department of Physical Sciences
I.K. Gujral Punjab Technical University
Main Campus

ScienceDirect

418

View PDF

Access through your institution

Purchase PDF

Materials Today: Proceedings
Volume 46, Part 11, 2021, Pages 5516-5522

Study of kinematic viscosity and density of biodiesels exposed to radiations

Amit Sarin [a], Neerja Sharma [b], Kusam Devgan [c], Meetu Singh [d]

Show more

Outline | Share Cite

https://doi.org/10.1016/j.matpr.2020.09.257 Get rights and content

Abstract

The storage of biodiesels is a major concern for its long term performance. The present work reports the kinematic viscosity and density of Jatropha biodiesel (JBD) and Pongamia biodiesel (PBD) when exposed to sunlight and ultraviolet (UV) irradiation for up to thirty days and ten hours respectively. Along with the exposure towards radiations, different antioxidants viz. Butylatedhydroxyanisole (BHA), Butylatedhydroxytoluene (BHT), Tert-butyl hydroquinone (TBHQ) were also added to the biodiesel samples to observe their impact along with varying storage ambiance. The study aimed to establish a concrete approach towards the stability of biodiesels when exposed to the diverse ambiance.

Previous Next

Head
Department of Physical Sciences
I.K. Gujral Punjab Technical University
Main Campus

Keywords

Biodiesel; Storage; Kinematic viscosity; Density; Antioxidants

FEEDBACK

Taylor & Francis Online

Log in | Register

Home ▸ All Journals ▸ Energy Sources, Part A: Recovery, Utilization, and Environmental Effects ▸ List of Issues ▸ Latest Articles ▸ Investigation of the shelf life of the o ....

Energy Sources, Part A: Recovery, Utilization, and Environmental Effects ›
Latest Articles

69 Views | 0 CrossRef citations to date | 0 Altmetric

Research Article

Investigation of the shelf life of the optimized Neem biodiesel and its execution and excretion characteristics on automotive diesel engine

Mayank Chhabra, Balraj Singh Saini, **Gaurav Dwivedi**, Arun Kumar Behura, Anuj Kumar, Siddharth Jain, Amit Sarin & Puneet Verma ...show less

Received 19 Aug 2020, Accepted 19 Jan 2021, Published online: 01 Feb 2021

Download citation https://doi.org/10.1080/15567036.2021.1881658 Check for updates

Sample our Economics, Finance, Business & Industry Journals
>> Sign in here to start your access to the latest two volumes for 14 days

STAR INITIATIVE
Free article access for authors from the Global South
Register for a voucher ›

Publish across Energy Sciences. Submit to F1000Research today.

ABSTRACT

The national biofuel policy of the Indian government support to put a great emphasis on the synthesis of biodiesel from the nonedible feedstock. A potential option in this regard is Neem oil which is found in abundance in India (~1,00,000 tonnes). The major hindrance to the commercialization of biodiesel is its shelf life due to poor oxidation and stability characteristics. The current work investigates the oxidation stability of Neem biodiesel as per

Head
Department of Physical Sciences
I.K. Gujral Punjab Technical University

420

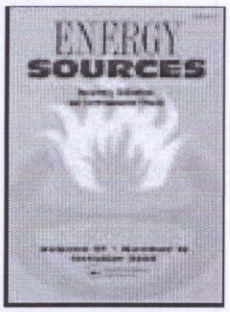

Taylor & Francis
Taylor & Francis Group

Energy Sources, Part A: Recovery, Utilization, and Environmental Effects

ISSN: (Print) (Online) Journal homepage: https://www.tandfonline.com/loi/ueso20

Comprehensive analysis of oxidation and storage stability of argemone biodiesel and development of correlations based on experimental results

Mandeep Singh , Amit Sarin & Sarbjot Singh Sandhu

To cite this article: Mandeep Singh , Amit Sarin & Sarbjot Singh Sandhu (2020): Comprehensive analysis of oxidation and storage stability of argemone biodiesel and development of correlations based on experimental results, Energy Sources, Part A: Recovery, Utilization, and Environmental Effects, DOI: 10.1080/15567036.2020.1773968

To link to this article: https://doi.org/10.1080/15567036.2020.1773968

Published online: 10 Jun 2020.

Submit your article to this journal

View related articles

View Crossmark data

Head
Department of Physical Sciences
I.K. Gujral Punjab Technical University
Main Campus

Full Terms & Conditions of access and use can be found at
https://www.tandfonline.com/action/journalInformation?journalCode=ueso20

Journal of Radioanalytical and Nuclear Chemistry
https://doi.org/10.1007/s10967-019-06935-6

Seasonal variation of indoor radon/thoron and their progeny levels in lesser-Himalayas of Jammu & Kashmir, India

Ajay Kumar[1] · Raman Vij[1,3] · Sumit Sharma[2] · Amit Sarin[3]

Received: 4 September 2019
© Akadémiai Kiadó, Budapest, Hungary 2019

Abstract
In this investigation, the passive estimation of radon (Rn^{222}), thoron (Rn^{220}) and their progenies have been measured in the dwellings of Reasi district of Jammu & Kashmir for a period of 1 year. These estimations have been done with the help of latest developed single entry Pin-hole based dosimeters and progeny sensors based on deposition. The annual Equilibrium factors for ^{222}Rn, ^{220}Rn, and their progenies have been calculated separately for each dwellings The average annual effective dose was found to be 0.9 ± 0.2 mSv/y for ^{222}Rn, which is less than prescribed limit of ICRP. The results obtained indicate no vital health hazards because of exposure of Rn^{222}, Rn^{220} and their progenies.

Keywords Deposition based sensors · Seasonal variation · Equilibrium factor · Prescribed level · House type

Introduction

Due to natural radiations, inhalation of ^{222}Rn, ^{220}Rn, and their decay-products contribute about 50% of world-wide effective dose to the general population [1]. Various case–control investigations of residential exposure to ^{222}Rn have been completed in different parts of the globe to enhance our understanding of the health risks of ionizing radiations. These controlled instigations provide the knowledge of an enchanting the risk of lung malignant with the expansion in exposure of ^{222}Rn [2]. ^{220}Rn, then again, has not been concentrated in detail because of reference to lung cancer risk. Recently, ^{220}Rn contribution is only recognized in the radiation dose [1, 3, 4].

The Inhalation dose due to ^{222}Rn and its short-lived progeny are the primary source and about 40% of the total radiation dose taken by the overall populace is the significant supporter to the issue in the respiratory tract, lung malady and sensitive tissue of the skin and cause skin disease [5, 6]. In Past decades, an equilibrium factor (fixed value = 0.4) (ratio of Equilibrium Equivalent Concentration of the short-lived to the Concentration of Radionuclide) can be utilized to measure the decay products of the radionuclide's [7], but in now a days, direct $^{222}Rn/^{220}Rn$ progeny sensors (DTPS/DRPS) have been utilized in this work for the progeny estimation. Unattached part, size distribution, and equilibrium factor are also the essential influent parameters related to the lung dose computation [8].

Radon (^{222}Rn) and thoron (^{220}Rn) decay into various short-lived radio-isotopes. After the decay of ^{222}Rn, the recently framed radio-active nuclides react with environmental gases and vapors and form a cluster of particles of size around 1 nm, which are Un-attached particles. These unattached radio-active nuclides may likewise combine with existed aerosols presented in the atmosphere within a time period of 1–100 s, framing the attached particles [9]. The buildup of activity of ^{222}Rn gas and its short-lived alpha emitters inside enclosed spaces may increase the radiation risk to the public. This applies especially to work environments like, underground mines, visitor surrenders, and water supply offices which deal with high radon ground water sources. By and large, health risk by radon (^{222}Rn) is considerably more far-reaching than by thoron (^{220}Rn). Since thoron (^{220}Rn) has a short span of life, it is less capable than the ^{222}Rn to move from the point where it is shaped [10]. As an outcome, materials used for building purposes are the most regular source of ^{220}Rn exposure. Conversely,

✉ Ajay Kumar
ajay782@rediffmail.com

1 Department of Physics, DAV College, Amritsar, Punjab 143001, India

2 Department of Applied Sciences, Swami Sarvanand Group of Institutes, Dinangar, Punjab 143531, India

3 Department of Physical Sciences, I. K. G. Punjab Technical University, Jalandhar, Punjab 144011, India

Published online: 18 November 2019

Head
Department of Physical Sciences
I.K. Gujral Punjab Technical University
Main Campus

422 24 2238

Effect of Metal Contaminants and Antioxidants on the Oxidation Stability of Argemone mexicana *Biodiesel: Experimental and Statistical Study*

Mandeep Singh, Deepak Kumar Singh, Surjit Kumar Gandhi, Amit Sarin, Sanjeev Saini, Sunil Kumar Mahla, Ajay Gupta & Sarbjot Singh Sandhu

Waste and Biomass Valorization

ISSN 1877-2641

Waste Biomass Valor
DOI 10.1007/s12649-019-00886-5

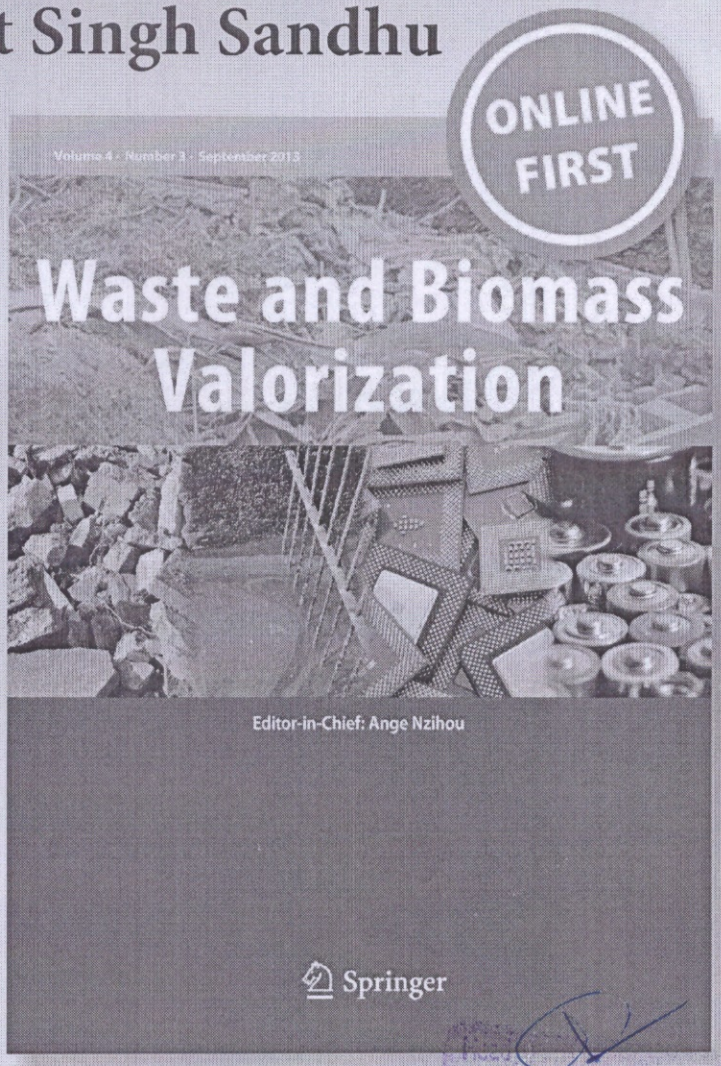

Department of Physical Sciences
I.K. Gujral Punjab Technical University
Main Campus

Springer

423

AIChE

Antioxidative Potential of *Phyllanthus emblica* for Oxidation Stability of Biodiesels

Meetu Singh,[a] Neerja Sharma,[b] Harkirat S. Paras,[c] Navneet S. Hans,[d] Narinder P. Singh,[e] and Amit Sarin[f]

[a]Department of Applied Sciences, I.K. Gujral Punjab Technical University, Kapurthala, India
[b]Department of Physics and Electronics, DAV College, Amritsar, India
[c]Department of Mechanical Engineering, Amritsar College of Engineering & Technology, Amritsar, India
[d]Department of Mechanical Engineering, Amritsar College of Engineering & Technology, Amritsar, India
[e]Department of Planning and External Development, I.K. Gujral Punjab Technical University, Kapurthala, India
[f]Department of Physical Sciences, I.K. Gujral Punjab Technical University, Kapurthala, India; amit.sarin@yahoo.com (for correspondence)

Published online 00 Month 2018 in Wiley Online Library (wileyonlinelibrary.com). DOI 10.1002/ep.13006

Biodiesel is an influential alternative fuel to petroleum-based diesel fuel due to its nontoxic, biodegradable and renewable nature. Oxidation stability (OS) is a significant feature to analyze the stability and shelf life of a biodiesel. To prevent biodiesel from being oxidized, various antioxidants are being used. In the present work, the antioxidant activity of Phyllanthus emblica has been investigated to enhance the OS of jatropha biodiesel (JBD) and pongamia biodiesel (PBD) synthesized by transesterification. The evaluation of functional groups vital for antioxidative potential in P. emblica has been identified by Fourier Transform Infrared (FTIR) spectroscopy technique and the presence of the phenolic group in it contributes toward the slowing down of auto-oxidation process in biodiesels. However, the antioxidant activity for it has been determined against 2,2-diphenyl-1-picrylhydrazyl-hydrate (DPPH) radical and total phenolic content (11.1 g of Gallic acid equivalent/100 g) was determined by the Folin–Ciocalteau method. OS of neat JBD and PBD was observed to be 4.24 h and 3.71 h, respectively. After doping P. emblica in different weight proportions, it has been found that the OS of JBD and PBD was increased up to 15.63 h and 14.26 h, respectively, with 1000 ppm blending. This study proves to be advantageous for exploring natural antioxidants to enhance the shelf life of biodiesels and to untarnish their renewable nature. © 2018 American Institute of Chemical Engineers Environ Prog, 2018

Keywords: biodiesel, oxidation, stability, antioxidants, P. emblica

INTRODUCTION

Biodiesel is defined as a monoalkyl ester derivative of long chain fatty acids, produced through the transesterification of vegetable oils, used frying oils or animal fats with alcohol and suitable catalysts. Biodiesel is one of the root alternatives to the petroleum diesel and can be used in blends in different proportions [1]. Biodiesel can be synthesized from various edible and nonedible oils. The edible feedstock such as soybean, palm, and sunflower oils are considered to be first generation biodiesel feedstock, whereas nonedible feedstock, such as jatropha, mahua, pongamia, jojoba, waste cooking oils, and animal fats are among the second-generation feedstocks [2]. Although biodiesel has an edge over other fossil fuels being environmentally friendly, yet certain limitations, such as declining oxidation stability, cold flow properties, storage stability etc. need to be taken care before their operational competitiveness with other fuels. Oxidation stability (OS) predicts the strength of biodiesel against oxidation which determines the shelf life and quality of biodiesel. Biodiesels are more prone to oxidative degradation as compared to petrol-based diesel due to the presence of a miscellaneous level of unsaturation in their fatty acid chains, containing allylic and bis-allylic sites [3]. During storage, oxidation occurs by a series of reactions categorized as initiation, propagation, and termination as clear from following reaction mechanism [4]:

Initiation:

$$RH + I \rightarrow R^{\bullet} + IH; \quad I \text{ is initiator radical}$$

Propagation:

$$R^{\bullet} + O_2 \rightarrow ROO^{\bullet}; \quad (\text{Peroxide radical})$$
$$ROO^{\bullet} + RH \rightarrow R\text{-}OOH + R^{\bullet}$$

Termination:

$$R^{\bullet} + R^{\bullet} \rightarrow R{-}R$$
$$ROO^{\bullet} + ROO^{\bullet} \rightarrow \text{Stable Product}$$

The OS of biodiesels, as a performance parameter is considered to be of paramount importance by several standards such as EN-14214 and ASTM D-6751, is evaluated through the induction period (IP). EN-14214 proposed a minimum IP of 6 h by the Rancimat method, whereas according to ASTM D-6751 standard, an IP of 3 h by the same method is considered

© 2018 American Institute of Chemical Engineers

Department of Physical Sciences
I.K. Gujral Punjab Technical University
Main Campus

Applied Physics A (2018) 124:830
https://doi.org/10.1007/s00339-018-2257-2

Applied Physics A
Materials Science & Processing

Optical characterisation of amorphous Se–Te–Sn thin films

Amit Sethi[1] · Surbhi Sharma[2] · Amit Sarin[3] · Rajesh Kumar[4] · Navjeet Sharma[5]

Received: 20 July 2018 / Accepted: 15 November 2018
© Springer-Verlag GmbH Germany, part of Springer Nature 2018

Abstract
Optical characterization of Sn doped Se–Te thin films has been carried out. The characterization has been carried out using transmission spectra in range 500–2500 nm. Bulk samples were prepared using melt quenching technique and thin films were deposited using thermal evaporation. XRD analysis was used to confirm the amorphous nature of prepared samples. Optical constants such as refractive index and extinction coefficient have been determined using Swanepoel's method. Variation of refractive index with wavelength has been analysed using single effective oscillator model. Optical band gap of the deposited films was calculated using Tauc plots. The observed properties have been explained using the chemical bond approach.

1 Introduction

Chalcogenide glasses (C.Gs) are attracting interest of scientific community owing to their unique properties viz. reversible phase transformation, high transparencies in low and middle IR region, relatively good thermo-mechanical, electrical and optical properties [1–3]. Such features make C.Gs appealing materials for the applications in switching, xerography, holography, memory, optical fibers etc. [4–10]. Studies reveals that Te based glasses have poor glass forming ability, narrow glass forming region, lower transmittance and are more susceptible towards crystallization [11]. Whereas, Se-based glasses are more stable than Te glasses because Se is the only one chalcogen which possesses vitreous state even in the room temperature [12]. Binary system of Se–Te have higher crystallization temperature, higher conductivity and show delayed ageing effects which makes these alloys much useful for various opto-electronic applications viz. IR spectroscopy, laser printing, photo-receptors etc. [13–15].

Additives like Sb, Sn, As, Ag added to binary alloys introduce defects in the system which create compositional disorder thereby making the system more flexible leading to enhanced glass forming area. However, studies shows that addition of heavy elements like Sn to a glass system may decrease its glass forming region but improves the transmittance in IR region due lower optical losses. Tin (Sn) containing Se–Te glassy alloy has been the material of interest for scientists owing to its higher refractive index and better non linear properties [16, 17].

In this paper an attempt is made to study optical properties of Se–Te-Sn ternary system. To reveal the structural disorder of $Se_{85-x}Te_{15}Sn_x$ ($x=0, 3, 6$) system through optical analysis various linear optical parameters viz. optical energy band gap, refractive index, extinction coefficient has been determined from the transmission spectra in the wavelength range of 500–2500 nm. Additionally, Wemple–DiDomenico effective oscillator model is used to enquire the dispersion behavior of the system.

2 Experimental technique

Conventional melt quenching technique was used for the preparation of bulk samples of $Se_{85-x}Te_{15}Sn_x$ ($x=0, 3, 6$) system. Constituent elements (5 N) were weighed according to their atomic percentage and were sealed in an evacuated quartz tube. Ampoules so obtained were then heated

✉ Navjeet Sharma
sharma_navjeet@yahoo.com

1 Department of Applied Sciences, I. K. G. Punjab Technical University, Kapurthala, Punjab, India

2 Department of Physics, Kanya Mahavidyalaya, Jalandhar, Punjab, India

3 Department of Applied Sciences, I.K.G. Punjab Technical University, Kapurthala, Punjab, India

4 Department of Physics, DAV College, Amritsar, Punjab, India

5 Department of Physics, DAV College, Jalandhar, Punjab, India

Published online: 19 November 2018

Department of Physical Sciences
I.K. Gujral Punjab Technical University
Main Campus

425

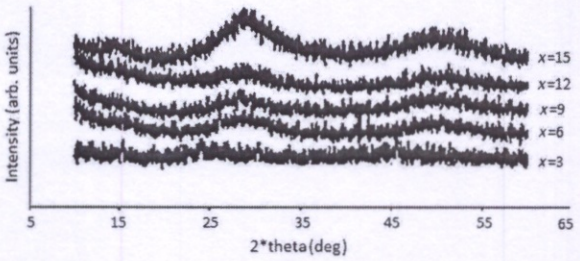

Fig. 1 XRD diffractograms of $Ge_{20}Sn_{10}Se_{70-x}Te_x$ ($x = 3, 6, 9, 12, 15$).

specimens. Figure 1 shows the XRD diffractograms of $Ge_{20}Sn_{10}Se_{70-x}Te_x$ ($x = 3, 6, 9, 12, 15$).

Subsequently, thermal evaporation technique was used to prepare thin films of $Ge_{20}Sn_{10}Se_{70-x}Te_x$ ($x = 3, 6, 9, 12, 15$) (Hind High Vacuum Coating Unit, 12A4D). Thin films were deposited onto a precleaned microscope borosilicate glass slides used as glass substrate at the rate of 5 to 8 nm/s, in a vacuum better than 10^{-5} Torr. To avoid substrate contamination, glass slides were rinsed using a detergent solution followed by boiling in distilled water to remove detergent traces. Further, these substrates were cleaned by an ultrasonic cleaner.

Optical transmittance of as-prepared thin films has been investigated in the wavelength range of 400 to 2500 nm using UV–VIS–NIR (Perkin Elmer Lambda 750) spectrophotometer.

Electrical characterization of thin films was carried out using a conventional two-probe method. Measurements were taken in the temperature range of 289 to 333 K. Electrodes were designed using silver paste with ~99.99% of purity. For I–V characteristics, DC voltage ranging 0 to 500 V was applied across the Ohmic contacts and the corresponding current was noted through Keithley picometer (model 6487).

3 Results and Discussion

3.1 *Study of Linear Optical Properties of the System*

3.1.1 *Investigation of refractive index, extinction coefficient, and film thickness of $Ge_{20}Sn_{10}Se_{70-x}Te_x$ ($x = 3, 6, 9, 12, 15$)*

The transmission spectra obtained from UV–VIS–NIR spectrophotometer have been used to determine the different optical constants of as-prepared thin films. The transmittance spectra for $Ge_{20}Sn_{10}Se_{70-x}Te_x$ ($x = 3, 6, 9, 12, 15$) thin films at the normal incidence are obtained in the spectral region from 400 to 2500 nm as shown in Fig. 2.

The presence of interference fringes in the transmission spectra is due to low absorption in thin films. Transmission curves are oscillatory in nature, which is due to the multiple interferences at three interfaces viz. air, film, and substrate. The transmission spectra as shown in Fig. 2 shift toward a higher wavelength, which is due to an increase in the concentration of heavier Te atoms in a Ge-Sn-Se matrix. This shift is a direct consequence of the compositional dependence of transmission spectra.[20] A sharp fundamental absorption edge is observed from ~493 to 574 nm, where its transmission % falls to about zero value as the concentration

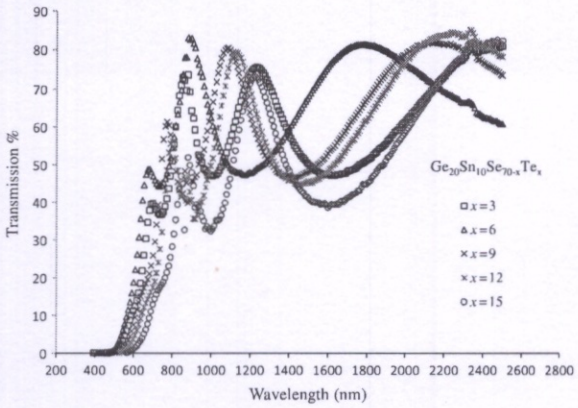

Fig. 2 Transmission spectra of $Ge_{20}Sn_{10}Se_{70-x}Te_x$ ($x = 3, 6, 9, 12, 15$) thin films.

of Te increases from 3 to 15 at. %. Cutoff wavelength of glasses reveals the stronger absorption of light in the visible region.[21–23]

Refractive index μ of thin films under study is calculated from transmission spectra using Swanepoel's method[24] based on the model manifested by Manifacier et al.[25] In the weak or medium absorption region of transmission spectra, the refractive index of a substrate has been calculated using standard equations as developed by Jenkins and White[26] and is available in the literature.[27]

From the plot of refractive index versus wavelength as shown in Fig. 3, it is inferred that refractive index decreases with an increase in the wavelength, whereas an increase in the refractive index can be observed with an increase in the Te concentration.

An increasing trend of refractive index with an increase in the concentration of Te is due to an increase in the resultant density, which makes the system rigid. Atomic radii of Te and Se are 1.6 and 1.14 Å,[28] respectively, and their respective densities are 6.24 and 4.28 g/cc, respectively.[29] Using Lorentz–Lorenz relation,[30] an effective increase in the refractive index can be attributed to the resultant increase in polarization with the incorporation of Te atoms of higher atomic radii:

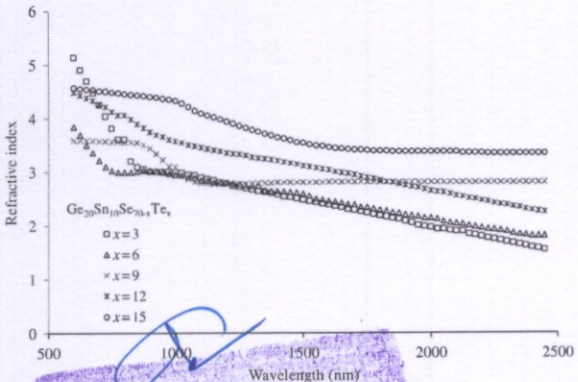

Fig. 3 Refractive index variation with wavelength for $Ge_{20}Sn_{10}Se_{70-x}Te_x$ ($x = 3, 6, 9, 12, 15$).

Head Department of Physical Sciences I.K. Gujral Punjab Technical University Main Campus

426 28 22038

Physica B: Condensed Matter 545 (2018) 210–214

Contents lists available at ScienceDirect

Physica B: Condensed Matter

journal homepage: www.elsevier.com/locate/physb

Crystallisation kinetics and thermal stability analysis of $Se_{82-x}Te_{15}Sn_3Sb_x$ ($0 \le x \le 6$) glassy alloys

Amit Sethi[a], Amit Sarin[a], Rajesh Kumar[b], Navjeet Sharma[c,*]

[a] Department of Physical Science, I. K. G. Punjab Technical University, Kapurthala, Punjab, India
[b] Department of Physics, DAV College, Amritsar, Punjab, India
[c] Department of Physics, DAV College, Jalandhar-144008, Punjab, India

ARTICLE INFO

Keywords:
Amorphous
Crystallisation
Activation energy
Glass transition

ABSTRACT

This paper reports the results of study of crystallization kinetics and thermal stability in $Se_{82-x}Te_{15}Sn_3Sb_x$ ($0 \le x \le 6$) glassy alloys. The alloys were analysed using DTA (differential thermal analysis) technique under non-isothermal conditions at heating rates of 5, 10, 15, 20 K/min, Activation energy of glass transition has been evaluated using Kissinger and Moynihan methods while Matusita, Kissinger and Augis and Bennett approaches has been employed to study the crystallization mechanism. Thermal stability and glass forming ability for all compositions has been analysed in terms of reduced glass transition temperature and Hruby's parameter.

1. Introduction

Chalcogenide glasses find numerous application in modern electronic devices, memory switching, optoelectronics and xerography etc. due to their special properties such as higher transparency in IR region and low optical losses [1–5]. These glasses offer the additional advantage of wide range tuning of their properties by varying the composition. Chalcogen elements S, Se and Te can be alloyed with elements from other groups to form binary, ternary or quaternary systems with tailor made properties and use in specific applications. Addition of a new element to a glass system introduces the configurational disorder in the system and changes its various physical properties such as thermal, optical and electrical [6]. This aspect of chalcogenide glasses has been extensively exploited by scientific community to form new glass systems with improved properties for specific applications [7–13]. Researchers have shown particular interest in glass systems containing heavy elements such as Sn and Sb for their advantage of better transmittance in IR region. Thermal and optical properties of Sn–Sb–Se–Te have been reported by Chander and Thangaraj [14]. Chen et al. reported the physical and thermal properties of Ge–Sb–Se–Sn glasses [16]. Addition of Sn to Se–Te matrix is known to improve its crystallization ability and affects the dimensionality of growth [17]. Nidhi and co-workers have reported the effect of Sb substitution on thermal properties of Te–Se–Ge glass system [15]. They concluded that incorporation of Sb in Te–Se–Ge network introduces strain in the system due to large size of Sb atoms and weakens the glass system. This leads to enhancement in the suitability of this system for phase change applications. This observation prompted the authors to study the effect of Sb addition in Se–Te–Sn glass system. All glasses have a tendency to crystallize and crystallization is a thermally activated process. Understanding of crystallization mechanism and glass transition of a system is very important for determining its suitability for memory and switching applications [18]. In the present work we have studied the crystallization kinetics of $Se_{82-x}Te_{15}Sn_3Sb_x$ ($0 \le x \le 6$) glass system using differential thermal analysis and computed the crystallization parameters for these compositions using different models. Composition dependence of crystallization parameters have been discussed.

2. Experimental techniques

Glass samples of $Se_{82-x}Te_{15}Sn_3Sb_x$ ($0 \le x \le 6$) were prepared using melt quenching technique. The constituent elements of 99.999% purity were weighed as per atomic percentages and sealed in evacuated quartz ampoules. The ampoules were heated in rocking furnace to 900 °C at a heating rate of 2–3 °C per minute. The ampoules were rocked at a constant rate to ensure homogeneity of the mixture. The samples were maintained at 900 °C for 24 h and then quenched in ice cold water. The amorphous nature of bulk samples prepared was confirmed using x-ray diffraction (XRD) technique. The XRD scans for prepared samples are shown in Fig. 1.

The samples in powder form were analysed for thermal studies using differential thermal analysis (DTA) technique in nitrogen atmosphere under non-isothermal conditions. DTA scans were obtained from room temperature to about 600 K at heating rates of 5, 10, 15 and 20 K/

* Corresponding author.
E-mail address: sharma_navjeet@yahoo.com (N. Sharma).

https://doi.org/10.1016/j.physb.2018.06.018
Received 12 April 2018; Received in revised form 16 June 2018; Accepted 18 June 2018
Available online 19 June 2018
0921-4526/ © 2018 Elsevier B.V. All rights reserved.

Department of Physical Sciences
I.K. Gujral Punjab Technical University
Main Campus

Author's personal copy

427

Acta Geophysica
https://doi.org/10.1007/s11600-018-0119-0

RESEARCH ARTICLE - SOLID EARTH SCIENCES

Assessment of radionuclide concentration and exhalation studies in soil of lesser Himalayas of Jammu and Kashmir, India

Ajay Kumar[1] · Raman Vij[1,2] · Sumit Sharma[1] · Amit Sarin[2] · Saurabh Narang[3]

Received: 6 December 2017 / Accepted: 6 February 2018
© Institute of Geophysics, Polish Academy of Sciences & Polish Academy of Sciences 2018

Abstract
Because to extensive utilization of soil as a building/construction stuff, the activities of ^{238}U, ^{40}K, ^{232}Th, and exhalation studies in solid samples have been measured using thallium activated sodium iodide (NaI(Tl)) gamma detector and scintillation-based smart RnDuo monitor. The measured activity concentration of radionuclides lies in the range of 2.76–38.96, 12.47–65.70, and 199–450 Bq/kg for uranium (C_U), thorium (C_{Th}), and potassium (C_K), respectively. The annual effective dose rate due to radionuclides is within the secure limit suggested by ICRP. The radium equivalent activity of all the samples is under 100 Bq/kg. The maximum outward and inside risk indices of all these samples are below the values of 0.37 and 0.43. No direct correlation has been seen between ^{238}U and its mass exhalation rate as well as ^{232}Th and its surface exhalation rate in soil samples.

Keywords Radionuclide concentration · Exhalation rate · RnDuo monitor · Air absorbed dose

Introduction

Since its formation, earth is radioactive in nature. Various radioactive elements such as uranium, radium, thorium, etc., are present in its abiotic components, i.e., rocks, soil, and water. Some of the radionuclides (^{238}U, ^{232}Th, and ^{40}K) of these elements have very long half-lives even in hundreds of years. The inhalation and ingestion of these radionuclides above the permissible level is a serious health hazard (Singh et al. 2007). Therefore, assessment of these radionuclides in any environment is of the level of interest due to its harmful effects. Inhalation of high uranium content increases the risk of lung and bone tumor and damage to internal organs particularly the kidneys (Lussenhop et al. 1958; Hursh and Spoor 1973; ATSDR 1999).

✉ Ajay Kumar
ajay782@rediffmail.com

[1] Department of Physics, D.A.V College, Amritsar, Punjab, India

[2] Department of Applied Sciences, I.K.G Punjab Technical University, Jalandhar, Punjab, India

[3] Department of Applied Sciences, Guru Kashi University, Talwandi Sabo, Punjab, India

Published online: 10 February 2018

According to UNSCEAR report, ^{40}K, ^{238}U, and ^{232}Th contributes 35, 25, and 40%, respectively, to the total radiation dose a population receives (UNSCEAR 1982). Soil and rocks are the one of the main sources of these background radiations. Radionuclides present in rocks are carried to soil through rain and the subsequent water streams (Taskin et al. 2009). When these radionuclides come in association with the soil, these can absorb the reactive layer of particles, perform ion interchange, precipitate as an oxide-hydroxide or sulphide, and form complexes with organic compounds or remain as such (Schulz 1965). Hence, once reached, these radionuclides remain in soil in one form or another. Now, these nuclides and their decay products come in contact with public mainly through ingestion and inhalation. Along with natural radioactivity, anthropogenic activities like industrial wastes and extensive use of phosphate fertilizers are also responsible for soil radioactivity (Abbady et al. 2008).

Prime contribution of the ionizing radiation (more than 50%) received by human population comes from Radon (^{222}Rn), thoron (^{220}Rn), and their naturally radioactive short-lived decay products taking all sources of radiation into account (Mazur and Kozak 2014). Therefore, this field has gained a lot of importance for last many years, both in terms of their transport properties and their influence on

Head
Department of Physical Sciences
I.K. Gujral Punjab Technical University
Main Campus

Acta Geophysica
https://doi.org/10.1007/s11600-018-0159-5

RESEARCH ARTICLE - SPECIAL ISSUE

Prediction of indoor radon/thoron concentration in a model room from exhalation rates of building materials for different ventilation rates

Manish Kumar[1,2] · Navjeet Sharma[1] · Amit Sarin[3]

Received: 9 October 2017 / Accepted: 12 May 2018
© Institute of Geophysics, Polish Academy of Sciences & Polish Academy of Sciences 2018

Abstract
Studies have confirmed that elevated levels of radon/thoron in the human–environments can substantially increase the risk of lung cancer in general population. The building materials are the second largest contributors to indoor radon/thoron after soil and bedrock beneath dwellings. In present investigation, the exhalation rates of radon/thoron from different building materials samples have been analysed using active technique. Radon/thoron concentrations in a model room have been predicted based on the exhalation rates from walls, floor and roof. The indoor concentrations show significant variations depending upon the ventilation rate and type of building materials used.

Keywords Radon · Exhalation · Ventilation rate

Introduction

Radioactivity is a part of human–environment and is present at all places on earth. All humans get exposure to ionizing radiations due to sources, natural as well as man-made. Radon/thoron are major contributors to the total ionizing radiation dose received by the general population (UNSCEAR 2008). The presence of radon/thoron in human environment above certain levels is a potential health hazard (UNSCEAR 2000; Darby et al. 2005; Krewski et al. 2006). The primary sources of indoor radon and thoron concentrations are bedrock soil underneath and building materials, which have high level of radium and thorium contents (UNSCEAR 1993; Sahoo et al. 2007). Radon/thoron reaches the indoor environment from the matrix of soil and building materials by a two stage process, emanation and exhalation. In emanation $^{222}Rn/^{220}Rn$ atoms escape from the mineral grains to the air-filled pores, and in exhalation these get transported to atmosphere by diffusion and convection (Sahoo et al. 2014). Exhalation rate of these gases from the sub-surface soil is controlled by many factors such as emanation factor, radium content of the soil and diffusion coefficient of the medium (Kumar et al. 2014). Radon, due to its relatively longer half-life, can diffuse over relatively long distances, before decaying. So contribution to indoor activity is generally from top few metres of sub-surface soil. In case of thoron, due to its short half-life, only the top layer of the sub-surface soil contributes to indoor activity. For characterizing the sources of indoor air activity concentrations of radon and thoron, measurement of exhalation rates of these gases is very important. Various methods have been developed by researchers to measure exhalation rates from building materials such as Can technique using SSNTD (solid state nuclear track detector) and closed-chamber method using online monitors (Abu-Jarad 1988; Stoulos et al. 2003). In recent years, many studies on exhalation rates from soil and building materials have been reported (Ramola et al. 2008, 2011; Chen et al. 2010; Chauhan et al. 2014; Aswal et al. 2016; Bourai et al. 2016; Singh et al. 2016; Yadav et al. 2016).

✉ Manish Kumar
manishpandit1313@gmail.com

[1] Department of Physics, DAV College, Jalandhar, Punjab, India

[2] Department of Applied Sciences, I.K.G. Punjab Technical University, Kapurthala, Punjab, India

[3] Department of Physical Sciences, I.K.G. Punjab Technical University, Kapurthala, Punjab, India

Published online: 23 May 2018

Head
Department of Physical Sciences
I.K. Gujral Punjab Technical University
Main Campus

3Type

429

Taylor & Francis

Human and Ecological Risk Assessment: An International Journal

ISSN: 1080-7039 (Print) 1549-7860 (Online) Journal homepage: http://www.tandfonline.com/loi/bher20

Radon and uranium concentrations in drinking water sources along the fault line passing through Reasi district, lesser Himalayas of Jammu and Kashmir State, India

Ajay Kumar, Raman Vij, Amit Sarin & Priya Kanwar

To cite this article: Ajay Kumar, Raman Vij, Amit Sarin & Priya Kanwar (2017): Radon and uranium concentrations in drinking water sources along the fault line passing through Reasi district, lesser Himalayas of Jammu and Kashmir State, India, Human and Ecological Risk Assessment: An International Journal, DOI: 10.1080/10807039.2017.1336426

To link to this article: http://dx.doi.org/10.1080/10807039.2017.1336426

Accepted author version posted online: 26 Jun 2017.
Published online: 26 Jun 2017.

Submit your article to this journal

Article views: 14

View related articles

View Crossmark data

Head
Department of Physical Sciences
I.K. Gujral Punjab Technical University
Main Campus

Full Terms & Conditions of access and use can be found at
http://www.tandfonline.com/action/journalInformation?journalCode=bher20

Download by: [169.149.253.42]

Date: 25 July 2017, At: 08:50

43c

6th Global Conference on Materials Science and Engineering IOP Publishing
IOP Conf. Series: Materials Science and Engineering **283** (2017) 012008 doi:10.1088/1757-899X/283/1/012008

Influence of Sb substitution on thermal and electrical characteristics of Ge-Sn-Se chalcogenide glass system

Surbhi Sharma[1*], Navjeet Sharma[2], Amit Sarin[3]
[1]Department of Applied Sciences, C. T. Institute of Engineering, Management, and Technology, Jalandhar, Punjab, India
[2]Department of Physics, DAV College, Jalandhar, Punjab, India
[3]Department of Physical Sciences, I.K.G. Punjab Technical University, Kapurthala, Punjab, India
Corresponding author: *physurbhi@gmail.com

Abstract. Present research work reports the systematic investigation of thermal and electrical characterizations of $Ge_{20}Sn_{10}Se_{70-x}Sb_x$ (x = 0, 3, 6, 9, 12, 15) glass system to probe the structural modifications. Bulk samples are prepared using melt quenching technique. Differential scanning calorimetric technique (DSC) is used at the constant heating rate of 10^0C under nonisothermal conditions. Different kinetic parameters viz. glass transition temperature T_g, Hruby parameter H_r, crystallization temperature T_c ,etc., have been calculated. Glasses under study shows good thermal stability, hence, can find practical applications especially in optical fiber technology. Further, in the current study, an attempt has been made to observe the variation in conductivity with respect to the increase in temperature for amorphous $Ge_{20}Sn_{10}Se_{70-x}Sb_x$ (x = 0, 3, 6, 9, 12, 15) using two probe method and hence the band structure and corresponding conduction mechanism is studied.

1. Introduction

Chalcogenide based thin films have attracted great attention of scientific community owing to their unique features like interesting electron transport mechanism, good thermal, mechanical and chemical properties [1-2]. Amorphous nano-scale structures have various advantages over crystalline nano- structures. It is well known that synthesis of crystalline nano-structures is controlled by deposition of atoms one by one. On the other hand in amorphous chalcogenide thin films atomic level handling is meaningless owing to its inherent property of disorderness. Thus chalcogenide films exhibit various varieties of structures due to lack of bonding constraints those arises in crystalline unit cells [3].

In Ge-Se system, Ge atoms acts as bond modifiers, which increase average bond strength by crosslinking with Se. This make the system more rigid, thus, increasing the glass transition temperature and resistivity [4]. The addition of third impurity introduces modifications into the local atomic structure, which further influence physical properties of the system. Various studies reveal that addition of Sn to Ge-Se matrix weakens the system and makes it at higher wavelength [5].

Head
Department of Physical Sciences
I.K. Gujral Punjab Technical University
Main Campus

Content from this work may be used under the terms of the Creative Commons Attribution 3.0 licence. Any further distribution of this work must maintain attribution to the author(s) and the title of the work, journal citation and DOI.
Published under licence by IOP Publishing Ltd

frontiers in Energy Research

ORIGINAL RESEARCH
published: 26 October 2017
doi: 10.3389/fenrg.2017.00028

Prospects of *Tectona Grandis* as a Feedstock for Biodiesel

Amit Sarin[1]*, *Meetu Singh*[2], *Neerja Sharma*[3] and *N. P. Singh*[4]

[1]Department of Physical Sciences, I.K. Gujral Punjab Technical University, Kapurthala, India, [2]Department of Applied Sciences, I.K. Gujral Punjab Technical University, Kapurthala, India, [3]PG Department of Physics and Electronics, DAV College, Amritsar, India, [4]Department of Planning and External Development, I.K. Gujral Punjab Technical University, Kapurthala, India

The limited availability of fossil fuels has encouraged the need of replacement fuels of renewable nature. Among the renewable fuels, biodiesel produced from oil seeds and food wastes has been favored by the majority of researchers. In this study, *Tectona Grandis* seed oil has been investigated as a non-edible feedstock for biodiesel. The oil content of seed is 43% which makes it suitable for commercial production of biodiesel. The synthesis of biodiesel from *T. Grandis* oil was done with transesterification reaction giving high percentage yield of biodiesel which reached to 89%. The *T. Grandis* biodiesel was subjected to determine various physicochemical parameters by standard testing methods and found in agreement with the ASTM D-6751 and EN-14214 standards. The fatty-acid methyl ester composition for the biodiesel is composed of 42.71% oleic acid, 13.1% palmitic acid, and 31.51% linoleic acid. The biodiesel showed low oxidation stability which is attributed to high percentage of unsaturation. To address this issue, synthetic antioxidants were added to increase its resistance towards oxidation. By considering all the parameters, the present study reveals that *T. Grandis* seed oil is reliable for the production of biodiesel with encouraging probability in future.

Keywords: biodiesel, feedstock, *Tectona Grandis*, transesterification, physicochemical properties

OPEN ACCESS

Edited by:
Liandong Zhu,
University of Vaasa, Finland

Reviewed by:
Jinxue Jiang,
Washington State University, United States
Baskar Gurunathan,
St. Joseph's College of Engineering, India
István Barabás,
Technical University of Cluj-Napoca, Romania
Perumal Varalakshmi,
Madurai Kamaraj University, India

***Correspondence:**
Amit Sarin
amit.sarin@yahoo.com

Specialty section:
This article was submitted to Bioenergy and Biofuels, a section of the journal Frontiers in Energy Research

Received: *15 August 2017*
Accepted: *04 October 2017*
Published: *26 October 2017*

Citation:
Sarin A, Singh M, Sharma N and Singh NP (2017) Prospects of Tectona Grandis as a Feedstock for Biodiesel. Front. Energy Res. 5:28. doi: 10.3389/fenrg.2017.00028

INTRODUCTION

The energy generated from the combustion of fossil fuels has indeed enabled many technological advancements and social-economic growth. However, the increasing demand of energy and environmental concerns arising due to the use of traditional fuels has become a threat to the sustainability of our ecosystem and sparked the need of energy sources of limitless duration with a smaller environmental impact. Biodiesel falls in the category of such fuels of renewable nature (Hu et al., 2004; Gui et al., 2008; Ullah et al., 2014). To address the issues related to pollution with petro-based fuels, Government of India has taken steps toward usage of biofuels. In this context, the Ministry of New and Renewable Energy has proposed 20% blending of transportation fuels, namely, diesel and petrol with bioethanol and biodiesel as a national biofuels policy by 2017 (Government of India, 2009). However, the contribution of energy from biomass has been estimated as one fourth of global energy by 2050 (Hossain and Davies, 2013).

The role of feedstock is significant for the characteristics and cost of any biodiesel. The possible feedstock for biodiesel production broadly categorized as edible and non-edible. Edible feedstocks such as soybean, palm, and sunflower are considered to be first-generation biodiesel feedstock because they were the first crops to be used to produce biodiesel and non-edible feedstock such as jatropha, mahua, jojoba oil, salmon oil, sea mango, waste cooking oils, and animal fats are considered

Head
Department of Physical Sciences
I.K. Gujral Punjab Technical University
Main Campus

Case study paper

Indoor and Built Environment

Indoor and Built Environment
0(0) 1–8
© The Author(s) 2017
Reprints and permissions:
sagepub.co.uk/
journalsPermissions.nav
DOI: 10.1177/1420326X17703773
journals.sagepub.com/home/ibe
SAGE

Measurement of uranium and radon concentration in drinking water samples and assessment of ingestion dose to local population in Jalandhar district of Punjab, India

Manish Kumar[1,4], Anjali Kaushal[1,4], B. K. Sahoo[2], Amit Sarin[1], Rohit Mehra[3], Rajan Jakhu[3], Atul Bhalla[4] and Navjeet Sharma[4]

Abstract

A study was conducted to assess the concentration of uranium and dissolved radon in drinking water samples collected from Jalandhar district of Punjab, India. The samples were analysed for dissolved radon using scintillation cell method. Laser fluorimetry was used for measurement of uranium concentration. Correlation analysis of radon and uranium concentrations and salinity and total dissolved solids with uranium was carried out. The uranium concentration in water samples varied from a minimum value of 1.53 ± 0.06 mg m^{-3} to 50.2 ± 0.08 mg m^{-3} with a geometric mean value of 14.85 mg m^{-3}. The radon concentration in water varied from a minimum value of 0.34 ± 0.07 kBq m^{-3} to a maximum value of 3.84 ± 0.48 kBq m^{-3} with a geometric mean value of 1.46 kBq m^{-3}. Ingestion dose to local population, due to radon and uranium in drinking water, for different age categories, was computed and results are being reported in this paper.

Keywords

Radon, Uranium, Ingestion dose

Accepted: 17 March 2017

Introduction

Radioactive contamination of ground water is a matter of great concern as it could lead to ingestion dose in humans. Uranium, a naturally occurring radioactive element, is important from a point of view of environmental radioactivity as it contributes a number of radioactive elements through its decay chain. Uranium is found naturally in different valance states from +2 to +6 with hexavalent state being most common.[1] It is found in nature in different types of rocks such as granites, sand stones and other mineral deposits.[2] Through the process of leaching from natural deposits, uranium enters the ground water and ultimately reaches the food chain through plants and drinking water. Though the normal concentration of uranium in ground water is reported to be in the range 0.1 to 10 mg m^{-3}, higher concentrations are possible in areas having elevated levels of uranium in rocks and soil.[3] Concentration of uranium in groundwater depends on geomorphological, lithological and

[1]Department of Physical Sciences, I. K. G. Punjab Technical University, Kapurthala, Punjab, India
[2]Radiological Physics & Advisory Division, Bhabha Atomic Research Center, Mumbai, India
[3]Department of Physics, Dr. B. R. Ambedkar NIT, Jalandhar, Punjab, India
[4]Department of Physics, DAV College, Jalandhar, Punjab, India

Corresponding author:
Navjeet Sharma, Department of Physics, DAV College, Mahatama Hans Raj Road, Jalandhar, Punjab 144008, India.
Email: navjeets@davjalandhar.com

Department of Physical Sciences
I.K. Gujral Punjab Technical University
Main Campus

433

J. Env. Bio-Sci., 2017: Vol. 31 (2):479-484 ISSN 0973-6913 (Print), ISSN 0976-3384 (On Line)

MEASUREMENT OF RADON CONCENTRATION IN THE DRINKING WATER AND ASSESSMENT OF AGE DEPENDENT INGESTION DOSE TO LOCAL POPULATION IN KAPURTHALA DISTRICT OF PUNJAB, INDIA

Manish Kumar[1,4], Amit Sarin[2], B. K. Sahoo[3] and Navjeet Sharma[4]

[1]Department of Applied Sciences, I.K.G. Punjab Technical University, Kapurthala 144601, Punjab India.

[2]Department of Physical Sciences, I.K.G. Punjab Technical University, Kapurthala 144601, Punjab India.

[3]Radiological Protection and Advisory Division, Bhabha Atomic Research Centre, Mumbai 400085, India.

[4]Department of Physics, DAV College Jalandhar 144008, Punjab, India

[Corresponding author E-mail[1,4]: manishpandit1313@gmail.com]

Received: 01-07-2017 **Accepted:** 29-08-2017

Radon, thoron and progeny constitute the single largest source of natural radiation exposure for humans. In addition to the dose due to inhalation, these elements also contribute significantly to radiation dose due to ingestion. Keeping this in view a study has been performed to assess the radon concentration in water and associated ingestion dose to local population in Kapurthala district of Punjab, India. The Smart RnDuo portable continuous radon (^{222}Rn) monitor was used to measure the dissolved radon concentration in drinking water samples collected from 37 different locations from Kapurthala district. The aim of the present investigation was to calculate the ingestion dose due to radon for different age group. The Radon concentration in drinking water samples are varied from a minimum value of 0.59 ± 0.22 Bql^{-1} to a maximum value 5.49 ± 0.67 Bql^{-1} with a geometric mean value of 1.99 Bql^{-1}. The recorded values are within the prescribed safe limit recommended by WHO, USEPA and UNSCEAR. The physico-chemical parameters such as TDS, salinity, EC, pH has been measured and correlated with radon concentration.

Radiation is an integral part of the environment. The major fraction of the natural radiation exposure we receive, comes from radioactive gas, Radon (^{222}Rn).Radon is present virtually everywhere on the earth, but particularly over land[1]. Radon is naturally occurring odourless, colourless and tasteless chemically inert gas, produced in the primordial radionuclide uranium (^{238}U) decay series[2]. Uranium is naturally occurring in the +2, +3, +4, +5 and +6 valence states, but it is most commonly found in the hexavalent form. It has very high density (19.0 g cm^{-3}) at 20 °C and insoluble in water[3] but their decay product speciallyradon (^{222}Rn) is soluble in water. Water is one of the prime elements for life on earth and drinking of uranium and radon rich water over a long period is unsafe as uranium is a documented radiological and chemical toxic effect on human health. The dissolved radon in groundwater enters in our body through ingestion. The alpha particles emitted from radon and their decay products damage the sensitive cells in the stomach and other human body organs like kidney and stomach and may lead to cancer[4]. Radon is the second major cause of lung cancer in the general population, after smoking[5]. The concentration and composition of these radioactive constituents vary from place to place, depending mainly on the radiochemical composition of the soil and rock strata and geological conditions through which the raw water may have passed[6].The concentration of indoor radon increases due to excess use of water inside the dwelling for laundering, washing, and cooking. It also depends on distance and height from principal source (rocks and soil) in the grounds[6]. The main source of uranium is soil, natural materials, food and water. The World Health Organization[7] has recommended the safe limit for uranium in drinking water as 30 µgL^{-1}. The Atomic Energy Regulatory Board, India has put the reference for Uranium in drinking water[8] as 60 µgL^{-1}.

Several investigators in the past decade focused on ingestion dose due to radon and provide reference data for Punjab, India. The joint report from GNDU, Amritsar and BARC Mumbai reveals that Uranium content in groundwater higher than the prescribed safe limit[8-9] in several places Bathinda, Mansa, Faridkot, Ferozepur and Moga Districts of Punjab[10-13]. The causes of high uranium in ground water may be the basement granite rocks, excess uses of Phosphatic fertilizers and chemical in field. By keeping this view, few data is available for Jalandhar district, so survey was conducted to measure theradon concentration in drinking water.

TDS, pH, conductivity and salinity are the physio-chemical parameters which plays vital role in water.Total dissolved solids (TDS) consists of inorganic salts such as calcium, magnesium, sodium and potassium cat ions and carbonate, hydrocarbonate, chloride, sulphate and nitrate anions and small

NAAS Rating (2017)-4.43

Head
Department of Physical Sciences
I.K. Gujral Punjab Technical University
Main Campus

434

Case Study

Indoor and Built Environment

Indoor and Built Environment
0(0) 1–9
© The Author(s) 2017
Reprints and permissions:
sagepub.co.uk/
journalsPermissions.nav
DOI: 10.1177/1420326X16687614
journals.sagepub.com/home/ibe
SAGE

Radon/thoron and progeny levels in dwellings: Regional variations and effect of dwelling characteristics – A case study in Jalandhar district of Punjab, India

Manish Kumar[1,2], Anjali Kaushal[1,2], Amit Sarin[3], Rajesh Kumar[4] and Navjeet Sharma[1]

Abstract

An extensive survey to measure natural radioactivity in human environment in Jalandhar district of Punjab was undertaken. Results of measurements of indoor radon/thoron and their progeny concentrations are being presented here. Single-entry, pin-hole dosemeters were used for the measurement of radon/thoron concentrations. Deposition-based direct radon/thoron progeny sensors were used for measurement of progeny concentrations. The results have been analysed on the basis of regional characteristics, type of construction and building material used. The radon concentration was found to vary from 6.64 ± 1.72 Bq/m^3 to 47.18 ± 4.43 Bq/m^3 with geometric mean value of 17.9 ± 2.91 Bq/m^3 while the thoron concentration varies from 7.75 ± 2.54 Bq/m^3 to 82.68 ± 8.33 Bq/m^3 with geometric mean value of 33.54 ± 5.09 Bq/m^3. The geometric mean value of equilibrium factor for indoor radon and thoron was found to be 0.43 and 0.02, respectively. The estimated annual inhalation dose varies from 0.22 mSv to 1.76 mSv with geometric mean value of 0.66 mSv. Correlation of indoor radon and air gamma dose rate was also studied.

Keywords

Radon, Thoron, Equilibrium factor, Dose

Accepted: 12 December 2016

Introduction

Presence of natural radioactivity in human environment is a potential health hazard. All human are being regularly exposed to ionising radiation.[1] This radiation exposure varies considerably by location, and background radiation levels are greatly influenced by local geological conditions. Radiation exposure to humans in indoor environment is controlled by various factors such as types of dwelling, building materials used and ventilation conditions.[2,3] Radon, along with its progenies is the largest contributors to the natural background radiation dose for general population. Many studies, reported world-wide, have established direct relationship between elevated levels of radon and increased incidence of lung cancers.[4–6] Some other types of cancers, besides lung, have also been linked to radon.[7] The health risk arises due to excess inhalation dose from various isotopes of radon and their progenies. Radon is a colourless, odourless and tasteless, radioactive ubiquitous, heaviest inert noble gas. It is naturally occurring on earth's crusts having 35 isotopes, but ^{222}Rn and ^{220}Rn

[1]Department of Physics, DAV College, Jalandhar, India
[2]Department of Applied Sciences, I.K.G. Punjab Technical University, Jalandhar, India
[3]Department of Applied Sciences, Amritsar College of Engineering & Technology, Amritsar, India
[4]Department of Physics, DAV College, Amritsar, India

Corresponding author:
Navjeet Sharma, Department of Physics, DAV College, Jalandhar, India.
Email: sharma_navjeet@yahoo.com

Department of Physical Sciences
I.K. Gujral Punjab Technical University
Main Campus

435 37

* UNKNOWN * | MPSJCA | JCA10.0.1465/W Unicode | ef-2016-01676y.3d (R3.6.i11:4432 | 2.0 alpha 39) 2015/07/15 14:30:00 | PROD-JCAVA | rq_7079245 | 9/19/2016 07:08:46 | 9 | JCA-DEFAULT

energy&fuels

Article

pubs.acs.org/EF

Experimental Study on Storage and Oxidation Stability of Bitter Apricot Kernel Oil Biodiesel

Virender Singh Gurau,[†] Mudit Shankar Agarwal,[†] Amit Sarin,[‡] and Sarbjot Singh Sandhu*[,†]

[†]Department of Mechanical Engineering, Dr. B. R. Ambedkar National Institute of Technology Jalandhar, Jalandhar, Punjab 144003, India

[‡]Department of Applied Sciences, Amritsar College of Engineering and Technology, Amritsar, Punjab 143001, India

ABSTRACT: Worldwide biodiesel is accepted as a substitute for mineral diesel for its almost similar physical and chemical properties. Because biodiesel is produced from vegetable oil, animal fat, or waste frying oil and is composed of a combination of saturated and unsaturated fatty acids, this makes it prone to oxidation with time. As a result of the oxidation, insoluble gums and deposits are formed, which adversely affect the characteristics of the biodiesel and result in corrosion of engine components, such as injectors, piston rings, piston liners, etc., during engine running. In this present study, storage and oxidation stability of biodiesel produced from bitter apricot kernel oil were investigated for 6 months under dark and sunlight storage conditions without being exposed to air. Five antioxidants in small quantity, viz., *tert*-butylhydroquinone, butylated hydroxytoluene, butylated hydroxyanisole, pyrogallol, and propyl gallate, one per sample, were used to enhance the induction period. The result shows that, by the dosage of antioxidants, biodiesel storage and oxidation stability can be maintained for 6 months in both storage conditions.

1. INTRODUCTION

Biodiesel can be produced from vegetable oil, animal fat, or waste frying oil by the transesterification reaction. Biodiesel is a fuel composed of mono-alkyl esters of long-chain fatty acids. These fatty acid chains are the combination of saturated and unsaturated fatty acids. The amount of unsaturated fatty acids present in the biodiesel defines its oxidation stability. The more unsaturated fatty acids in biodiesel, the more it is prone to oxidation. The most common unsaturated fatty acids present in biodiesel are oleic (C18:1), linoleic (C18:2), and linolenic (C18:3) acids. A previous study shows the relative oxidation rate for oleic, linoleic, and linolenic acids as 1:12:25.[1]

Although degradation of biodiesel as a result of oxidation instability is undesirable, it is advantageous from an environmental point of view because it makes biodiesel relatively more biodegradable compared to mineral diesel. Oxidation of biodiesel is an auto-oxidation reaction,[2] which involves three steps: initiation, propagation, and termination. The complete process is shown in Figure 1. As a result of the oxidation, insoluble gums and deposits are produced, which affect the properties and characteristics of the biodiesel and its engine application.

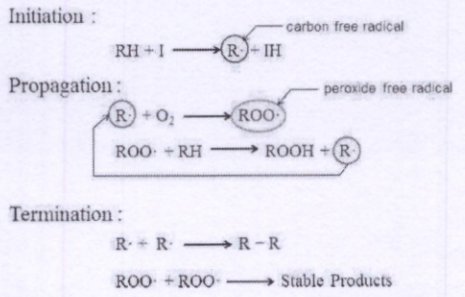

Figure 1. Auto-oxidation reaction.

As per ASTM D6751 and EN 14214 standards, the biodiesel must have a minimum of 3 and 6 h of oxidation stability, respectively, at 110 °C, and thus, it has become an important fuel quality parameter. During biodiesel production, some natural antioxidants become removed during water washing and the subsequent moisture removal process, and thus, biodiesel becomes more prone to oxidation. Although it is not possible to avoid the oxidation of biodiesel, it can be delayed using synthetic antioxidants.

Previous studies[3−14] found that the oxidation of biodiesel during storage results in an increase in the acid number, density, and kinematic viscosity, whereas the induction period decreases. Sarin et al.[3] carried out an oxidation stability study of *Jatropha* biodiesel using five antioxidants: α-tocopherol (α-T), butylated hydroxytoluene (BHT), *tert*-butylated phenol derivative (TBP), octylated butylated diphenyl amine (OBPA), and *tert*-butylhydroquinone (TBHQ). The research concluded that, to maintain the induction period of 6 h, the order of efficiency of antioxidants is TBHQ > BHT > TBP > OBPA > α-T. Kivevele et al.[5] studied the oxidation stability of *Croton megalocarpus* biodiesel using three antioxidants: pyrogallol (PY), propyl gallate (PG), and butylated hydroxyanisole (BHA). The effectiveness of antioxidants was found to be PY > PG > BHA. In another study by Jain et al.[6] on 6 months of storage stability of *Jatropha* biodiesel using PY antioxidants, it was found that the viscosity, peroxide value, and acid number of biodiesel increase with the storage time and 200 ppm of PY was sufficient to make the *Jatropha* biodiesel stable for 6 months. Shahabuddin et al.[8] carried out experiments on 3 months of storage stability of fuels, viz., *Jatropha* biodiesel and its blends, palm oil biodiesel and its blend, and coconut oil biodiesel, without using any antioxidants. The study concluded

Received: July 11, 2016
Revised: September 9, 2016

ACS Publications © XXXX American Chemical Society

DOI: 10.1021/acs.energyfuels.6b01676
Energy Fuels XXXX, XXX, XXX−XXX

Head
Department of Physical Sciences
I.K. Gujral Punjab Technical University
Main Campus

436

Optical Materials 51 (2016) 56–61

Contents lists available at ScienceDirect

Optical Materials

journal homepage: www.elsevier.com/locate/optmat

Effect of Sb addition on linear and non-linear optical properties of amorphous Ge–Se–Sn thin films

Navjeet Sharma [a], Surbhi Sharma [b,c,*], Amit Sarin [d], Rajesh Kumar [e]

[a] Department of Physics, DAV College, Jalandhar, India
[b] Department of Applied Sciences, C.T. Institute of Engineering, Management and Technology, Jalandhar, India
[c] Punjab Technical University, Kapurthala, India
[d] Department of Applied Sciences, Amritsar College of Engineering and Technology, Amritsar, India
[e] Department of Physics, DAV College, Amritsar, India

ARTICLE INFO

Article history:
Received 27 October 2015
Received in revised form 12 November 2015
Accepted 13 November 2015

Keywords:
Chalcogenide glasses
Optical constants

ABSTRACT

Optical characterization of amorphous thin films of $Ge_{20}Sn_{10}Se_{70-x}Sb_x$ ($x = 0, 3, 6, 9, 12, 15$) has been carried out. Thin films were deposited onto pre cleaned glass substrates using thermal evaporation technique. Transmission spectra of the films were recorded, for normal incidence, in range 400–2400 nm. Refractive index of the films was calculated using the envelope method by Swanepoel. Dispersion analysis has been carried out using single effective oscillator model. Other optical constants such as absorption coefficients, extinction coefficients have also been evaluated. Tauc plots were used to evaluate the optical band gap. The refractive index has been found to be increasing while the band gap decreases with increasing Sb concentration. The observed optical behavior of the films has been explained using chemical bond approach. Cohesive energy is found to be decreasing in the present work, which reflects that bond strength decreases with the increasing content of Sb. Non-linear optical parameters (i.e. n_2 and $\chi^{(3)}$) have been derived from linear optical parameters (i.e. n, k, Eg). Observed changes in linear and non-linear parameters have been reported in this study.

© 2015 Elsevier B.V. All rights reserved.

1. Introduction

Chalcogens (S, Se, Te) alloyed with elements of group 14 and 15 (i.e. Ge, In, As, Sb, etc.) of modern periodic table forms an important category of optical materials. Dynamic properties of chalcogenide glasses (C.Gs) viz. reversible phase transformation [1–4], high transparencies in middle and far IR region, low optical absorption, negligible susceptibility towards atmospheric moisture, etc. have furnished them great attention in optical and photonic technology as well. C.Gs have emerged as the important candidate for various applications viz. Optical Fibers, Holography, Switching, CO_2 Laser, etc. [5–7]. Study of optical properties is important not only because it suggests different phenomenon of light absorption by the amorphous system but also clarifies the dependence of optical properties and energy spectrum on the disorder structure of the system [8].

Study of optical properties is important because it not only suggests different processes of light absorption by the amorphous system but also reveals the dependence of optical properties and energy spectrum on the disorder structure of the system [8].

C.Gs have high atomic masses which generate low energy phonons within their amorphous network and thus grants them the wide optical transparency which extends into middle and far infrared region [9]. This property enables the optical applications of C. Gs in far infrared region. Large data has been reported on the glass formation, electrical conductivity and refractive index dependence on Ge content in Ge_xSe_{1-x} C.G thin films [10–12]. Ge–Se glass system is one of the most studied glass system which found to have good glass forming ability over wide area of compositions [13]. Additional impurity like Sn added to binary Ge–Se system introduces defects in the system. The presence of unshared electrons leads to the flexibility in the structure which in turn favors the glass forming ability. This increase in glass transition temperature further indicates the shift of absorption to higher wavelength [14]. Addition of Sb in C.G system reportedly enhances glass forming region and stability of the system and thus increases the glass transition temperature [15]. In multi-chalcogenide glasses, compositional disorders create localized states in the forbidden gap leading to the perturbation in refractive index [16].

Optical properties of the system can be altered by varying the composition of glass. Various properties of glass viz. band gap, conductivity, photo-resistivity, etc. are characterized by localized

* Corresponding author at: Punjab Technical University, Kapurthala, India.
E-mail address: physurbhi@gmail.com (S. Sharma).

http://dx.doi.org/10.1016/j.optmat.2015.11.021
0925-3467/© 2015 Elsevier B.V. All rights reserved.

Department of Physical Sciences
I.K. Gujral Punjab Technical University
Main Campus

437

PHYSICAL REVIEW C 97, 024610 (2018)

Fusion hindrance for the positive Q-value system $^{12}C + ^{30}Si$

G. Montagnoli,[1] A. M. Stefanini,[2] C. L. Jiang,[3] K. Hagino,[4,5] F. Galtarossa,[2,6] G. Colucci,[1] S. Bottoni,[3,*] C. Broggini,[1] A. Caciolli,[1] P. Čolović,[7] L. Corradi,[2] S. Courtin,[8] R. Depalo,[1] E. Fioretto,[2] G. Fruet,[8] A. Gal,[8] A. Goasduff,[1] M. Heine,[8] S. P. Hu,[9] M. Kaur,[10] T. Mijatović,[7] M. Mazzocco,[1] D. Montanari,[8] F. Scarlassara,[1] E. Strano,[1] S. Szilner,[7] and G. X. Zhang[11]

[1]*Dipartimento di Fisica e Astronomia, Università di Padova, INFN, Sez. di Padova, I-35131 Padova, Italy*

[2]*INFN, Laboratori Nazionali di Legnaro, I-35020 Legnaro (Padova), Italy*

[3]*Physics Division, Argonne National Laboratory, Argonne, Illinois 60439, USA*

[4]*Department of Physics, Tohoku University, Sendai 980-8578, Japan*

[5]*Research Center for Electron Photon Science, Tohoku University, 1-2-1 Mikamine, Sendai 982-0826, Japan*

[6]*Dipartimento di Fisica e Scienze della Terra, Università di Ferrara, I-44121 Ferrara, Italy*

[7]*Ru er Bošković Institute, HR-10002 Zagreb, Croatia*

[8]*IPHC, CNRS-IN2P3, Université de Strasbourg, F-67037 Strasbourg Cedex 2, France*

[9]*College of Physics and Energy, Shenzhen University, Shenzhen, 518060, China*

[10]*Department of Physical Sciences, I.K. Gujral Punjab Technical University, Kapurthala 144603, India*

[11]*School of Physics and Nuclear Energy Engineering, Beihang University, Beijing, 100191, China*

(Received 6 November 2017; published 12 February 2018)

Background: The fusion reaction $^{12}C + ^{30}Si$ is a link between heavier cases studied in recent years, and the light heavy-ion systems, e.g., $^{12}C + ^{12}C$, $^{16}O + ^{16}O$ that have a prominent role in the dynamics of stellar evolution. $^{12}C + ^{30}Si$ fusion itself is not a relevant process for astrophysics, but it is important to establish its behavior below the barrier, where couplings to low-lying collective modes and the hindrance phenomenon may determine the cross sections. The excitation function is presently completely unknown below the barrier for the $^{12}C + ^{30}Si$ reaction, thus no reliable extrapolation into the astrophysical regime for the C+C and O+O cases can be performed.
Purpose: Our aim was to carry out a complete measurement of the fusion excitation function of $^{12}C + ^{30}Si$ from well below to above the Coulomb barrier, so as to clear up the consequence of couplings to low-lying states of ^{30}Si, and whether the hindrance effect appears in this relatively light system which has a positive Q value for fusion. This would have consequences for the extrapolated behavior to even lighter systems.
Methods: The inverse kinematics was used by sending ^{30}Si beams delivered from the XTU Tandem accelerator of INFN-Laboratori Nazionali di Legnaro onto thin ^{12}C (50 $\mu g/cm^2$) targets enriched to 99.9% in mass 12. The fusion evaporation residues (ER) were detected at very forward angles, following beam separation by means of an electrostatic deflector. Angular distributions of ER were measured at $E_{beam} = 45$, 59, and 80 MeV, and they were angle integrated to derive total fusion cross sections.
Results: The fusion excitation function of $^{12}C + ^{30}Si$ was measured with high statistical accuracy, covering more than five orders of magnitude down to a lowest cross section $\simeq 3$ μb. The logarithmic slope and the S factor have been extracted and we have convincing phenomenological evidence of the hindrance effect. These results have been compared with the calculations performed within the model that considers a damping of the coupling strength well inside the Coulomb barrier.
Conclusions: The experimental data are consistent with the coupled-channels calculations. A better fit is obtained by using the Yukawa-plus-exponential potential and a damping of the coupling strengths inside the barrier. The degree of hindrance is much smaller than the one in heavier systems. Also a phenomenological estimate reproduces quite closely the hindrance threshold for $^{12}C + ^{30}Si$, so that an extrapolation to the C+C and O+O cases can be reliably performed.

DOI: 10.1103/PhysRevC.97.024610

I. INTRODUCTION

Recent measurements on fusion of medium-heavy systems [1] revealed that going to very low energies the intervening so-called "hindrance" effect shows up, as a noteworthy increase of the slope of the excitation function, not reproduced by standard coupled-channels (CC) calculations.

In the sudden approach, Misicu and Esbensen proposed [2,3] to describe this phenomenon using the M3Y interaction with an additional short-range term from the incompressibility of nuclear matter. The resulting shallow potential was very successful in reproducing the hindrance effect in several cases [4,5]. An adiabatic model was instead proposed by Ichikawa, Hagino, and Iwamoto [6] considering

*Present address: University of Milan and INFN-Milan, Italy.

 ©2018 American Physical Society

Head
Department of Physical Sciences
I.K. Gujral Punjab Technical University
Main Campus

438

PHYSICAL REVIEW C **98**, 064612 (2018)

Investigating the fusion enhancement for neutron-rich mid-mass nuclei using the dynamical cluster-decay model

Rupinder Kaur,[1,2] Maninder Kaur,[1] Varinderjit Singh,[1,*] Sarbjeet Kaur,[3] BirBikram Singh,[3] and B. S. Sandhu[2]

[1]*Department of Physical Sciences, I.K.G. Punjab Technical University, Kapurthala 144603, India*

[2]*Department of Physics, Punjabi University, Patiala 147002, India*

[3]*Department of Physics, Sri Guru Granth Sahib World University, Fatehgarh Sahib 140406, India*

(Received 8 September 2018; published 28 December 2018)

The mechanism involved in compound nucleus formation through heavy ion induced fusion reactions at near- and sub-barrier energies has been stimulating the interest of both experimentalists and theoreticians. The study of fusion reactions is important not only for the production of superheavy elements but also to unfold the mysteries involved in the evolution of neutron stars and nucleosynthesis of elements in astrophysical scenarios. The detection of gravitational waves originating from the merging of two black holes, and the possibility of observing similar events originating from black-hole–neutron-star mergers, highlighted the necessity of understanding the behavior of neutron-rich nuclear matter. One of the potential methods to understand the character of neutron-rich matter is through the study of fusion of an isotopic chain of reactions. Recently, the first experimental evidence of fusion enhancement at near-barrier energies for neutron-rich nuclei was reported for the light and mid-mass regime. To understand the dynamics involved in such reactions, the investigation of K-induced reactions has been performed using the quantum mechanical fragmentation based dynamical cluster-decay model (DCM). The experimental fusion cross sections of $^{39,47}\mathrm{K} + {}^{28}\mathrm{Si}$ are reproduced using DCM and, further, the fusion cross sections are predicted for other isotopes of K beam on ^{28}Si to investigate the fusion enhancement as a function of neutron number. It has been observed that fusion enhancement is significant at near-barrier energies for neutron-rich nuclei. The fusion enhancement observed is larger for odd neutron number nuclei as compared to adjacent neutron nuclei. This indicates the influence of unpaired neutrons on fusion cross sections. Also, the fusion cross sections predicted in the present work will act as input for planning more experimental measurements.

DOI: 10.1103/PhysRevC.98.064612

I. INTRODUCTION

Neutrons not only play a crucial role in the physics of nuclear reactors under terrestrial conditions, they also play a decisive role in astrophysical scenarios during nucleosynthesis, via neutron capture processes: namely the r and s processes (on different time scales) in neutron-rich environments. The valence neutrons in these neutron rich nuclei provide an opportunity to understand the channel coupling and transfer probability effects using a different formalisms, thus revealing the anticipated enhancement of fusion cross sections at near- and sub-barrier regimes [1,2]. A number of authors have investigated the sub-barrier fusion of neutron-rich nuclei using the coupled-channel model [3,4] and time-dependent Hartree-Fock theory [5,6].

Experimentally, with the availability of radioactive ion beams of nuclei away from β stability, it is now possible to investigate the fusion of neutron-rich beams, which consequently provides insight into the fusion mechanism. Understanding the fusion mechanism of neutron-rich nuclei is necessary to get a better estimate of neutron star composition, which in turn will help in the accurate prediction of x-ray superbursts and neutron-star–black-hole merger events. Also, the understanding of fusion of neutron-rich nuclei will be helpful for exploring the production mechanism of heavy elements in nature. So, the study of structural and dynamical aspects involved in the fusion reaction of neutron-rich nuclei is of paramount importance.

A few initial measurements in this direction suggested an enhancement of fusion probability as compared to the standard statistical model at near-barrier energies [7]. Various studies indicated the importance of interplay between nuclear structural and reaction dynamical aspects present in these many-body systems, which can be incorporated through spin and energy dependent potentials [8], sensitivity to coupling of fusion degree of freedom to other degrees of freedom [9], neck formation [3,10], static deformations [11], increased collectivity through increased coupling of weakly bound neutron-rich nuclei [12], etc. Several studies have also revealed the strong isotopic dependence of the fusion cross sections near the barrier [13–15]. The enhancement of fusion cross sections observed through these isotopic chains of nuclear reactions is being considered as one of the best methods to understand the character of neutron-rich matter.

*vickymangat3@gmail.com

Head
Department of Physical Sciences
I.K. Gujral Punjab Technical University
Main Campus

 ©2018 American Physical Society

439

PHYSICAL REVIEW C 97, 024610 (2018)

Fusion hindrance for the positive Q-value system $^{12}C + ^{30}Si$

G. Montagnoli,[1] A. M. Stefanini,[2] C. L. Jiang,[3] K. Hagino,[4,5] F. Galtarossa,[2,6] G. Colucci,[1] S. Bottoni,[3,*] C. Broggini,[1] A. Caciolli,[1] P. Čolović,[7] L. Corradi,[2] S. Courtin,[8] R. Depalo,[1] E. Fioretto,[2] G. Fruet,[8] A. Gal,[8] A. Goasduff,[1] M. Heine,[8] S. P. Hu,[9] M. Kaur,[10] T. Mijatović,[7] M. Mazzocco,[1] D. Montanari,[8] F. Scarlassara,[1] E. Strano,[1] S. Szilner,[7] and G. X. Zhang[11]

[1]*Dipartimento di Fisica e Astronomia, Università di Padova, INFN, Sez. di Padova, I-35131 Padova, Italy*

[2]*INFN, Laboratori Nazionali di Legnaro, I-35020 Legnaro (Padova), Italy*

[3]*Physics Division, Argonne National Laboratory, Argonne, Illinois 60439, USA*

[4]*Department of Physics, Tohoku University, Sendai 980-8578, Japan*

[5]*Research Center for Electron Photon Science, Tohoku University, 1-2-1 Mikamine, Sendai 982-0826, Japan*

[6]*Dipartimento di Fisica e Scienze della Terra, Università di Ferrara, I-44121 Ferrara, Italy*

[7]*Ru er Bošković Institute, HR-10002 Zagreb, Croatia*

[8]*IPHC, CNRS-IN2P3, Université de Strasbourg, F-67037 Strasbourg Cedex 2, France*

[9]*College of Physics and Energy, Shenzhen University, Shenzhen, 518060, China*

[10]*Department of Physical Sciences, I.K. Gujral Punjab Technical University, Kapurthala 144603, India*

[11]*School of Physics and Nuclear Energy Engineering, Beihang University, Beijing, 100191, China*

(Received 6 November 2017; published 12 February 2018)

Background: The fusion reaction $^{12}C + ^{30}Si$ is a link between heavier cases studied in recent years, and the light heavy-ion systems, e.g., $^{12}C + ^{12}C$, $^{16}O + ^{16}O$ that have a prominent role in the dynamics of stellar evolution. $^{12}C + ^{30}Si$ fusion itself is not a relevant process for astrophysics, but it is important to establish its behavior below the barrier, where couplings to low-lying collective modes and the hindrance phenomenon may determine the cross sections. The excitation function is presently completely unknown below the barrier for the $^{12}C + ^{30}Si$ reaction, thus no reliable extrapolation into the astrophysical regime for the C+C and O+O cases can be performed.

Purpose: Our aim was to carry out a complete measurement of the fusion excitation function of $^{12}C + ^{30}Si$ from well below to above the Coulomb barrier, so as to clear up the consequence of couplings to low-lying states of ^{30}Si, and whether the hindrance effect appears in this relatively light system which has a positive Q value for fusion. This would have consequences for the extrapolated behavior to even lighter systems.

Methods: The inverse kinematics was used by sending ^{30}Si beams delivered from the XTU Tandem accelerator of INFN-Laboratori Nazionali di Legnaro onto thin ^{12}C (50 $\mu g/cm^2$) targets enriched to 99.9% in mass 12. The fusion evaporation residues (ER) were detected at very forward angles, following beam separation by means of an electrostatic deflector. Angular distributions of ER were measured at $E_{beam} = 45$, 59, and 80 MeV, and they were angle integrated to derive total fusion cross sections.

Results: The fusion excitation function of $^{12}C + ^{30}Si$ was measured with high statistical accuracy, covering more than five orders of magnitude down to a lowest cross section $\simeq 3$ μb. The logarithmic slope and the S factor have been extracted and we have convincing phenomenological evidence of the hindrance effect. These results have been compared with the calculations performed within the model that considers a damping of the coupling strength well inside the Coulomb barrier.

Conclusions: The experimental data are consistent with the coupled-channels calculations. A better fit is obtained by using the Yukawa-plus-exponential potential and a damping of the coupling strengths inside the barrier. The degree of hindrance is much smaller than the one in heavier systems. Also a phenomenological estimate reproduces quite closely the hindrance threshold for $^{12}C + ^{30}Si$, so that an extrapolation to the C+C and O+O cases can be reliably performed.

DOI: 10.1103/PhysRevC.97.024610

I. INTRODUCTION

Recent measurements on fusion of medium-heavy systems [1] revealed that going to very low energies the intervening so-called "hindrance" effect shows up, as a noteworthy increase of the slope of the excitation function, not reproduced by standard coupled-channels (CC) calculations.

In the sudden approach, Misicu and Esbensen proposed [2,3] to describe this phenomenon using the M3Y interaction with an additional short-range term from the incompressibility of nuclear matter. The resulting shallow potential was very successful in reproducing the hindrance effect in several cases [4,5]. An adiabatic model was instead proposed by Ichikawa, Hagino, and Iwamoto [6] considering

*Present address: University of Milan and INFN-Milan, Italy.

 ©2018 American Physical Society

Head
Department of Physical Sciences
I.K. Gujral Punjab Technical University
Main Campus

440

PHYSICAL REVIEW C **101**, 044605 (2020)

Dynamical aspects of ^{48}Ti + ^{58}Fe, ^{58}Ni → ^{106}Cd*, ^{106}Sn* reactions at energies near the Coulomb barrier

Rupinder Kaur,[1,2,3,*] Maninder Kaur,[2] Varinderjit Singh,[2] Mandeep Kaur,[3] BirBikram Singh,[3,†] and B. S. Sandhu[1]

[1]*Department of Physics, Punjabi University, Patiala-147002, India*

[2]*Department of Physical Sciences, I.K.G. Punjab Technical University, Kapurthala-144603, India*

[3]*Department of Physics, Sri Guru Granth Sahib World University, Fatehgarh Sahib-140406, India*

(Received 12 June 2019; revised manuscript received 10 January 2020; accepted 9 March 2020; published 14 April 2020)

The study of the heavy-ion reactions at the near- and sub-barrier regimes gives immense information about the nuclear structure and the involved reaction dynamics. It has been observed that a slight difference in the nuclear structure may lead to a significant change in the sub-barrier fusion excitation functions. The studies of different trends of excitation functions below the Coulomb barrier region due to dissimilar structures of the nuclei, which are involved in the reaction, are available in literature. To understand the role of different structures and dynamics involved in such reactions, an investigation of ^{48}Ti-induced reactions on ^{58}Fe and ^{58}Ni forming ^{106}Cd* and ^{106}Sn* compound nuclei (CN), respectively, has been made at similar $E_{\text{c.m.}}/V_b$ values within the framework of the dynamical cluster decay model (DCM). The difference in the structure between the nuclei is quite notable with ^{58}Ni and ^{106}Sn* having a proton shell closure ($Z = 28$ and 50, respectively). Within the DCM, the experimental fusion evaporation cross sections are reproduced using deformed configurations effects included up to quadruple deformations (β_{2i}) for two nuclei having optimum orientations $\theta^{\text{opt.}}$. The fusion evaporation data at near- and sub-barriers has been explained through the calculated enhanced ΣP_0 values of the decaying channels in the case of ^{106}Cd* in comparison to ^{106}Sn*. Moreover, it is observed that the quantum tunneling of the fragments is less hindered in the case of ^{106}Cd* as compared to ^{106}Sn* at the lower values of $E_{\text{c.m.}}/V_b$, i.e., having less barrier modification (ΔV_B) in the case of the former. The role of magicity has been further explored with the plotted values of the ratio of fusion cross sections (σ_{fus}) of CN ^{106}Sn* and ^{112}Xe* (formed in the reaction with both the projectile ^{58}Ni and target ^{54}Fe having proton and neutron magicity, respectively) with respect to ^{106}Cd*, which are highly suppressed in the case of the latter in comparison to the former, particularly, below the Coulomb barrier.

DOI: 10.1103/PhysRevC.101.044605

I. INTRODUCTION

In the past few decades, a thorough study of sub-barrier heavy-ion interactions have uncovered the various unexpected characteristics involved in the reaction dynamics. The most notable outcome of these studies, observed experimentally, is the hinderance phenomenon at deep sub-barrier energies in some systems in comparison to others. This suggests existence of an experimentally determined threshold limit E_s in sub-barrier energies which varies from one system to another. The investigation of the physical cause for such phenomena will help to understand the involved reaction dynamics. Thus, to ascertain the reaction mechanisms involved in observed phenomena requires a consistent study of various systems. The apparent dynamical picture of the sub-barrier fusion has been acknowledged by the considerable experimental and theoretical efforts made by various authors in this direction [1]. Several experiments have provided a clear example of fusion hindrance at the deep sub-barrier region. One of such studies in which the effect on the fusion excitation function due to the associated nuclear structure of the interacting nuclei, has been investigated by Jiang *et al.* in ^{64}Ni + ^{64}Ni fusion reaction [2]. The author has explained the associated phenomenon of hinderance by considering stiff to open-shell nuclei in the entrance channel in the sub-barrier regime in terms of the S factor where the steep falloff in cross sections translates into a maximum of the S factor. Fusion hindrance in the ^{58}Ni + ^{54}Fe reaction at lower energies is also investigated by Stefanini *et al.* [3]. They observed that, at lower energies, fusion cross sections drop faster than conventional Woods-Saxon potential calculations with a steep slope. Recently, Stefanini *et al.* [4] have also shown that distinct low-energy nuclear structures of the involved nuclei leads to different trends in the fusion excitations functions for the ^{48}Ti + ^{58}Fe and ^{58}Ni + ^{54}Fe reactions at the sub-barrier regime. Large fusion cross sections has been observed in the measured energy range in ^{48}Ti + ^{58}Fe as compared to ^{58}Ni + ^{54}Fe (with closed-shell protons and neutrons in the entrance channel). The cross-section trends are explained in the ^{48}Ti + ^{58}Fe reaction through the involved strong quadrupole modes of both ^{48}Ti and ^{58}Fe and the two-neutron transfer channel.

*roopisaini87@gmail.com

†birbikramsingh@sggswu.edu.in

Department of Physical Sciences I.K. Gujral Punjab Technical University Main Campus

 ©2020 American Physical Society

IOP Publishing Journal of Physics G: Nuclear and Particle Physics

J. Phys. G: Nucl. Part. Phys. **48** (2021) 075104 (17pp) https://doi.org/10.1088/1361-6471/abe8cd

Measurement of fission excitation function for $^{19}F + ^{194,196,198}Pt$ reactions

Varinderjit Singh[1,2,*], B R Behera[1], Maninder Kaur[1,2], A Jhingan[3], Rupinder Kaur[2], P Sugathan[3], Davinder Siwal[1,4], S Goyal[4], K P Singh[1], Santanu Pal[5], A Saxena[6] and S Kailas[7]

[1] Department of Physics, Panjab University, Chandigarh 160014, India
[2] Department of Physical Sciences, IKG Punjab Technical University, Kapurthala 144603, India
[3] Inter University Accelerator Centre, New Delhi 110067, India
[4] Department of Physics and Astrophysics, University of Delhi, Delhi 110007, India
[5] CS-6/1, Golf Green, Kolkata 700095, India
[6] Nuclear Physics Division, Bhabha Atomic Research Centre, Mumbai 400085, India
[7] UM-DAE Centre for Excellence in Basic Sciences, University of Mumbai, Mumbai 400098, India

E-mail: vickymangat3@gmail.com

Received 3 December 2020, revised 18 February 2021
Accepted for publication 22 February 2021
Published 21 May 2021

Abstract

Experimental fission cross-sections are reported for the $^{19}F + ^{194,196,198}Pt$ reactions populating an isotopic chain of compound nuclei comprising both closed and non-closed shell nuclei. The fission cross-sections are obtained at near and above Coulomb barrier energies by measuring fission fragment angular distributions. The present work aims to estimate nuclear dissipation and find its isotopic and shell closure dependence from statistical model (SM) analysis of experimental data. Pre-scission neutron multiplicity data for the same systems is also included in the SM analysis. An updated version of SM is used in the present analysis, which includes shell corrections in level density and fission barrier as well as the effect of collective enhancement of level density and orientation effect of the compound nucleus along the symmetry axis. An isotopic dependence of the dissipation strength fitting the fission excitation functions is observed. The pre-scission neutron multiplicity, however, is underestimated by the SM.

Keywords: nuclear reactions, fusion–fission reaction, fission fragment angular distribution, statistical model of nuclear reactions

(Some figures may appear in colour only in the online journal)

*Author to whom any correspondence should be addressed.

0954-3899/21/075104+17$33.00 © 2021 IOP Publishing Ltd Printed in the UK

Head
Department of Physical Sciences
I.K. Gujral Punjab Technical University
Main Campus

442

Nuclear Instruments and Methods in Physics Research A 837 (2016) 28–33

Contents lists available at ScienceDirect

Nuclear Instruments and Methods in Physics Research A

journal homepage: www.elsevier.com/locate/nima

High-rate axial-field ionization chamber for particle identification of radioactive beams

J. Vadas [a,b], Varinderjit Singh [a,b], G. Visser [b], A. Alexander [a], S. Hudan [a,b], J. Huston [a,b], B.B. Wiggins [a,b], A. Chbihi [c], M. Famiano [d], M.M. Bischak [d], R.T. deSouza [a,b,*]

[a] Department of Chemistry, Indiana University, 800 E. Kirkwood Ave., Bloomington, IN 47405, USA
[b] Center for Exploration of Energy and Matter, Indiana University, 2401 Milo B. Sampson Lane, Bloomington, IN 47408, USA
[c] GANIL, 1 Blvd. Henri Becquerel, Caen 14000, France
[d] Department of Physics, Western Michigan University, Kalamazoo, MI 49008, USA

ARTICLE INFO

Article history:
Received 8 August 2016
Received in revised form
18 August 2016
Accepted 27 August 2016
Available online 29 August 2016

Keywords:
Ionization chamber
Particle identification
Radioactive beam

ABSTRACT

The design, construction and performance characteristics of a simple axial-field ionization chamber suitable for identifying ions in a radioactive beam are presented. Optimized for use with low-energy radioactive beams (< 5 MeV/A) the detector presents only three 0.5 μm/cm^2 foils to the beam in addition to the detector gas. A fast charge sensitive amplifier (CSA) integrated into the detector design is also described. Coupling this fast CSA to the axial field ionization chamber produces an output pulse with a risetime of 60–70 ns and a fall time of 100 ns, making the detector capable of sustaining a relatively high rate and providing a time resolution of 6–8 ns. Tests with an α source establish the detector energy resolution as ~8% for an energy deposit of ~3.5 MeV. The energy resolution with beams of 2.5 and 4.0 MeV/A ^{39}K ions and the dependence of the energy resolution on beam intensity is measured. At an instantaneous rate of 3×10^5 ions/s the energy resolution has degraded to 14% with a pileup of 12%. The good energy resolution of this detector at rates up to 3×10^5 ions/s makes it an effective tool in the characterization of low-energy radioactive beams.

© 2016 Elsevier B.V. All rights reserved.

1. Introduction

The development of radioactive isotope beams (RIBs) has enabled the investigation of nuclei away from β-stability [1–4], which is crucial in understanding nucleosynthesis in exotic astrophysical environments [3], as well as the structure of exotic nuclei [3,4]. RIBs can be produced by a variety of techniques including projectile fragmentation [5], ISOL [6], and photofission [7]. As the primary nuclear reaction produces a distribution of product nuclei, to provide a useful secondary radioactive beam, it is necessary to select the nuclide of interest from this distribution. This separation is typically accomplished through electromagnetic means [8]. Often, however, this separation does not produce a pure beam, and other reaction products with similar mass-to-charge ratios contaminate the beam. An effective way to address this challenge is to identify each ion in the beam on a particle-by-particle basis. A commonly used approach to accomplish this is through measurement of the energy loss (ΔE) and time-of-flight (TOF) of each ion [9].

The ΔE information is often obtained from gas ionization chambers [10] used in transmission mode. The uniform thickness achieveable with these detectors, as well as their robustness against radiation damage are key factors in their utility. A common geometry of an ion chamber utilizes an electric field transverse to the incident ion direction [11], with a Frisch grid used to remove the dependence of the pulse amplitude on position. In this geometry of ion chambers, however, the drift time of the electrons in the direction transverse to the beam direction typically limits the rate to ~10^4 ions/s. To overcome this limitation of a slow response time, an axial field design can be employed. Axial field ionization chambers have been successfully employed as ΔE detectors for heavy-ions since the 1980s [12,13]. Recently, the high rate capability of this design has been exploited at both high [14] and low energies [15] by using multiple tilted electrodes in the beam path to identify reaction products in a radioactive beam. When the incident energy is sufficiently high (~100 MeV/A) thin metallized foils have been utilized for the electrodes. In contrast, at low incident energies (~5 MeV/A) the electrodes consist of wire harps. Both designs involve the insertion of multiple electrode planes (15–24) into the beam path, a source of considerable scattering and energy loss for the incident ion. In the subsequent sections,

* Corresponding author at: Department of Chemistry, Indiana University, 800 E. Kirkwood Ave., Bloomington, IN 47405, USA
E-mail address: desouza@indiana.edu (R.T. deSouza).

http://dx.doi.org/10.1016/j.nima.2016.08.056
0168-9002/© 2016 Elsevier B.V. All rights reserved.

Head
Department of Physical Sciences
I.K. Gujral Punjab Technical University
Main Campus

443

Physics Letters B 765 (2017) 99–103

Contents lists available at ScienceDirect

Physics Letters B

www.elsevier.com/locate/physletb

Fusion enhancement at near and sub-barrier energies in $^{19}O + ^{12}C$

Varinderjit Singh [a], J. Vadas [a], T.K. Steinbach [a], B.B. Wiggins [a], S. Hudan [a], R.T. deSouza [a,*], Zidu Lin [b], C.J. Horowitz [b], L.T. Baby [c], S.A. Kuvin [c], Vandana Tripathi [c], I. Wiedenhöver [c], A.S. Umar [d]

[a] Department of Chemistry and Center for Exploration of Energy and Matter, Indiana University, 2401 Milo B. Sampson Lane, Bloomington, IN 47408, USA
[b] Department of Physics and Center for Exploration of Energy and Matter, Indiana University, 2401 Milo B. Sampson Lane, Bloomington, IN 47408, USA
[c] Department of Physics, Florida State University, Tallahassee, FL 32306, USA
[d] Department of Physics and Astronomy, Vanderbilt University, Nashville, TN 37235, USA

ARTICLE INFO

Article history:
Received 16 September 2016
Received in revised form 28 October 2016
Accepted 7 December 2016
Available online 12 December 2016
Editor: D.F. Geesaman

Keywords:
Near-barrier fusion
Neutron-rich fusion
RIB fusion
Fusion enhancement

ABSTRACT

Measuring the fusion excitation function for an isotopic chain of projectile nuclei provides a stringent test of a microscopic description of fusion. We report the first measurement of the fusion excitation function at near-barrier energies for the $^{19}O + ^{12}C$ system. The measured excitation function is compared with the fusion excitation function of $^{18}O + ^{12}C$. A significant enhancement in the fusion probability of ^{19}O ions with a ^{12}C target as compared to ^{18}O ions is observed. The experimental cross-sections observed at near-barrier energies are compared with a state-of-the-art microscopic model.

© 2016 The Authors. Published by Elsevier B.V. This is an open access article under the CC BY license (http://creativecommons.org/licenses/by/4.0/). Funded by SCOAP[3].

1. Introduction

While the fusion of both light and heavy β-stable nuclei has been studied for several decades, only recently has the investigation of fusion of neutron-rich nuclei become feasible due to radioactive beam facilities [1–5]. In particular, examination of the fusion excitation function for an isotopic chain of neutron-rich nuclei represents an unique opportunity. Since the charge distribution of the neutron-rich projectile nuclei is essentially unaffected by the additional neutrons, the repulsive Coulomb potential is largely unchanged. Consequently, the comparison of the fusion excitation functions for the different projectiles provides access to the change in the attractive nuclear potential with an increasing number of neutrons. As the initial step in fusion at near-barrier energies involves overlap of the low density tails of the nuclear matter distribution, these reactions provide a sensitive probe of the composition and extent of the nuclear surface. An accurate microscopic description of the fusion of neutron-rich nuclei is thus relevant to the asymmetry term in the nuclear equation-of-state and in particular its density dependence [6].

Despite the opportunity presented to learn about structure and dynamics of low-density nuclear matter by examining the fusion of light nuclei, relatively few isotopic chains have been investigated, as radioactive beams are necessary. An initial measurement of fusion induced with a neutron-rich oxygen nucleus, ^{20}O, on a ^{12}C target suggested an enhancement of the fusion probability as compared to a standard fusion–evaporation model [7]. However, technical difficulties in the experiment prevented extraction of the total fusion cross-section. Recently, the fusion of $^{10,14,15}C + ^{12}C$ has been investigated using a novel active target approach [8]. At the above barrier energies studied, no significant fusion enhancement was observed relative to a simple barrier penetrability model. However, close examination of the $^{15}C + ^{12}C$ data presented reveals that at lowest energies measured, the data slightly exceed the model predictions. It can be argued on general grounds that fusion enhancement is best studied at near and below barrier energies. At low incident energies, the importance of central (low l-wave) collisions, which emphasize the attractive nuclear interaction, is enhanced. In addition, low relative energy allows the changing internuclear potential to effectively couple with collective excitations in the two nuclei, resulting in a fusion enhancement. These expectations are supported by the observation of an enhancement at sub-barrier energies for the mass asymmetric system $^{15}C + ^{232}Th$ [9].

* Corresponding author.
E-mail address: deSouza@indiana.edu (R.T. deSouza).

http://dx.doi.org/10.1016/j.physletb.2016.12.017
0370-2693/© 2016 The Authors. Published by Elsevier B.V. This is an open access article under the CC BY license (http://creativecommons.org/licenses/by/4.0/). Funded by SCOAP[3].

Department of Physical Sciences
I.K. Gujral Punjab Technical University
Main Campus

444

PHYSICAL REVIEW C **96**, 045804 (2017)

Experimental measurement of $^{12}C + ^{16}O$ fusion at stellar energies

X. Fang,[1,2] W. P. Tan,[1,*] M. Beard,[1] R. J. deBoer,[1] G. Gilardy,[1] H. Jung,[1] Q. Liu,[1] S. Lyons,[1] D. Robertson,[1] K. Setoodehnia,[1] C. Seymour,[1] E. Stech,[1] B. Vande Kolk,[1] M. Wiescher,[1] R. T. deSouza,[3] S. Hudan,[3] V. Singh,[3] X. D. Tang,[4] and E. Uberseder[5]

[1]*Institute for Structure and Nuclear Astrophysics and Joint Institute for Nuclear Astrophysics, University of Notre Dame, Notre Dame, Indiana 46556, USA*

[2]*Sino-French Institute of Nuclear Engineering and Technology, Sun Yat-Sen University, Zhuhai 519082, People's Republic of China*

[3]*Department of Chemistry and Center for Exploration of Energy and Matter, Indiana University, Bloomington, Indiana 47405, USA*

[4]*Institute of Modern Physics, Chinese Academy of Science, Lanzhou, Gansu 730000, People's Republic of China*

[5]*Cyclotron Institute, Texas A&M University, College Station, Texas 77843, USA*

(Received 9 September 2016; revised manuscript received 3 April 2017; published 9 October 2017)

The total cross section of the $^{12}C + ^{16}O$ fusion reaction has been measured at low energies to investigate the role of this reaction during late stellar evolution burning phases. A high-intensity oxygen beam, produced by the 5 MV pelletron accelerator at the University of Notre Dame, impinged on a thick, ultrapure graphite target. Protons and γ rays were simultaneously measured in the center-of-mass energy range from 3.64 to 5.01 MeV for singles and from 3.73 to 4.84 MeV for coincidence events, using silicon and Ge detectors. Statistical model calculations were employed to interpret the experimental results. The emergence of a new resonance-like broad structure and a decreasing trend in the S-factor data towards lower energies (opposite to previous data) are found for the $^{12}C + ^{16}O$ fusion reaction. Based on these results the uncertainty range of the reaction rate within the temperature range of late stellar burning environments is discussed.

DOI: 10.1103/PhysRevC.96.045804

I. INTRODUCTION

The fusion of light nuclei at sub-barrier energies plays an important role in the evolution of massive stars, as well as in the ignition of type Ia supernova [1,2] and the ignition of explosive burning processes in the atmospheres of accreting neutron stars [3,4]. The cross sections of fusion reactions are governed by the penetrability of the nuclei through the Coulomb and orbital angular momentum barriers, and therefore drop off exponentially with decreasing energy. This translates into extremely low values of the cross section near and within the energy range of astrophysical interest, i.e., the Gamow window. The direct experimental study of fusion reactions at stellar energies is therefore extremely difficult.

Carbon burning and oxygen burning in massive stars ($M \geqslant 8M_{\odot}$) [1] are important burning phases in late stellar evolution following helium burning as well as in cataclysmic burning phases of type Ia supernovae. In both cases the critical reactions are the $^{12}C + ^{12}C$, $^{12}C + ^{16}O$, and $^{16}O + ^{16}O$ fusion processes. Extensive efforts, both experimentally and theoretically, have been invested in the determination of the reaction rates for all associated reaction channels [1,2]. Despite these efforts, large uncertainties remain in the reaction rates due to the extrapolation of the data into the Gamow range [5]. The predicted rates depend sensitively on adopted model parameters, hindrance effects, and the possibility of cluster or molecular resonances at relevant energies [2,6,7].

Extending and improving the quality of experimental data towards lower energies is therefore crucial for reducing the uncertainties—in particular, the uncertainty associated with extrapolating the data towards lower energies—and providing more reliable reaction rates for the study of late stellar evolution. The $^{12}C + ^{16}O$ reaction plays a particularly important role in both the carbon and oxygen burning phases of stars [8,9]. Core and shell carbon burning is expected to be dominated by the $^{12}C + ^{12}C$ fusion reaction, yet near the end of the carbon burning phase the abundance of ^{16}O in the ashes of stellar helium burning is substantially higher than that of ^{12}C, due to the $^{12}C(\alpha,\gamma)^{16}O$ reaction [10,11]. With a high abundance of ^{16}O and a competitive reaction rate, the $^{12}C + ^{16}O$ reaction could play an important role in shell carbon burning nucleosynthesis. A similar situation exists in oxygen burning, which is dominated by the $^{16}O + ^{16}O$ fusion. Temperature and density increase towards the final stage of this burning phase will enable the photodissociation of ^{16}O to occur, which results in the release of free ^{12}C into the hot burning environment. The produced ^{12}C will be consumed either by reacting with itself or with ^{16}O, affecting the transition to subsequent stellar burning, when intershell mixing processes transfers carbon into the oxygen burning shell of a pre-supernova star [12]. Type Ia supernovae (SN) are interpreted as the consequence of explosive carbon burning ignited near the core of white dwarf stars. The $^{12}C + ^{12}C$ fusion process is supposed to be the dominant energy source for pre-ignition processes such as carbon simmering and the ignition itself; however, the $^{12}C + ^{16}O$ reaction may also play a significant role depending on the associated fusion rates and the environmental conditions such as ^{16}O abundance, temperature, and density [2,13]. Recent studies showed indeed that the $^{12}C + ^{16}O$ rate is expected to have an unusually large effect on the calcium and sulfur yields in type Ia SN; e.g., the higher $^{12}C + ^{16}O$ rate suppresses the alpha-particle abundance, which in turn decreases the Ca/S ratio [13].

The study of the total low energy fusion cross section of the $^{12}C + ^{16}O$ reaction is therefore of similar importance as the measurements of the competing $^{12}C + ^{12}C$ and $^{16}O + ^{16}O$

*wtan@nd.edu

 ©2017 American Physical Society

Head
Department of Physical Sciences
I.K. Gujral Punjab Technical University
Main Campus

445
47 474

Nuclear Inst. and Methods in Physics Research, A 866 (2017) 202–206

Contents lists available at ScienceDirect

Nuclear Inst. and Methods in Physics Research, A

journal homepage: www.elsevier.com/locate/nima

Development of a compact $E \times B$ microchannel plate detector for beam imaging

B.B. Wiggins, Varinderjit Singh, J. Vadas, J. Huston, T.K. Steinbach, S. Hudan, R.T. deSouza *

Department of Chemistry and Center for Exploration of Energy and Matter, Indiana University, 2401 N. Milo B. Sampson Ln, Bloomington, IN 47408, USA

ARTICLE INFO

Keywords:
Microchannel plate detector
Beam imaging
Tracking detector
Position-sensitive microchannel plate detector

ABSTRACT

A beam imaging detector was developed by coupling a multi-strip anode with delay line readout to an $E \times B$ microchannel plate (MCP) detector. This detector is capable of measuring the incident position of the beam particles in one-dimension. To assess the spatial resolution, the detector was illuminated by an α-source with an intervening mask that consists of a series of precisely-machined slits. The measured spatial resolution was 520 μm FWHM, which was improved to 413 μm FWHM by performing an FFT of the signals, rejecting spurious signals on the delay line, and requiring a minimum signal amplitude. This measured spatial resolution of 413 μm FWHM corresponds to an intrinsic resolution of 334 μm FWHM when the effect of the finite slit width is de-convoluted. To understand the measured resolution, the performance of the detector is simulated with the ion-trajectory code SIMION.

© 2017 Published by Elsevier B.V.

1. Introduction

A new generation of radioactive beam facilities provide unique opportunities to investigate nuclei far from β-stability. However, the beam intensity of the most N/Z exotic nuclei is typically less than 1000 ions/s posing significant challenges in imaging these beams. In the case of low energy beams, it is particularly important that the imaging detector introduce the least amount of material into the beam path in order to minimally distort the beam. In addition, as most accelerator facilities are pulsed it is beneficial if the imaging detector has good timing characteristics. Due to their high gain, fast temporal response, sensitivity to a single electron, and compact size, microchannel plates (MCPs) are often used as an electron amplifier for these imaging detectors [1].

There are several methods for providing position sensitivity with an MCP detector including: multi-strip anode [2], helical delay line [3,4], cross-strip anode [5], induced signal [6,7], resistive anode [8–10], and Timepix CMOS readout [11]. To realize a beam imaging detector requires transport of electrons produced at a secondary-emission foil onto the surface of the position sensitive MCP detector situated away from the beam axis. In one approach, a clever magnetic field arrangement provided transport of the electrons on helical trajectories onto the surface of a MCP detector [12–14]. This technique resulted in a spatial resolution of 588 μm FWHM [13]. The most serious limitation of this approach is the large space occupied by this detector making its use prohibitive in many experiments.

A beam timing detector which is compact and introduces a minimal amount of material into the beam path is an $E \times B$ detector [15–18]. Such a detector has been used to measure the time-of-flight of beam particles and reaction products in nuclear reaction studies [19–21]. To make the MCP in an $E \times B$ detector position-sensitive we employed a multi-strip anode with delay line readout, which is a particularly appealing because of its simplicity and low cost. Moreover, due to the fast time response of the detector it is capable of resolving two particles that arrive simultaneously but are spatially separated. Two principal factors influence one's ability to accurately image the beam: the impact of electron transport from the electron-emission foil to the MCP and the inherent spatial resolution of the position-sensitive element. In this article, we describe the design, development, and performance of an $E \times B$ position-sensitive detector suitable for imaging low-intensity radioactive beams. We explore the impact of the electron transport for this detector geometry on the measured resolution using the ion trajectory code SIMION [22].

2. Experimental setup

Presented in Fig. 1(a) is a schematic drawing of the experimental setup used to determine the spatial resolution of the position-sensitive

* Corresponding author.
E-mail address: desouza@indiana.edu (R.T. deSouza).

http://dx.doi.org/10.1016/j.nima.2017.06.006
Received 21 March 2017; Received in revised form 17 May 2017; Accepted 4 June 2017
Available online 17 June 2017
0168-9002/© 2017 Published by Elsevier B.V.

Head
Department of Physical Sciences
I.K. Gujral Punjab Technical University
Main Campus

446

PHYSICAL REVIEW C **96**, 054605 (2017)

Fission time scale from pre-scission neutron and α multiplicities in the $^{16}O + ^{194}Pt$ reaction

K. Kapoor, S. Verma, P. Sharma, R. Mahajan, N. Kaur, G. Kaur, B. R. Behera, K. P. Singh, and A. Kumar*
Department of Physics, Panjab University, Chandigarh 160014, India

H. Singh
Department of Physics, Kurukshetra University, Kurukshetra-136119, India

R. Dubey, N. Saneesh, A. Jhingan, and P. Sugathan
Inter University Accelerator Centre, New Delhi-110067, India

G. Mohanto, B. K. Nayak, and A. Saxena
Nuclear Physics Division, Bhabha Atomic Research Centre, Mumbai-400085, India

H. P. Sharma
Department of Physics, Banaras Hindu University, Varanasi-221005, India

S. K. Chamoli
Department of Physics and Astrophysics, University of Delhi, Delhi-110007, India

I. Mukul
Department of Particle Physics and Astrophysics, Weizmann Institute of Science, Rehovot-76100, Israel

V. Singh
Department of Physics, Punjab Technical University, Jalandhar-144603, India
(Received 29 April 2017; revised manuscript received 11 October 2017; published 20 November 2017)

Pre- and post-scission α-particle multiplicities have been measured for the reaction $^{16}O + ^{194}Pt$ at 98.4 MeV forming ^{210}Rn compound nucleus. α particles were measured at various angles in coincidence with the fission fragments. Moving source technique was used to extract the pre- and post-scission contributions to the particle multiplicity. Study of the fission mechanism using the different probes are helpful in understanding the detailed reaction dynamics. The neutron multiplicities for this reaction have been reported earlier. The multiplicities of neutrons and α particles were reproduced using standard statistical model code JOANNE2 by varying the transient (τ_{tr}) and saddle to scission (τ_{ssc}) times. This code includes deformation dependent-particle transmission coefficients, binding energies and level densities. Fission time scales of the order of 50–65 $\times 10^{-21}$ s are required to reproduce the neutron and α-particle multiplicities.

DOI: 10.1103/PhysRevC.96.054605

I. INTRODUCTION

The study of fusion-fission dynamics is one of the interesting areas of heavy-ion-induced nuclear reactions. Depending upon the excitation energy, temperature, and various other factors, the compound nucleus may tend towards the fission process. Fusion-fission dynamics of the excited nucleus can be studied by characterizing the emitted particles, such as α, p, ν, and γ during the course of deexcitation [1,2]. Fission time scale measurements are carried out by measuring the multiplicities of neutrons [3,4], charged particles [2,5,6], and giant dipole resonance (GDR) [7] emitted during fusion-fission. Fission time is divided into two major parts, the transient time (τ_{tr}) and the saddle to scission time (τ_{ssc}). The study of fission time scale gives insight into fission dynamics [8]. It has been reported earlier that the fission process slows down to an order (10^{-20}–10^{-19} s) due to nuclear viscosity [9].

Various theories have been formulated to elucidate the nature and magnitude of nuclear viscosity [10]. The standard statistical model was found to be insufficient to reproduce the measured particle multiplicities and the fission lifetimes [11]. Based on this observation, Kramer modified the Bohr-Wheeler's standard statistical model pointing toward the longer fission lifetime due to which higher particle emission is expected [12]. Measured excessive particle emission indicates the hindrance in the fission process. To discern the fission process, emission of the particles is divided into two major components. Particles emitted from the compound nucleus are called pre-scission particles whereas the particles emitted from the fragments are called post-scission particles [5]. The contribution of the pre- and post-scission particles in the measured spectra can be extracted using the moving source analysis. Investigation of the emitted particles provides paramount facts on the dynamical and statistical aspects of

*Corresponding author: ashok@pu.ac.in

 ©2017 American Physical Society

Head
Department of Physical Sciences
I.K. Gujral Punjab Technical University
Main Campus

Nuclear Inst. and Methods in Physics Research, A 903 (2018) 326–334

Contents lists available at ScienceDirect

Nuclear Inst. and Methods in Physics Research, A

journal homepage: www.elsevier.com/locate/nima

HYTAR: A HYbrid Telescope ARray detection system for heavy ion nuclear reactions around Coulomb barrier

Akhil Jhingan [a,*], Gurpreet Kaur [b], N. Saneesh [a], R. Ahuja [a], Tathagata Banerjee [a], Rakesh Dubey [a], Varinderjit Singh [c], Ruchi Mahajan [b], Meenu Thakur [b], M. Kumar [a], Abhishek Yadav [a], B.R. Behera [b], P. Sugathan [a]

[a] Inter University Accelerator Centre, P.O. Box 10502, New Delhi 110067, India
[b] Department of Physics, Panjab University, Chandigarh 160014, India
[c] Department of Physical Sciences, IKGPTU, Kapurthala 144603, India

ARTICLE INFO

Keywords:
ΔE-E technique
Ionization chamber
Silicon detector
Charge sensitive pre-amplifier

ABSTRACT

Characteristics and performance of a HYbrid Telescope ARray (HYTAR) detector system for heavy ions are presented. The system has been developed for the study of reaction mechanisms in nuclear physics experiments around the Coulomb barrier. HYTAR apparatus is an array of hybrid telescopes, each unit comprising of a gas ionization chamber followed by a silicon detector. Gas ionization chamber, operated in axial field mode, measures the differential energy loss (ΔE), while the residual energies are measured by silicon detector. Particle identification is realized by implementing ΔE-E technique. Use of gas ionization chamber as ΔE detector allows identification of reaction channels down to low energy thresholds ~ 0.1 MeV/A in $A \sim 100$ region. The detector system has been developed to investigate the fusion and fusion–fission dynamics by performing quasi-elastic scattering and fission angular distribution experiments. Processing of the detector signals is realized with compact and simple high density front-end electronics, which consists of custom developed low noise charge sensitive preamplifiers (operated inside vacuum) and differential driver NIM modules, followed by commercially available spectroscopy amplifiers, logic modules, analog to digital converters etc. Design features of the HYTAR and measurements performed with it are described in this article.

1. Introduction

The nuclear physics program at Inter University Accelerator Centre, or IUAC (formerly Nuclear Science Centre or NSC) [1,2], is focused at heavy-ion reactions around the Coulomb barrier. These include experiments related to fusion [3] and fusion–fission reactions [4], and quasi-elastic scattering [5]. The dependence of the fusion cross-section on incident kinetic energy, called the fusion excitation function [3], provides a useful insight into the fusion mechanism. Barrier distributions [6] in fusion reactions can be extracted from the experimental fusion excitation function. Quasi-elastic (QE) scattering, which combines elastic and inelastic scattering, and transfer reactions, yields information about the QE excitation functions and fusion barrier distributions. The study of heavy-ion induced fission fragment angular distributions [7] is a rich source of information as regards fission process, its dynamics and cross-section. Observation of anomalous fission fragment anisotropies with reference to the prediction of statistical models has led to new explanations such as presence of non-compound nuclear fission events (pre-equilibrium fission and quasi-fission etc.). Such reactions around the Coulomb barrier are characterized by measuring the yield of reaction products at desired angles. An efficient and granular detection system with particle identification capability is required for such studies. In the past several years, variety of apparatus have been used to study different kind of nuclear reactions which includes detector arrays such as 8πLP [8], MEGHA [9], INDRA [10], etc. A detector system based on gas–silicon hybrid telescopes has been developed at IUAC. The prime motive behind the development of these telescopes is to perform QE scattering and fission fragment angular distribution experiments in the energy domain near the Coulomb barrier, using the 1.5 m diameter General Purpose Scattering Chamber (GPSC) [11] and NAND facility [12] at IUAC. The hybrid telescopes have gas ionization chambers as ΔE detectors, providing the differential energy loss information, and silicon as E detector. Currently the array consists of 16 such telescopes. Dedicated low noise and low power charge sensitive preamplifiers (CSPA) were developed for extracting signals from telescopes. The CSPAs are

* Corresponding author.
E-mail addresses: akhil@iuac.res.in, jhinganakhil@gmail.com (A. Jhingan).

https://doi.org/10.1016/j.nima.2018.04.064
Received 30 March 2018; Accepted 30 April 2018
0168-9002/© 2018 Elsevier B.V. All rights reserved.

Head
Department of Physical Sciences
I.K. Gujral Punjab Technical University
Main Campus

PHYSICAL REVIEW C **97**, 031601(R) (2018)

Rapid Communications | Editors' Suggestion

Probing the fusion of neutron-rich nuclei with re-accelerated radioactive beams

J. Vadas, Varinderjit Singh, B. B. Wiggins, J. Huston, S. Hudan, and R. T. deSouza*
Department of Chemistry, Center for Exploration of Energy and Matter, Indiana University, 2401 Milo B. Sampson Lane, Bloomington, Indiana 47408, USA

Z. Lin and C. J. Horowitz
Department of Physics, Center for Exploration of Energy and Matter, Indiana University, 2401 Milo B. Sampson Lane, Bloomington, Indiana 47408, USA

A. Chbihi and D. Ackermann
GANIL, 1 Boulevard Henri Becquerel, Caen 14000, France

M. Famiano
Department of Physics, Western Michigan University, Kalamazoo, Michigan 49008, USA

K. W. Brown
Department of Physics and Astronomy, National Superconducting Cyclotron Laboratory, Michigan State University, East Lansing, Michigan 48824, USA

(Received 14 September 2017; revised manuscript received 6 November 2017; published 27 March 2018)

We report the first measurement of the fusion excitation functions for $^{39,47}K + ^{28}Si$ at near-barrier energies. Evaporation residues resulting from the fusion process were identified by direct measurement of their energy and time of flight with high geometric efficiency. At the lowest incident energy, the cross section measured for the neutron-rich ^{47}K-induced reaction is $\approx$6 times larger than that of the β-stable system. This experimental approach, both in measurement and in analysis, demonstrates how to efficiently measure fusion with low-intensity re-accelerated radioactive beams, establishing the framework for future studies.

DOI: 10.1103/PhysRevC.97.031601

The recent coincident detection of gravitational waves in GW170817 [1] and a γ-ray burst in GRB170817A [2] marks the first observation of a binary neutron star merger [3,4]. The delayed optical emission spectrum that followed indicated the presence of heavy elements in the neutron star ejecta [5]. This result clearly established binary neutron star mergers as an important, potentially primary, site for heavy element nucleosynthesis. Ejecta resulting from the tidal disruption of the neutron stars as they merge reflects both their initial composition as well as the reactions that occur during the merger. Understanding the composition of the neutron stars is thus an important question in understanding heavy element nucleosynthesis.

Insight into the composition of some neutron stars prior to merging may be realized by considering the case of accreting neutron stars [6]. Heavy elements in the outer crust of an accreting neutron star are produced by fusion reactions [7,8]. Some of the resulting heavy nuclei become neutron rich through electron-capture reactions [9]. It has been proposed that fusion of neutron-rich nuclei occurring in the outer crust may be enhanced relative to their β-stable counterparts providing an important heat source that triggers an x-ray superburst [10].

As a nucleus becomes increasingly neutron rich, the extent of the neutron density distribution increases. Consequently, even if the density distributions were frozen through the fusion process the fusion cross section would increase in response to the larger geometric cross section. However, the fusion process is not static but dynamic. The decreased average binding energy of the outermost neutrons with increasing neutron number and the existence of low-energy collective modes act to make neutron-rich nuclei more polarizable. This increased polarizability, which can be viewed as the prelude to neutron transfer, increases the likelihood for fusion to occur. Thus, both static and dynamic factors impact the fusion cross section. By examining the fusion cross section with an increasing neutron number for an isotopic chain and observing an increase beyond the geometric expectation, one might extract the increased role of dynamics. Such general expectations are borne out by microscopic time-dependent Hartree-Fock calculations [11].

To determine how fusion evolves for increasingly neutron-rich nuclei in an isotopic chain, it is advantageous to measure fusion at near-barrier energies. It is in this near and sub-barrier regime that one is most sensitive to the shape of the barrier which reflects both structure and dynamics. A new generation of radioactive beam facilities [12–14] with the capability of high-quality re-accelerated beams provides, for the first time, the opportunity to systematically address this question. These

*desouza@indiana.edu

 ©2018 American Physical Society

Head
Department of Physical Sciences
I.K. Gujral Punjab Technical University
Main Campus

PHYSICAL REVIEW C **98**, 064612 (2018)

Investigating the fusion enhancement for neutron-rich mid-mass nuclei using the dynamical cluster-decay model

Rupinder Kaur,[1,2] Maninder Kaur,[1] Varinderjit Singh,[1,*] Sarbjeet Kaur,[3] BirBikram Singh,[3] and B. S. Sandhu[2]

[1]*Department of Physical Sciences, I.K.G. Punjab Technical University, Kapurthala 144603, India*

[2]*Department of Physics, Punjabi University, Patiala 147002, India*

[3]*Department of Physics, Sri Guru Granth Sahib World University, Fatehgarh Sahib 140406, India*

(Received 8 September 2018; published 28 December 2018)

The mechanism involved in compound nucleus formation through heavy ion induced fusion reactions at near- and sub-barrier energies has been stimulating the interest of both experimentalists and theoreticians. The study of fusion reactions is important not only for the production of superheavy elements but also to unfold the mysteries involved in the evolution of neutron stars and nucleosynthesis of elements in astrophysical scenarios. The detection of gravitational waves originating from the merging of two black holes, and the possibility of observing similar events originating from black-hole–neutron-star mergers, highlighted the necessity of understanding the behavior of neutron-rich nuclear matter. One of the potential methods to understand the character of neutron-rich matter is through the study of fusion of an isotopic chain of reactions. Recently, the first experimental evidence of fusion enhancement at near-barrier energies for neutron-rich nuclei was reported for the light and mid-mass regime. To understand the dynamics involved in such reactions, the investigation of K-induced reactions has been performed using the quantum mechanical fragmentation based dynamical cluster-decay model (DCM). The experimental fusion cross sections of $^{39,47}K + ^{28}Si$ are reproduced using DCM and, further, the fusion cross sections are predicted for other isotopes of K beam on ^{28}Si to investigate the fusion enhancement as a function of neutron number. It has been observed that fusion enhancement is significant at near-barrier energies for neutron-rich nuclei. The fusion enhancement observed is larger for odd neutron number nuclei as compared to adjacent neutron nuclei. This indicates the influence of unpaired neutrons on fusion cross sections. Also, the fusion cross sections predicted in the present work will act as input for planning more experimental measurements.

DOI: 10.1103/PhysRevC.98.064612

I. INTRODUCTION

Neutrons not only play a crucial role in the physics of nuclear reactors under terrestrial conditions, they also play a decisive role in astrophysical scenarios during nucleosynthesis, via neutron capture processes: namely the *r* and *s* processes (on different time scales) in neutron-rich environments. The valence neutrons in these neutron rich nuclei provide an opportunity to understand the channel coupling and transfer probability effects using a different formalisms, thus revealing the anticipated enhancement of fusion cross sections at near- and sub-barrier regimes [1,2]. A number of authors have investigated the sub-barrier fusion of neutron-rich nuclei using the coupled-channel model [3,4] and time-dependent Hartree-Fock theory [5,6].

Experimentally, with the availability of radioactive ion beams of nuclei away from β stability, it is now possible to investigate the fusion of neutron-rich beams, which consequently provides insight into the fusion mechanism. Understanding the fusion mechanism of neutron-rich nuclei is necessary to get a better estimate of neutron star composition, which in turn will help in the accurate prediction of x-ray superbursts and neutron-star–black-hole merger events. Also, the understanding of fusion of neutron-rich nuclei will be helpful for exploring the production mechanism of heavy elements in nature. So, the study of structural and dynamical aspects involved in the fusion reaction of neutron-rich nuclei is of paramount importance.

A few initial measurements in this direction suggested an enhancement of fusion probability as compared to the standard statistical model at near-barrier energies [7]. Various studies indicated the importance of interplay between nuclear structural and reaction dynamical aspects present in these many-body systems, which can be incorporated through spin and energy dependent potentials [8], sensitivity to coupling of fusion degree of freedom to other degrees of freedom [9], neck formation [3,10], static deformations [11], increased collectivity through increased coupling of weakly bound neutron-rich nuclei [12], etc. Several studies have also revealed the strong isotopic dependence of the fusion cross sections near the barrier [13–15]. The enhancement of fusion cross sections observed through these isotopic chains of nuclear reactions is being considered as one of the best methods to understand the character of neutron-rich matter.

*vickymangat3@gmail.com

Head
Department of Physical Sciences
I.K. Gujral Punjab Technical University
Main Campus

 ©2018 American Physical Society

450

PHYSICAL REVIEW C **101**, 044605 (2020)

Dynamical aspects of $^{48}Ti + {}^{58}Fe$, $^{58}Ni \rightarrow {}^{106}Cd^*$, $^{106}Sn^*$ reactions at energies near the Coulomb barrier

Rupinder Kaur,[1,2,3,*] Maninder Kaur,[2] Varinderjit Singh,[2] Mandeep Kaur,[3] BirBikram Singh,[3,†] and B. S. Sandhu[1]

[1]*Department of Physics, Punjabi University, Patiala-147002, India*

[2]*Department of Physical Sciences, I.K.G. Punjab Technical University, Kapurthala-144603, India*

[3]*Department of Physics, Sri Guru Granth Sahib World University, Fatehgarh Sahib-140406, India*

(Received 12 June 2019; revised manuscript received 10 January 2020; accepted 9 March 2020; published 14 April 2020)

The study of the heavy-ion reactions at the near- and sub-barrier regimes gives immense information about the nuclear structure and the involved reaction dynamics. It has been observed that a slight difference in the nuclear structure may lead to a significant change in the sub-barrier fusion excitation functions. The studies of different trends of excitation functions below the Coulomb barrier region due to dissimilar structures of the nuclei, which are involved in the reaction, are available in literature. To understand the role of different structures and dynamics involved in such reactions, an investigation of ^{48}Ti-induced reactions on ^{58}Fe and ^{58}Ni forming $^{106}Cd^*$ and $^{106}Sn^*$ compound nuclei (CN), respectively, has been made at similar $E_{c.m.}/V_b$ values within the framework of the dynamical cluster decay model (DCM). The difference in the structure between the nuclei is quite notable with ^{58}Ni and $^{106}Sn^*$ having a proton shell closure ($Z = 28$ and 50, respectively). Within the DCM, the experimental fusion evaporation cross sections are reproduced using deformed configurations effects included up to quadruple deformations (β_{2i}) for two nuclei having optimum orientations $\theta^{opt.}$. The fusion evaporation data at near- and sub-barriers has been explained through the calculated enhanced ΣP_0 values of the decaying channels in the case of $^{106}Cd^*$ in comparison to $^{106}Sn^*$. Moreover, it is observed that the quantum tunneling of the fragments is less hindered in the case of $^{106}Cd^*$ as compared to $^{106}Sn^*$ at the lower values of $E_{c.m.}/V_b$, i.e., having less barrier modification (ΔV_B) in the case of the former. The role of magicity has been further explored with the plotted values of the ratio of fusion cross sections (σ_{fus}) of CN $^{106}Sn^*$ and $^{112}Xe^*$ (formed in the reaction with both the projectile ^{58}Ni and target ^{54}Fe having proton and neutron magicity, respectively) with respect to $^{106}Cd^*$, which are highly suppressed in the case of the latter in comparison to the former, particularly, below the Coulomb barrier.

DOI: 10.1103/PhysRevC.101.044605

I. INTRODUCTION

In the past few decades, a thorough study of sub-barrier heavy-ion interactions have uncovered the various unexpected characteristics involved in the reaction dynamics. The most notable outcome of these studies, observed experimentally, is the hinderance phenomenon at deep sub-barrier energies in some systems in comparison to others. This suggests existence of an experimentally determined threshold limit E_s in sub-barrier energies which varies from one system to another. The investigation of the physical cause for such phenomena will help to understand the involved reaction dynamics. Thus, to ascertain the reaction mechanisms involved in observed phenomena requires a consistent study of various systems. The apparent dynamical picture of the sub-barrier fusion has been acknowledged by the considerable experimental and theoretical efforts made by various authors in this direction [1]. Several experiments have provided a clear example of fusion hindrance at the deep sub-barrier region. One of such studies in which the effect on the fusion excitation function due to the associated nuclear structure of the interacting nuclei, has been investigated by Jiang *et al.* in $^{64}Ni + {}^{64}Ni$ fusion reaction [2]. The author has explained the associated phenomenon of hinderance by considering stiff to open-shell nuclei in the entrance channel in the sub-barrier regime in terms of the S factor where the steep falloff in cross sections translates into a maximum of the S factor. Fusion hindrance in the $^{58}Ni + {}^{54}Fe$ reaction at lower energies is also investigated by Stefanini *et al.* [3]. They observed that, at lower energies, fusion cross sections drop faster than conventional Woods-Saxon potential calculations with a steep slope. Recently, Stefanini *et al.* [4] have also shown that distinct low-energy nuclear structures of the involved nuclei leads to different trends in the fusion excitations functions for the $^{48}Ti + {}^{58}Fe$ and $^{58}Ni + {}^{54}Fe$ reactions at the sub-barrier regime. Large fusion cross sections has been observed in the measured energy range in $^{48}Ti + {}^{58}Fe$ as compared to $^{58}Ni + {}^{54}Fe$ (with closed-shell protons and neutrons in the entrance channel). The cross-section trends are explained in the $^{48}Ti + {}^{58}Fe$ reaction through the involved strong quadrupole modes of both ^{48}Ti and ^{58}Fe and the two-neutron transfer channel.

*roopisaini87@gmail.com

†birbikramsingh@sggswu.edu.in

 ©2020 American Physical Society

Head Department of Physical Sciences I.K. Gujral Punjab Technical University Main Campus

451

IOP Publishing Journal of Physics G: Nuclear and Particle Physics

J. Phys. G: Nucl. Part. Phys. **48** (2021) 075104 (17pp) https://doi.org/10.1088/1361-6471/abe8cd

Measurement of fission excitation function for $^{19}F + ^{194,196,198}Pt$ reactions

Varinderjit Singh[1,2,*], B R Behera[1], Maninder Kaur[1,2], A Jhingan[3], Rupinder Kaur[2], P Sugathan[3], Davinder Siwal[1,4], S Goyal[4], K P Singh[1], Santanu Pal[5], A Saxena[6] and S Kailas[7]

[1] Department of Physics, Panjab University, Chandigarh 160014, India
[2] Department of Physical Sciences, IKG Punjab Technical University, Kapurthala 144603, India
[3] Inter University Accelerator Centre, New Delhi 110067, India
[4] Department of Physics and Astrophysics, University of Delhi, Delhi 110007, India
[5] CS-6/1, Golf Green, Kolkata 700095, India
[6] Nuclear Physics Division, Bhabha Atomic Research Centre, Mumbai 400085, India
[7] UM-DAE Centre for Excellence in Basic Sciences, University of Mumbai, Mumbai 400098, India

E-mail: vickymangat3@gmail.com

Received 3 December 2020, revised 18 February 2021
Accepted for publication 22 February 2021
Published 21 May 2021

Abstract

Experimental fission cross-sections are reported for the $^{19}F + ^{194,196,198}Pt$ reactions populating an isotopic chain of compound nuclei comprising both closed and non-closed shell nuclei. The fission cross-sections are obtained at near and above Coulomb barrier energies by measuring fission fragment angular distributions. The present work aims to estimate nuclear dissipation and find its isotopic and shell closure dependence from statistical model (SM) analysis of experimental data. Pre-scission neutron multiplicity data for the same systems is also included in the SM analysis. An updated version of SM is used in the present analysis, which includes shell corrections in level density and fission barrier as well as the effect of collective enhancement of level density and orientation effect of the compound nucleus along the symmetry axis. An isotopic dependence of the dissipation strength fitting the fission excitation functions is observed. The pre-scission neutron multiplicity, however, is underestimated by the SM.

Keywords: nuclear reactions, fusion–fission reaction, fission fragment angular distribution, statistical model of nuclear reactions

(Some figures may appear in colour only in the online journal)

*Author to whom any correspondence should be addressed.

0954-3899/21/075104+17$33.00 © 2021 IOP Publishing Ltd Printed in the UK

Head
Department of Physical Sciences
IKG Punjab Technical University
Main Campus

Physics Letters B 814 (2021) 136115

Contents lists available at ScienceDirect

Physics Letters B

www.elsevier.com/locate/physletb

Effect of increasing neutron-excess on the fusion cross-section in $^{12-15}C + ^{12}C$ at above-barrier energies

R.T. deSouza [a,*], Varinderjit Singh [a], S. Hudan [a], Z. Lin [b,c], C.J. Horowitz [b]

[a] Department of Chemistry and Center for Exploration of Energy and Matter, Indiana University, 2401 Milo B. Sampson Lane, Bloomington, IN 47408, USA
[b] Department of Physics and Center for Exploration of Energy and Matter, Indiana University, 2401 Milo B. Sampson Lane, Bloomington, IN 47408, USA
[c] Department of Physics, Arizona State University, 450 E. Tyler Mall, Tempe, AZ 85287-1504, USA

ARTICLE INFO

Article history:
Received 24 November 2020
Received in revised form 12 January 2021
Accepted 27 January 2021
Available online 29 January 2021
Editor: D.F. Geesaman

Keywords:
Near-barrier fusion
Neutron-rich fusion
RIB fusion
Fusion enhancement

ABSTRACT

Fusion excitation functions at energies above the fusion barrier for $^{12-15}C + ^{12}C$ are examined. From these excitation functions the average fusion cross-section, $< \sigma_F >$, is calculated. For this isotopic chain, the measured dependence of $< \sigma_F >$ on neutron excess is compared with static barrier penetration models. The more rapid increase observed for the experimental cross-sections above the geometric increase predicted by the static models suggests that the stronger dependence on neutron-excess measured may be attributable to dynamics. Calculations with a time-dependent Hartree-Fock model also fail to describe the observed trend suggesting that for neutron-rich nuclei, neutron dynamics may play a larger role than is presently accounted for.

© 2021 The Authors. Published by Elsevier B.V. This is an open access article under the CC BY license (http://creativecommons.org/licenses/by/4.0/). Funded by SCOAP[3].

1. Introduction

Nuclei are extremely interesting quantal systems. Despite a limited number of constituent particles, they manifest collective behavior. This collective behavior is observed in many forms including giant multipole resonances [1], shape coexistence [2], and the quintessential case of fission [3]. In the case of nuclear fission the evolution of collective degrees of freedom is key to understanding the process. Although typically associated with the structure and reactions of mid-mass and heavy nuclei, collectivity for very light nuclei has recently been reported [4]. Nuclear fusion provides another example in which collective degrees of freedom undergo substantial change as the reaction proceeds. Of particular interest is the role of collectivity for neutron-rich nuclei as for these nuclei the dependence of collective behavior on the asymmetry between the neutron and proton densities can be probed. Fusion reactions provide a powerful means to assess the response of neutron-rich nuclei to perturbation. As fusion involves the interplay of the repulsive Coulomb and attractive nuclear potentials, by examining fusion for an isotopic chain one probes the neutron density distribution and how that density distribution evolves as the two nuclei approach and overlap [5–8]. On qualitative grounds, increasing neutron excess leads to a larger range of the nuclear interaction, resulting in a lower value for the height of the s-wave fusion barrier and a larger barrier radius. Consequently, a larger fusion cross-section is expected with increasing neutron excess. At near-barrier energies this fusion cross-section reflects both the increase in the static size as well as any dynamics present. In addition to an improved fundamental understanding of the dynamics of neutron-rich nuclei, investigating the fusion of neutron-rich nuclei is also important for describing reactions occurring in the crusts of accreting neutron stars [9]. In this manuscript, careful comparison of the experimental above-barrier fusion cross-section for an isotopic chain with the prediction of both static and dynamical models, reveals the failure of these models to describe the dependence of the fusion cross-section on neutron excess. The stronger dependence of the average fusion cross-sections on neutron-excess observed may reflect the increasing importance of dynamics for neutron-rich nuclei.

At high incident energy one expects the sudden approximation to be valid. Consequently, the nuclear densities do not have enough time to rearrange in the contact region and the cross-section is a manifestation of nuclear size and other geometrical features such as ground-state deformation, all of which are considered "static". Hence, the measured interaction cross-section, σ_I, provides a direct and effective measure of the extent of the matter distribution. Collision of nuclei at lower energy is more complex with a multitude of processes that constitute the "dynamics". These processes include excitation of the entrance channel nuclei and formation of a neck where multi-nucleon transfer occurs, all influenced by the quantal Pauli exclusion principle [10]. Comparison of high-energy

* Corresponding author.
E-mail address: desouza@indiana.edu (R.T. deSouza).

https://doi.org/10.1016/j.physletb.2021.136115
0370-2693/© 2021 The Authors. Published by Elsevier B.V. This is an open access article under the CC BY license (http://creativecommons.org/licenses/by/4.0/). Funded by SCOAP[3].

Department of Physical Sciences
I.K. Gujral Punjab Technical University
Main Campus

453

PHYSICAL REVIEW C **103**, 064606 (2021)

Assessing the impact of valence *sd* neutrons and protons on fusion

Varinderjit Singh, J. Vadas, T. K. Steinbach, B. B. Wiggins, S. Hudan, and R. T. deSouza*
Department of Chemistry and Center for Exploration of Energy and Matter, Indiana University, 2401 Milo B. Sampson Lane, Bloomington, Indiana 47408, USA

(Received 13 April 2021; accepted 1 June 2021; published 10 June 2021)

Experimental near-barrier fusion cross sections for $^{17}F + ^{12}C$ are compared to the fusion excitation functions for $^{16,17,18}O$, ^{19}F, and ^{20}Ne ions on a carbon target. Normalized or reduced fusion cross sections are utilized in order to compare the different systems and account for the differing static size of the incident ions as well as changes in fusion barrier. Fusion excitation functions for the case of the mirror nuclei ^{17}F and ^{17}O with a single *sd* nucleon are compared. The ^{17}F data are also juxtaposed with nuclei involving multiple *sd* nucleons. Trends of the fusion cross section above the barrier beyond the expected systematic behavior are observed. These trends are interpreted as the interplay of the *sd* protons and neutrons. The experimental data are also compared to a widely used analytic model of near-barrier fusion, a time-dependent Hartree-Fock model, and coupled channels calculations.

DOI: 10.1103/PhysRevC.103.064606

I. INTRODUCTION

Nuclear fusion is a topic of considerable interest both from a fundamental perspective as well as in the field of nuclear astrophysics [1]. Nuclei just beyond a closed shell present a unique opportunity to probe the interplay of shell and collective effects on the fusion process. In particular, light nuclei just beyond the $1p_{1/2}$ shell, namely isotopes of oxygen, fluorine, and neon, are good candidates for examination. In this work, the fusion of various isotopes of these elements with a carbon target at near-barrier energies is examined. The results of this work, which combines both stable and radioactive beams, point to the potential of low-energy beams at radioactive beam facilities [2,3] for examining the impact of neutron excess on fusion.

Addition of neutrons and protons just beyond the $1p_{1/2}$ shells of ^{16}O clearly changes both the matter and charge distributions of the nuclei. Theoretical calculations indicate that for a large neutron excess, e.g., ^{24}O as compared to ^{16}O, fusion with ^{16}O target is significantly enhanced [4]. The impact of adding just a few neutrons or protons beyond the $1p_{\frac{1}{2}}$ shell on fusion is less clear. With increased atomic or mass number, the fusion barrier and consequently the fusion cross section are clearly impacted. We propose to go beyond these trivial systematic differences and examine the detailed differences in the fusion cross section. A particularly interesting case to investigate is fusion of the nucleus ^{17}F, which exhibits a proton halo when in its $2s_{1/2}$ excited state [5]. It is presently unclear whether an increased radial extent results in a fusion enhancement or weak binding results in a decreased fusion cross section. For the case of $^{17}F + ^{208}Pb$, neither an enhancement nor a suppression of fusion was observed relative to $^{19}F + ^{208}Pb$ [6]. However, in the case of fusion with a large target nucleus, such as ^{208}Pb, the impact on fusion of adding two neutrons might be diminished. Recently, the fusion cross section for $^{17}F + ^{12}C$ both at near-barrier energies [7] and higher energies [8] has been reported, indicating that the low binding energy of ^{17}F and the halo properties of the low-lying first excited state do not affect the low-energy fusion cross section. In this work we report an independent, higher statistics measurement of near barrier fusion for $^{17}F + ^{12}C$. By comparing the present measurement with fusion induced by O, F, and Ne beams on ^{12}C the impact of adding a few protons and neutrons to the *sd* shell on the fusion cross section is examined.

II. EXPERIMENTAL DETAILS

Discovery of halo nuclei, notably ^{11}Li [9,10] was achieved through systematic examination of the interaction cross sections for lithium isotopes. At high incident energy one expects the sudden approximation to be valid in describing the collision of the nuclei. Consequently, the nuclear densities do not have enough time to rearrange as the projectile and target nuclei come into contact. Thus, a measurement of the interaction cross section at high energy probes the nuclear size and other geometrical features such as deformation, all of which are considered "static" [9]. Hence, the measured interaction cross section, σ_I, provides a direct and effective measure of the extent of the matter distribution.

To better understand the change in the static size of the different nuclei considered in this work, we examine the interaction cross sections measured at high energy. Presented in Table I are σ_I for O, F, and Ne nuclei with a carbon target [11] with the number of protons and neutrons in the *sd* shell indicated. The closure of the $1p_{\frac{1}{2}}$ with $N = 8$ provides a natural reference from which to examine the impact made by

*desouza@indiana.edu

Head
Department of Physical Sciences
I.K. Gujral Punjab Technical University
Main Campus

 ©2021 American Physical Society

Nuclear Inst. and Methods in Physics Research, A 1014 (2021) 165697

Contents lists available at ScienceDirect

Nuclear Inst. and Methods in Physics Research, A

journal homepage: www.elsevier.com/locate/nima

MuSIC@Indiana: An effective tool for accurate measurement of fusion with low-intensity radioactive beams

J.E. Johnstone [a,b], Rohit Kumar [a,b], S. Hudan [a,b], Varinderjit Singh [a,b], R.T. deSouza [a,b,*], J. Allen [c], D.W. Bardayan [c], D. Blankstein [c], C. Boomershine [c], S. Carmichael [c], A. Clark [c], S. Coil [c], S.L. Henderson [c], P.D. O'Malley [c]

[a] Department of Chemistry, Indiana University, 800 E. Kirkwood Ave., Bloomington, IN 47405, USA
[b] Center for Exploration of Energy and Matter, Indiana University, 2401 Milo B. Sampson Lane, Bloomington, IN 47408, USA
[c] Department of Physics, University of Notre Dame, Notre Dame, IN 46556, USA

ARTICLE INFO

Keywords:
MuSIC
Multi-sampling ionization chamber
Active target
Fusion

ABSTRACT

The design, construction, and characterization of the Multi-Sampling Ionization Chamber, MuSIC@Indiana, are described. This detector provides efficient and accurate measurement of the fusion cross-section at near-barrier energies. The response of the detector to low-intensity beams of ^{17,18}O, ^{19}F, ^{23}Na, ^{24,26}Mg, ^{27}Al, and ^{28}Si at E_{lab} = 50–60 MeV was examined. MuSIC@Indiana was commissioned by measuring the ^{18}O+^{12}C fusion excitation function for 11 < E_{cm} < 20 MeV using CH_4 gas. A simple, effective analysis cleanly distinguishes proton capture and two-body scattering events from fusion on carbon. With MuSIC@Indiana, measurement of 15 points on the excitation function for a single incident beam energy is achieved. The resulting excitation function is shown to be in good agreement with literature data.

1. Introduction

The structure and reactions of neutron-rich isotopes is presently a topic of significant interest [1]. As nuclei become more neutron-rich their properties are expected to change and new collective modes may emerge. The availability of neutron-rich beams at radioactive beam facilities now allows the systematic exploration of fusion for an isotopic chain of neutron-rich nuclei [2–6]. While the next generation of radioactive beam facilities, such as the Facility for Rare Isotope Beams (FRIB), will provide radioactive beams closer to the neutron drip-line than ever before [7], it also presents experimental challenges. Due to their short half-lives, these exotic beams will only be available at low intensity mandating use of an effective and efficient means for accurately measuring fusion probability.

The low intensity of exotic radioactive beams suggests that a thick target approach should be used. Thick target approaches have previously been used in the measurement of fusion by identifying the fusion products via their characteristic γ-radiation as they de-excite [8]. However, utilizing this approach requires accurate knowledge of the γ detection efficiency – which is often low – as well as knowledge of the decay properties of the neutron-rich fusion products — which may not exist.

An alternative approach is to use an active target in which direct detection of the primary charged fusion products provides the signal that fusion has occurred. A Multi-Sampling Ionization Chamber (MuSIC) detector [2] provides an effective means of measuring the fusion cross-section by identifying the heavy fusion product. While MuSIC detectors were originally developed for use in high-energy heavy-ion experiments [9–11], more recently their use has been extended to low energy nuclear reactions namely the measurement of the fusion excitation function for $^{10-15}$C+^{12}C [2,12] and ^{17}F+^{12}C [13], or studies of (α,n)/(α,p) reactions [14,15].

The MuSIC approach provides a couple of intrinsic advantages over the typical thin-target measurement. Traditional thin-target measurements were performed with limited angular coverage, identifying the fusion products by either ΔE-E [16,17] or ETOF [18] techniques. Extraction of the fusion cross-section thus required integration of the angle and energy distributions for the individual heavy product introducing an uncertainty into the total extracted fusion cross-section. Use of a MuSIC detector provides a direct integrated measure of the fusion cross-section. In contrast to the thin-target approach where the incident beam energy must be changed, MuSIC detectors allow measurement of multiple points on the excitation function simultaneously [12]. In addition, MuSIC detectors are self-normalizing since the incident beam is detected by the same detector as the reaction products. These advantages make MuSIC detectors an efficient means for measuring fusion excitation functions for neutron-rich nuclei when available beam intensities are limited.

* Corresponding author at: Department of Chemistry, Indiana University, 800 E. Kirkwood Ave., Bloomington, IN 47405, USA.
E-mail address: desouza@indiana.edu (R.T. deSouza).

https://doi.org/10.1016/j.nima.2021.165697
Received 11 July 2021; Accepted 27 July 2021
Available online 3 August 2021
0168-9002/© 2021 Elsevier B.V. All rights reserved.

Head
Department of Physical Sciences
I.K. Gujral Punjab Technical University
Main Campus

455

61

PRAMANA
— journal of
physics

© Indian Academy of Sciences

Vol. 86, No. 2
February 2016
pp. 479–485

Nucleon-generalized parton distributions in the light-front quark model

NEETIKA SHARMA

Indian Institute of Science Education and Research Mohali, S.A.S. Nagar, Mohali 140 306, India
E-mail: neetika@iisermohali.ac.in

DOI: 10.1007/s12043-015-1169-3; ***e*Publication:** 12 January 2016

Abstract. We calculate the generalized parton distributions (GPDs) for the up- and down-quarks in nucleon using the effective light-front wavefunction. The results obtained for GPDs in momentum and impact parameter space are comparable with phenomenological parametrization methods.

Keywords. Eelectromagnetic form factors; properties of baryons; Compton scattering by hadrons.

PACS Nos 13.40.Gp; 14.20.Dh; 13.60.Fz

1. Introduction

Generalized parton distributions (GPDs) are the important set of parameters that give us essential information about the non-perturbative structure of hadrons. GPDs have gained a lot of theoretical and experimental interest in the recent past. At the leading order, there are two GPDs: helicity-dependent $H(x, \zeta, t)$ and helicity-independent $E(x, \zeta, t)$. These are functions of three variables, namely, longitudinal momentum fraction (x), square of the total momentum transferred (t), and skewness (ζ), which represents the longitudinal momentum transferred in the process. GPDs are experimentally extracted from hard exclusive processes such as deeply virtual Compton scattering and vector meson production [1]. Recent measurements at DESY [2] and Jefferson Lab [3] will significantly advance our knowledge about the GPDs.

GPDs are expressed as off-forward matrix elements of bilocal light-front current in the overlap representation. Their first moments are related to form factors and they do not have probabilistic interpretation. For the zero skewness, the Fourier transform (FT) of the GPDs with respect to the momentum transfer in the transverse direction, gives the impact parameter-dependent GPDs. The impact parameter GPDs have probabilistic interpretation [4] and provide us information about partonic distributions in the impact parameter or transverse position space [5].

Head
Department of Physical Sciences
I.K. Gujral Punjab Technical University
Main Campus

Eur. Phys. J. A (2016) **52**: 91
DOI 10.1140/epja/i2016-16091-4

THE EUROPEAN PHYSICAL JOURNAL A

Regular Article – Theoretical Physics

Hard gluon evolution of nucleon generalized parton distributions in the light-front quark model

Hard gluon evolution of nucleon GPDs

Neetika Sharma[a]

Indian Institute of Science Education and Research Mohali, S.A.S. Nagar, Mohali-140306, Punjab, India

Received: 13 January 2016 / Revised: 22 February 2016
Published online: 19 April 2016 – © Società Italiana di Fisica / Springer-Verlag 2016
Communicated by S. Hands

Abstract. We incorporate the perturbative evolution effects in the generalized parton distributions (GPDs) calculated in effective light-front quark model for the nucleon. The perturbative effects enter into formalism through the evolution of GPDs according to the Dokshitzer-Gribov-Lipatov-Altarelli-Parisi-like (DGLAP) equation. We obtain the evolved GPDs in the momentum space and transverse impact parameter space. We observe that combining the light-front quark model with the perturbative evolution effects, give the effective model for studying the phenomenological GPDs.

1 Introduction

Quantum chromodynamics (QCD) is the widely accepted fundamental description of strong interaction in terms of quark and gluon degrees of freedom. It has been proved successful in explaining the physical phenomena at high-energy range; however, the applicability of QCD to low energies is limited to some extent. Because of color confinement no quarks and gluons have ever been directly observed by any detector in high-energy scattering experiments. The QCD factorization theorem enables us to connect the dynamics of quarks and gluons to physically measured hard-scattering cross sections of the known spectrum of hadrons, by systematically factorizing the physics taking place at different momentum scales [1–4].

Both the exclusive and inclusive processes, can be factorized into the perturbative and non-perturbative part. The scattering of the virtual photon off the parton is the short-distance part which can be evaluated using the perturbation theory. The universal long-distance part is parametrized in terms of PDFs, GPDs, or other kinds of form factors and require the knowledge of either non-perturbative methods or a global fit to experimental data. The initial distributions of quark and gluon are parameterized as functions of longitudinal momentum of quarks x for a chosen initial scale μ^2 and then evolved to numerically larger values. The independence of the physical observable from the physical scale leads to the DGLAP equation in the perturbative QCD.

The study of GPDs has been of enormous interest as they contain vital information about the 3-D structure information of the nucleon [5–7]. Many models have been proposed theoretically in the recent past to explain the hadronic properties in terms of GPDs [8]. Primarily, GPDs are parametrized in terms of three variables, namely, longitudinal momentum of quark, x, the invariant momentum transfer, t, and the skewness parameter, ζ, which gives the fraction of the longitudinal momentum transfer to the nucleon in the process. The recent experiments are performed at high luminosity with large momentum transfer and give remarkable precise data for the measurement of GPDs. Several experiments, for example, H1 Collaboration [9], ZEUS Collaboration [10] at the HERA collider, HERMES at DESY [11], have already collected data for the deeply virtual Compton scattering experiments. Experiments presently running at Hall A and B at Jefferson Laboratory [12–14], COMPASS at CERN [15], etc., will provide more accurate data in a wider kinematic range. This will significantly help us in advancing our present understanding of hadron structure.

Recently, light-front holography, has emerged as a semiclassical approximation for strongly coupled quantum field theories. It is based on the remarkable connection between the quantum gauge field theory in four dimensions and the classical gravity theory in five dimensions [16–18]. The light-front holography also successfully predicts the hadron spectrum [19], the color confinement potential [20], running coupling at low scales [21], and other physical quantities. The successes of this approach to non-perturbative QCD are really remarkable.

[a] e-mail: neetika@iisermohali.ac.in

Head
Department of Physical Sciences
I.K. Gujral Punjab Technical University
Main Campus

PHYSICAL REVIEW D **94,** 074018 (2016)

Diffractive ρ and ϕ production at HERA using a holographic AdS/QCD light-front meson wave function

Mohammad Ahmady*
Department of Physics, Mount Allison University, Sackville, New Brunswick E4L 1E6, Canada

Ruben Sandapen†
Department of Physics, Acadia University, Wolfville, Nova Scotia B4P 2R6, Canada and Department of Physics, Mount Allison University, Sackville, New Brunswick E4L 1E6, Canada

Neetika Sharma‡
Department of Physical Sciences, Indian Institute of Science Education and Research Mohali, S.A.S. Nagar, Mohali-140306, Punjab, India

(Received 26 May 2016; published 13 October 2016)

We use an anti–de Sitter/quantum chromodynamics holographic light-front wave function for the ρ and ϕ mesons, in conjunction with the color glass condensate dipole cross section whose parameters are fitted to the most recent 2015 high precision HERA data on inclusive deep inelastic scattering, in order to predict the cross sections for diffractive ρ and ϕ electroproduction. Our results suggest that the holographic meson light-front wave function is able to give a simultaneous description of ρ and ϕ production data provided we use a set of light quark masses with $m_{u,d} < m_s \approx 0.14$ GeV.

DOI: 10.1103/PhysRevD.94.074018

I. INTRODUCTION

We use the QCD color dipole model [1,2] together with a nonperturbative holographic meson light-front wave function [3] to predict the cross sections for diffractive ρ and ϕ electroproduction measured at the HERA collider [4–9]. In Ref. [10], successful predictions were obtained for diffractive ρ production using the holographic wave function for the ρ and the color glass condensate (CGC) dipole cross section [11] whose parameters were fitted to the 2001 HERA deep inelastic scattering (DIS) structure function data [12,13]. In 2015, the latest high precision combined HERA data on inclusive DIS were released [14]. This definitive DIS data set supersedes the earlier ones and is one of the major legacies of the HERA collider. We shall use these new data here to update the parameters of the CGC dipole cross section and thus repeat the predictions of Ref. [10]. We shall also extend our predictions to diffractive ϕ production, thereby testing the holographic wave function for the heavier ϕ meson.

The holographic meson wave function is predicted in holographic light-front QCD proposed by Brodsky and de Téramond [15–17]. A recent review of holographic light-front QCD can be found in Ref. [3]. In a semiclassical approximation of light-front QCD with massless quarks, there is an exact correspondence between the light-front Schrödinger equation for QCD bound states in physical spacetime and the equation of motion of spin-J modes in the higher dimensional anti–de Sitter (AdS) space. A dilaton field breaking the conformal symmetry of AdS space then dictates the form of the confining potential in physical spacetime. A phenomenologically successful choice is a dilaton that is quadratic in the fifth dimension of AdS space, and this maps onto a light-front harmonic oscillator in physical spacetime. Remarkably, group theoretical arguments based on the underlying conformality of the classical Lagrangian of QCD reveal that the light-front harmonic potential is unique [18].

A single mass scale, κ, appears in the quadratic dilaton field and thus in the light-front harmonic oscillator in physical spacetime. The holographic light-front Schrödinger equation can then be solved to predict the meson mass spectrum. The latter has a string model Regge form as is observed experimentally. The parameter κ can then be fixed to fit the observed slopes of the Regge trajectories for the various meson families. It is found that for all light mesons, $\kappa \approx 0.5$ GeV [3]. Furthermore, the pion is predicted to be massless, consistent with chiral symmetry.

Accounting for nonzero quark masses goes beyond the AdS/QCD correspondence, and in Ref. [19], Brodsky and de Téramond propose an ansatz for including small (on a hadronic scale) quark masses. The key observation is that the evolution variable for the momentum space light-front wave function is the quark-antiquark invariant mass, and this can be appropriately modified to account for nonzero quark masses. With the modified holographic wave function, the shift in meson masses can be computed as a first

*mahmady@mta.ca
†ruben.sandapen@acadiau.ca
‡neetika@iisermohali.ac.in

 © 2016 American Physical Society

Department of Physical Sciences
I.K. Gujral Punjab Technical University
Main Campus

458

Eur. Phys. J. A (2016) **52**: 338
DOI 10.1140/epja/i2016-16338-0

THE EUROPEAN PHYSICAL JOURNAL A

Regular Article – Theoretical Physics

Momentum transfer dependence of generalized parton distributions

Neetika Sharma[a]

Indian Institute of Science Education and Research Mohali, S.A.S. Nagar, Mohali-140306, Punjab, India

Received: 5 July 2016 / Revised: 6 October 2016
Published online: 21 November 2016 – © Società Italiana di Fisica / Springer-Verlag 2016
Communicated by Shi-Lin Zhu

Abstract. We revisit the model for parametrization of the momentum dependence of nucleon generalized parton distributions in the light of recent MRST measurements of parton distribution functions (A.D. Martin *et al.*, Eur. Phys. J. C **63**, 189 (2009)). Our parametrization method with a minimum set of free parameters give a sufficiently good description of data for Dirac and Pauli electromagnetic form factors of proton and neutron at small and intermediate values of momentum transfer. We also calculate the GPDs for up- and down-quarks by decomposing the electromagnetic form factors for the nucleon using the charge and isospin symmetry and also study the evolution of GPDs to a higher scale. We further investigate the transverse charge densities for both the unpolarized and transversely polarized nucleon and compare our results with Kelly's distribution.

1 Introduction

The study of fundamental quantities like generalized partion distributions (GPDs) and electromagnetic form factors (EFFs) have been of tremendous interest in the recent past. GPDs are parametrized in terms of longitudinal momentum x and invariant momentum transfer squared $t = -q^2$, thus giving vital information about the 3D structure of nucleon. The EFFs measure the probability for a nucleon to absorb a virtual photon of momentum q^2. Ji sum rule states that the GPDs for unpolarized nucleon reduce to EFFs when integrated over x [1]:

$$F_1^N(q^2) = \int_0^1 \mathrm{d}x\, H^N(x, q^2), \tag{1}$$

$$F_2^N(q^2) = \int_0^1 \mathrm{d}x\, E^N(x, q^2), \tag{2}$$

where $H(x, q^2)$ and $E(x, q^2)$ (with $N = p, n$) are, respectively, the spin-independent and spin-dependent GPDs and the functions F_1 and F_2 are Dirac and Pauli form factors for the nucleon.

GPDs are measured in processes like deeply virtual Compton scattering ($\gamma^* p \to \gamma p$) and diffractive vector meson production ($\gamma^* p \to V p$). Various experiments at Jefferson Lab (JLAB) [2,3], and HERA [4] have extracted information about GPDs and new data is expected in the near future from the experiments at JLAB12, COMPASS, and electron-ion collider [5]. On the other hand, GPDs are calculated in the Euclidean lattice QCD using the first-principle approach [6, 7]. This is a method based upon numerical simulations, however, the applicability is limited by enormous computational complexities, dependence upon the free parameters, and the fact that dynamical observables in Minkowski spacetime cannot be directly observed in the Euclidean lattice computations. Recently, there has been a lot of activity in calculating GPDs in the anti-de Sitter AdS/QCD holography-based models as well [8, 9]. In this approach, information on GPDs is obtained via matching the matrix elements of electromagnetic current with QCD sum rules in the hard- and soft-wall models [10, 11].

There are several other phenomenological models in the literature to obtain GPDs in a functional form that represent the data over a wide range of momentum transfer [12–17]. These approaches are based on parametrizations of the quark wave function or directly the EFFs, using the constraint imposed by sum rules in eq. (1). It is also interesting to formulate a simple parametrization in term of x and q^2 dependences. The x-dependence was measured accurately in terms of the quark distribution functions and the q^2-dependence can be added using different functional forms from the phenomenological description of nucleon EFFs.

In this work, we will follow the parametrization approach with a functional form of quark distribution functions based on the latest global analysis by "MSTW2009" [18] combined with the Guassian ansatz to incorporate the q^2-dependence [19]. Though this approach is model dependent, one can reach much higher values of

[a] e-mail: neetika@iisermohali.ac.in

Head
Department of Physical Sciences
I.K. Gujral Punjab Technical University
Main Campus

Eur. Phys. J. A (2017) **53**: 237
DOI 10.1140/epja/i2017-12433-0

THE EUROPEAN PHYSICAL JOURNAL A

Regular Article – Theoretical Physics

Gravitational form factors and angular momentum densities in light-front quark-diquark model

Narinder Kumar[1], Chandan Mondal[2,a], and Neetika Sharma[3,4]

[1] Department of Physics, Indian Institute of Technology Kanpur, Kanpur-208016, India
[2] Institute of Modern Physics, Chinese Academy of Sciences, Lanzhou-730000, China
[3] Department of Physical Sciences, I K Gujral Punjab Technical University, Jalandhar 144603, Punjab, India
[4] Department of Physics, Panjab University, Chandigarh 160014, India

Received: 2 June 2017 / Revised: 24 September 2017
Published online: 14 December 2017 – © Società Italiana di Fisica / Springer-Verlag 2017
Communicated by G. Torrieri

Abstract. We investigate the gravitational form factors (GFFs) and the longitudinal momentum densities (p^+ densities) for proton in a light-front quark-diquark model. The light-front wave functions are constructed from the soft-wall AdS/QCD prediction. The contributions from both the scalar and the axial vector diquarks are considered here. The results are compared with the consequences of a parametrization of nucleon generalized parton distributions (GPDs) in the light of recent MRST measurements of parton distribution functions (PDFs) and a soft-wall AdS/QCD model. The spatial distribution of angular momentum for up and down quarks inside the nucleon has been presented. At the density level, we illustrate different definitions of angular momentum explicitly for an up and down quark in the light-front quark-diquark model inspired by AdS/QCD.

1 Introduction

Nucleon tomography has become an important tool in the modern study of the nucleon structure [1, 2]. One can characterize the distribution of quarks in high energy nucleon not only by the momentum fraction x but also by the transverse position $\mathbf{b}_\perp$ and transverse momentum $\mathbf{k}_\perp$. This important information is encoded in the generalized parton distributions (GPDs) and transverse momentum distributions (TMDs). We can access the GPDs in hard exclusive processes like deep virtual Compton scattering (DVCS) or deep virtual meson production (DVMP) and TMDs in the semi-inclusive processes like semi-inclusive deep inelastic scattering (SIDIS). Worldwide, several experiments such as the H1 Collaboration [3, 4], ZEUS Collaboration [5, 6] and fixed target experiments at HERMES [7] have finished taking data on DVCS. Experiments are also being done at JLAB, Hall A and B [8] and COMPASS at CERN [9] to access GPDs and new data is expected from the upcoming experimental facilities at JLAB12 and electron ion collider (EIC) [10].

In literature, several models [11–16] and parametrizations [17–19] are present for GPDs. The Fourier transform of GPDs with skewness equal to zero gives the impact parameter dependent parton distribution function (ipdpdf) providing the information of the partons of a given longitudinal momentum distributed in transverse position space. The x moments of GPDs give the form factors accessible in exclusive processes whereas in the forward limit they reduce to parton distributions, accessible in inclusive processes. Electromagnetic form factors (EFFs) [20] describe the spatial distributions of electric charge and magnetization densities inside the nucleon and thus are intimately related to its internal structure; these form factors are among the most basic observables of the nucleon. The Fourier transform of EFFs gives the charge and magnetization distributions of nucleon respectively. One can obtain the Dirac, $F_1(Q^2)$ and Pauli, $F_2(Q^2)$ form factors from the first moment of spin non-flip $H(x, Q^2)$ and spin flip $E(x, Q^2)$ GPDs [21].

Gravity plays a major role at two extreme but completely different scales *i.e.*, Planck and cosmic. At the subatomic levels, gravity has little effect due to its weak coupling. In classical mechanics, mass distribution and moment of inertia are important concepts but barely discussed for quantum systems like nucleon. The second moment of charge distribution gives the mass distribution for nucleon. However, it is very interesting that the second Mellin moments GPDs give the gravitational form factors (GFFs) without actual gravitational scattering. In hadron physics, matrix elements of the energy-momentum tensor ($T^{\mu\nu}$) relate to the GFFs $A(Q^2)$ and $B(Q^2)$ [22].

[a] e-mail: mondal@impcas.ac.cn

Department of Physical Sciences
I.K. Gujral Punjab Technical University
Main Campus

3.4.5 Number of research papers per teacher in the Journals notified on UGC website during the last five years (15)

3.4.5.1: Number of research papers in the Journals notified on UGC website during the last five years

Sr. No.	Title of paper	Name of the author/s	Department of the teacher	Name of journal	Year of publication	ISSN number	Link to the recognition in UGC enlistment of the Journal	University Website Link
1	Lattice Thermal Conductivity of pure and doped (B,N) Graphene	Sarita Mann, Isha Mudahar, **Hitesh Sharma**, V.K. Jindal, G. Dubey	Department of Physical Sciences	Material Research Express	2020	2053-1591	https://mjl.clarivate.com:/search-results?issn=2053-1591&hide_exact_match_fl=true&utm_source=mjl&utm_medium=share-by-link&utm_campaign=search-results-share-this-journal	https://ptu.ac.in/faculty/?fid=7
2	Effect of Twist Angle on Structural, Electronic and Magnetic Properties of Carbon Nano Hybrids: A DFT Study	Amrish Sharma, Sandeep Kaur, **Hitesh Sharma**, Neha Kapila, V.K. Jindal, Vladimir Bubanja	Department of Physical Sciences	Computational Materials Science	2020	0927-0256 / 1879-0801	https://mjl.clarivate.com:/search-results?issn=0927-0256&hide_exact_match_fl=true&utm_source=mjl&utm_medium=share-by-link&utm_campaign=search-results-share-this-journal	https://ptu.ac.in/faculty/?fid=7
3	Graphene nanoribbons under axial compressive and point tensile stresses	Sandeep Kaur, **Hitesh Sharma**, V.K. Jindal, Vladimir Bubanja and Isha Mudahar	Department of Physical Sciences	Physica E: Low dimensional System and Nanostructures **111**, 1-12	2019	1386-9477	https://mjl.clarivate.com:/search-results?issn=1386-9477&hide_exact_match_fl=true&utm_source=mjl&utm_medium=share-by-link&utm_campaign=search-results-share-this-journal	https://ptu.ac.in/faculty/?fid=7
4	Substitutional doping of symmetrical sized small fullerene dimmers	Sandeep Kaur, Amrish Sharma, **Hitesh Sharma** and Isha Mudahar	Department of Physical Sciences	In. Journal of Quantum Chemistry **119,23**, 1-12	2019	1097-461X	https://mjl.clarivate.com:/search-results?issn=0020-7608&hide_exact_match_fl=true&utm_source=mjl&utm_medium=share-by-link&utm_campaign=search-results-share-this-journal	https://ptu.ac.in/faculty/?fid=7
5	Substitutional Doping of Asymmetrical Small Fullerene Dimar	Sandeep Kaur, Amrish Sharma, Isha and **Hitesh Sharma**	Department of Physical Sciences	Advanced Science Letters **24**, 888-892	2018	ISSN 1936-6612 (Print)	https://mjl.clarivate.com:/search-results?issn=2055-0340&hide_exact_match_fl=true&utm_source=mjl&utm_medium=share-by-link&utm_campaign=search-results-share-this-journal	https://ptu.ac.in/faculty/?fid=7
6	A First Principle Study on C_{20} and C_{40} Carbon Nanobuds,	Sandeep Kaur, Amrish Sharma, Isha and **Hitesh Sharma**	Department of Physical Sciences	Advance Science letters **24**, 888-892	2018	ISSN 1936-6612 (Print)	https://mjl.clarivate.com:/search-results?issn=2055-0340&hide_exact_match_fl=true&utm_source=mjl&utm_medium=share-by-link&utm_campaign=search-results-share-this-journal	https://ptu.ac.in/faculty/?fid=7
7	Structural and Magnetic Properties of Small Symmetrical and Asymmetrical sized Fullerene Dimers	Sandeep Kaur, Amrish Sharma, Isha and **Hitesh Sharma**	Department of Physical Sciences	Mater. Res. Express **5**, 016105	2018	2053-1591	https://mjl.clarivate.com:/search-results?issn=2053-1591&hide_exact_match_fl=true&utm_source=mjl&utm_medium=share-by-link&utm_campaign=search-results-share-this-journal	https://ptu.ac.in/faculty/?fid=7
8	Effect of Dopant and Defects in GNRs on Adsorption of Gas Molecules	Sandeep Kumar, Meenakshi and **Hitesh Sharma**	Department of Physical Sciences	Mater. Res. Express **5**, 105007	2018	2053-1591	https://mjl.clarivate.com:/search-results?issn=2053-1591&hide_exact_match_fl=true&utm_source=mjl&utm_medium=share-by-link&utm_campaign=search-results-share-this-journal	https://ptu.ac.in/faculty/?fid=7
9	Chemical State analysis of Cl, K and kB13 x-ray emission lines using polychromatic WDXRF spectrometer	Harpreet Singh Kainth, Arun Upmanyu, **Hitesh Sharma**, Tejbir Singh and Sanjeev Kumar	Department of Physical Sciences	Nuclear Inst. And Methods in Physics Research **B416**, 62	2018	0168-583X / 1872-9584	https://mjl.clarivate.com:/search-results?issn=0168-583X&hide_exact_match_fl=true&utm_source=mjl&utm_medium=share-by-link&utm_campaign=search-results-share-this-journal	https://ptu.ac.in/faculty/?fid=7
10	Electronic and magnetic properties of small fullerene carbon nanobuds: A DFT study	Amrish Sharma, Sandeep Kaur, Isha and **Hitesh Sharma**	Department of Physical Sciences	Mater. Res. Express, **5**, 065032	2018	2053-1591	https://mjl.clarivate.com:/search-results?issn=2053-1591&hide_exact_match_fl=true&utm_source=mjl&utm_medium=share-by-link&utm_campaign=search-results-share-this-journal	https://ptu.ac.in/faculty/?fid=7
11	Adsorption of gas molecules on ultra-thin pristine and doped graphene nanoribbons	Sandeep Kaumar and **Hitesh Sharma**	Department of Physical Sciences	Mater. Res. Express **5**, 105007	2018	2053-1591	https://mjl.clarivate.com:/search-results?issn=2053-1591&hide_exact_match_fl=true&utm_source=mjl&utm_medium=share-by-link&utm_campaign=search-results-share-this-journal	https://ptu.ac.in/faculty/?fid=7
12	Electronic and magnetic properties of small fullerene carbon nanobuds: A DFT study,	Amrish Sharma, Sandeep Kaur, **Hitesh Sharma** and Isha	Department of Physical Sciences	Mater. Res. Express, **5**, 065032	2018	2053-1591	https://mjl.clarivate.com:/search-results?issn=2053-1591&hide_exact_match_fl=true&utm_source=mjl&utm_medium=share-by-link&utm_campaign=search-results-share-this-journal	https://ptu.ac.in/faculty/?fid=7
13	Cross section measurements of radiative KL2,3 in case of 24Cr and L3M4,5RR5 in 59Pr for Mn Ka1,2X –rays	Veena Sharma, Arun Upmanyu, R.Singh, G.Singh, **Hitesh Sharma,** Sanjeev Kumar and D. Mehta	Department of Physical Sciences	Radiation Physics and Chemistry **135**, 55-62	2017	0969-806X	https://mjl.clarivate.com:/search-results?issn=0969-806X&hide_exact_match_fl=true&utm_source=mjl&utm_medium=share-by-link&utm_campaign=search-results-share-this-journal	https://ptu.ac.in/faculty/?fid=7
14	A first principle investigation into effect of B and BN doped C60 in lowering dehydrogenation of MXH4 (where M= Na, Li and X = Al, B)	Meenakshi, Deepak Agnihotri and **Hitesh Sharma**	Department of Physical Sciences	Bulletin of Materials Science **40**, 7, 1397–1403	2017	0250-4707	https://mjl.clarivate.com:/search-results?issn=0250-4707&hide_exact_match_fl=true&utm_source=mjl&utm_medium=share-by-link&utm_campaign=search-results-share-this-journal	https://ptu.ac.in/faculty/?fid=7
15	Effect of Gas Adsorption on Graphene Nanoribbons: A Density Functional Theory	Sandeep Kaumar and **Hitesh Sharma**	Department of Physical Sciences	Materials Today: Proceedings **4**, 10441–10445	2017	2214-7853	https://mjl.clarivate.com:/search-results?issn=1369-7021&hide_exact_match_fl=true&utm_source=mjl&utm_medium=share-by-link&utm_campaign=search-results-share-this-journal	https://ptu.ac.in/faculty/?fid=7
16	Effect of nitrogen as co-dopant in carbon and boron-doped ZnO clusters	Neha Kapila, Isha, Gaurav and **Hitesh Sharma**	Department of Physical Sciences	Journal of Magnetism and Magnetic Materials **405**, 187-196	2016	0304-8853	https://mjl.clarivate.com:/search-results?issn=0304-8853&hide_exact_match_fl=true&utm_source=mjl&utm_medium=share-by-link&utm_campaign=search-results-share-this-journal	https://ptu.ac.in/faculty/?fid=7
17	Carbon nanotubes for improving dehydrogenation from NaAlH4	Meenakashi, Deepak Agnihotri and **Hitesh Sharma**	Department of Physical Sciences	Computational and Theoretical Chemistry, **1097**, 61–69	2016	2210-271X	https://mjl.clarivate.com:/search-results?issn=2210-271X&hide_exact_match_fl=true&utm_source=mjl&utm_medium=share-by-link&utm_campaign=search-results-share-this-journal	https://ptu.ac.in/faculty/?fid=7
18	Improvement in dehydrogenation of MXH4 where M = Na, Li and X = Al, B confined in CNTs: a DFT investigation,	Meenakshi,Deepak Agnihotri and **Hitesh Sharma**	Department of Physical Sciences	Mater. Res. Express **3**, 115013	2016	2053-1591	https://mjl.clarivate.com:/search-results?issn=2053-1591&hide_exact_match_fl=true&utm_source=mjl&utm_medium=share-by-link&utm_campaign=search-results-share-this-journal	https://ptu.ac.in/faculty/?fid=7
19	Size dependent electronic and magnetic properties of ultra-thin graphene nanoribbons	Sandeep Kaumar and **Hitesh Sharma**	Department of Physical Sciences	Mater. Res. Express **3**, 095007	2016	2053-1591	https://mjl.clarivate.com:/search-results?issn=2053-1591&hide_exact_match_fl=true&utm_source=mjl&utm_medium=share-by-link&utm_campaign=search-results-share-this-journal	https://ptu.ac.in/faculty/?fid=7
20	Study of kinematic viscosity and density of biodiesels exposed to radiations	**Amit Sarin**, Neerja Sharma, Kusum Devgan and Meetu Singh	Department of Physical Sciences	Materials Today Proceedings, 46, 5516-5522	2021	2214-7853	https://www.scopus.com/sourceid/21100370037	https://ptu.ac.in/faculty/?fid=85
21	Investigation of the shelf life of the optimized Neem biodiesel and its execution and excretion characteristics on automotive diesel engine	Mayank Chhabra, Balraj Singh Saini, Gaurav Dwivedi, Arun Kumar Behura, Anuj Kumar, Siddharth Jain, **Amit Sarin** and Puneet Verma	Department of Physical Sciences	Energy Sources, Part A: Recovery, Utilization, and Environmental Effects	2021	1556-7036	https://mjl.clarivate.com:/search-results?issn=1556-7036&hide_exact_match_fl=true&utm_source=mjl&utm_medium=share-by-link&utm_campaign=search-results-share-this-journal	https://ptu.ac.in/faculty/?fid=85
22	Comprehensive analysis of oxidation and storage stability of argemone biodiesel and development of correlations based on experimental results	Mandeep Singh, **Amit Sarin** and Sarabjot Singh Sandhu	Department of Physical Sciences	Energy Sources, Part A: Recovery, Utilization, and Environmental Effects	2020	1556-7036	https://mjl.clarivate.com:/search-results?issn=1556-7036&hide_exact_match_fl=true&utm_source=mjl&utm_medium=share-by-link&utm_campaign=search-results-share-this-journal	https://ptu.ac.in/faculty/?fid=85
23	Seasonal Variation of Indoor radon/thoron and their progeny levels in lesser Himalayas of Jammu & Kashmir	Ajay Kumar, Raman Vij, Sumit Sharma, Amit Sarin	Department of Physical Sciences	Journal of Radioanalytical and Nuclear Chemistry, 323, 495-506	2020	0236-5731	https://mjl.clarivate.com:/search-results?issn=0236-5731&hide_exact_match_fl=true&utm_source=mjl&utm_medium=share-by-link&utm_campaign=search-results-share-this-journal	https://ptu.ac.in/faculty/?fid=85
24	Effect of metal contaminants and antioxidants on the oxidation stability of Argemone Mexicana biodiesel, Experimental and Statistical study	Mandip Singh, Deepak Kumar Singh, Surjit Kumar Gandhi, **Amit Sarin**, Sanjeev Saini, Sunil Kumar Malha, Ajay Gupta and Sarabjot Singh Sandhu	Department of Physical Sciences	Waste and biomass valorization	2019	1877-2641	https://mjl.clarivate.com:/search-results?issn=1877-2641&hide_exact_match_fl=true&utm_source=mjl&utm_medium=share-by-link&utm_campaign=search-results-share-this-journal	https://ptu.ac.in/faculty/?fid=85
25	Antioxidative Potential of Phyllanthus emblica for Oxidation Stability of Biodiesels	Meetu Singh, Neerja Sharma, Harkirat S. Paras, Navneet S. Hans, Narinder P. Singh, and **Amit Sarin**	Department of Physical Sciences	Environmental Progress & Sustainable Energy	2019	1944-7450	https://mjl.clarivate.com:/search-results?issn=1944-7442&hide_exact_match_fl=true&utm_source=mjl&utm_medium=share-by-link&utm_campaign=search-results-share-this-journal	https://ptu.ac.in/faculty/?fid=85
26	Optical characterisation of amorphous Se-Te-Sn thin films	Amit Sethi, Surbhi Sharma, **Amit Sarin**, Rajesh Kumar, Navjeet Sharma	Department of Physical Sciences	Applied Physics A: Materials Science & Processing	2018	1432-0630	https://mjl.clarivate.com:/search-results?issn=0947-8396&hide_exact_match_fl=true&utm_source=mjl&utm_medium=share-by-link&utm_campaign=search-results-share-this-journal	https://ptu.ac.in/faculty/?fid=85
27	Influence of compositional variations on optoelectrical properties of Ge20Sn10Se70-xTex glass system	Surbhi Sharma; Navjeet Sharma; **Amit Sarin**	Department of Physical Sciences	Optical Engineering	2018	0091-3286	https://mjl.clarivate.com:/search-results?issn=0091-3286&hide_exact_match_fl=true&utm_source=mjl&utm_medium=share-by-link&utm_campaign=search-results-share-this-journal	https://ptu.ac.in/faculty/?fid=85

Head
Department of Physical Sciences
I.K. Gujral Punjab Technical University
Main Campus

28	Crystallisation kinetics and thermal stability analysis of Se82-xTe15Sn3Sbx(0=x=6) glass alloys	Sethi, **Amit & Sarin**, Amit & Kumar, Rajesh & Sharma, Navjeet	Department of Physical Sciences	Physica b: Condensed matter	2018	0921-4526	https://mjl.clarivate.com:/search-results?issn=0921-4526&hide_exact_match_fl=true&utm_source=mjl&utm_medium=share-by-link&utm_campaign=search-results-share-this-journal	https://ptu.ac.in/faculty/?fid=85
29	Assessment of radionuclide concentration and exhalation studies in soil of lesser Himalayas of Jammu and Kashmir, India	Ajay Kumar, Raman Vij, Sumit Sharma, **Amit Sarin**, Saurabh Narang	Department of Physical Sciences	Acta Geophysica	2018	1895-7455	https://mjl.clarivate.com:/search-results?issn=1895-6572&hide_exact_match_fl=true&utm_source=mjl&utm_medium=share-by-link&utm_campaign=search-results-share-this-journal	https://ptu.ac.in/faculty/?fid=85
30	Prediction of indoor radon/thoron concentration in a model room from exhalation rates of building materials for different ventilation rates	Manish Kumar, Navjeet Sharma, **Amit Sarin**	Department of Physical Sciences	Acta Geophysica	2018	1895-7455	https://mjl.clarivate.com:/search-results?issn=1895-6572&hide_exact_match_fl=true&utm_source=mjl&utm_medium=share-by-link&utm_campaign=search-results-share-this-journal	https://ptu.ac.in/faculty/?fid=85
31	Radon and uranium concentrations in drinking water sources along the fault line passing through Reasi district, lesser Himalayas of Jammu and Kashmir State, India	Ajay Kumar, Raman Vij, **Amit Sarin** & Priya Kanwar	Department of Physical Sciences	Human and Ecological Risk Assessment: An International Journal	2017	1549-7860	https://mjl.clarivate.com:/search-results?issn=1080-7039&hide_exact_match_fl=true&utm_source=mjl&utm_medium=share-by-link&utm_campaign=search-results-share-this-journal	https://ptu.ac.in/faculty/?fid=85
32	Influence of Sb substitution on thermal and electrical characteristics of Ge-Sn-Se chalcogenide glass system	Surbhi Sharma, Navjeet Sharma and **Amit Sarin**	Department of Physical Sciences	Materials Science and Engineering	2017	1757-8981	https://www.scopus.com/sourceid/19700200831	https://ptu.ac.in/faculty/?fid=85
33	Prospects of Tectona Grandis as a feedstock for Biodiesel.	**Amit Sarin**, Meetu Singh, Neerja Sharma, N.P. Singh	Department of Physical Sciences	Frontiers in Energy Research	2017	2296-598X	https://mjl.clarivate.com:/search-results?issn=2296-598X&hide_exact_match_fl=true&utm_source=mjl&utm_medium=share-by-link&utm_campaign=search-results-share-this-journal	https://ptu.ac.in/faculty/?fid=85
34	Measurement of uranium and radon concentration in drinking water samples and assessment of ingestion dose to local population in Jalandhar district	Manish Kumar, , Anjali Kaushal, B. K. Sahoo, **Amit Sarin**, Rohit Mehra, Rajan Jakhu, Atul Bhalla, Navjeet Sharma	Department of Physical Sciences	Indoor and Built Environment	2017	1420-326X	https://mjl.clarivate.com:/search-results?issn=1420-326X&hide_exact_match_fl=true&utm_source=mjl&utm_medium=share-by-link&utm_campaign=search-results-share-this-journal	https://ptu.ac.in/faculty/?fid=85
35	Measurement of radon concentration in the drinking water and assessment of age dependent ingestion dose to local population in Kapurthala district of Punjab, India	Manish Kumar, **Amit Sarin**, B. K. Sahoo, and Navjeet Sharma	Department of Physical Sciences	journal of environment and bio-sciences	2017	0973-6913	https://mjl.clarivate.com:/search-results?issn=0973-6913&hide_exact_match_fl=true&utm_source=mjl&utm_medium=share-by-link&utm_campaign=search-results-share-this-journal	https://ptu.ac.in/faculty/?fid=85
36	Radon/thoron and progeny levels in dwellings: Regional variations and effect of dwelling characteristics A case study in Jalandhar district of Punjab, India	Manish Kumar, Anjali Kaushal, **Amit Sarin**, Rajesh Kumar, Navjeet Sharma	Department of Physical Sciences	Indoor and Built Environment	2017	1420-326X	https://mjl.clarivate.com:/search-results?issn=1420-326X&hide_exact_match_fl=true&utm_source=mjl&utm_medium=share-by-link&utm_campaign=search-results-share-this-journal	https://ptu.ac.in/faculty/?fid=85
37	An Experimental Study on Storage and Oxidation Stability of Bitter Apricot Kernel Oil Biodiesel/	Virender Singh Gurau, Mudit Shankar Agarwal, **Amit Sarin**, and Sarbjot Singh Sandhu	Department of Physical Sciences	Energy & Fuels	2016	0887-0624	https://mjl.clarivate.com:/search-results?issn=0887-0624&hide_exact_match_fl=true&utm_source=mjl&utm_medium=share-by-link&utm_campaign=search-results-share-this-journal	https://ptu.ac.in/faculty/?fid=85
38	Effect of Sb addition on linear and nonlinear optical properties of amorphous GeSeSn thin films	Navjeet Sharma, Surbhi Sharma, **Amit Sarin**, Rajesh Sharma	Department of Physical Sciences	Optical Materials	2016	0925 -3467	https://mjl.clarivate.com:/search-results?issn=0925-3467&hide_exact_match_fl=true&utm_source=mjl&utm_medium=share-by-link&utm_campaign=search-results-share-this-journal	https://ptu.ac.in/faculty/?fid=85
39	Fusion hindrance for the positive Q-value system $^{12}C+^{30}Si$	G. Montagnoli, A.M. Stefanini, C.L. Jiang, K.Hagino, F. Galtarossa, G. Colucci, S. Bottoni, C. Broggini, A. Caciolli, P. Colovi'c, L. Corradi, S.	Department of Physical Sciences	Physical Review C	2018	0556-2813 / 1089-490X	https://mjl.clarivate.com:/search-results?issn=0556-2813&hide_exact_match_fl=true&utm_source=mjl&utm_medium=share-by-link&utm_campaign=search-results-share-this-journal	https://ptu.ac.in/faculty/?fid=8
40	Investigation of fusion enhancement for the neutron-rich mid-mass nuclei using dynamical cluster- decay model	Rupinder Kaur, **Maninder Kaur, Varinderjit Singh**, Sarbjeet Kaur, BirBikram Singh, and B. S. Sandhu	Department of Physical Sciences	Physical Review C **98**, 064612	2018	0556-2813 / 1089-490X	https://mjl.clarivate.com:/search-results?issn=0556-2813&hide_exact_match_fl=true&utm_source=mjl&utm_medium=share-by-link&utm_campaign=search-results-share-this-journal	https://ptu.ac.in/faculty/?fid=8
41	Fusion hindrance for the positive **Q**-value system $^{12}C+^{30}Si$	G. Montagnoli, … , **M. Kaur.**. *et. al*	Department of Physical Sciences	Physical Review C **97**, 024610	2018	0556-2813 / 1089-490X	https://mjl.clarivate.com:/search-results?issn=0556-2813&hide_exact_match_fl=true&utm_source=mjl&utm_medium=share-by-link&utm_campaign=search-results-share-this-journal	https://ptu.ac.in/faculty/?fid=8
42	Dynamical aspects of $^{48}Ti+^{58}Fe$, $^{58}Ni \rightarrow ^{106}Cd^{*}, ^{106}Sn^{*}$ reactions at energies near the coulomb barrier	Rupinder Kaur, **Maninder Kaur**, Varinderjit Singh, Mandeep Kaur, BirBikram Singh, and B. S.	Department of Physical Sciences	Phys. Rev. C **101**, 044605	2020	0556-2813 / 1089-490X	https://mjl.clarivate.com:/search-results?issn=0556-2813&hide_exact_match_fl=true&utm_source=mjl&utm_medium=share-by-link&utm_campaign=search-results-share-this-journal	https://ptu.ac.in/faculty/?fid=8
43	Measurement of fission excitation function for $^{19}F+^{194,196,198}Pt$.	Varinderjit Singh, Bivash R. Behera, **Maninder Kaur**, Akhil Jhingan, Rupinder Kaur, Pullanhiotan Sugathan, Davinder Siwal, Savi Goyal, K. P. Singh	Department of Physical Sciences	Journal of Physics G: Nuclear and Particle Physics **48**, 075104	2021	0954-3899	https://mjl.clarivate.com:/search-results?issn=0954-3899&hide_exact_match_fl=true&utm_source=mjl&utm_medium=share-by-link&utm_campaign=search-results-share-this-journal	https://ptu.ac.in/faculty/?fid=8
44	High-rate axial-field ionization chamber for particle identification of radioactive beams	J. Vadas, **Varinderjit Singh**, G. Visser, A. Alexander, S. Hudan, J. Huston, B.B. Wiggins, A. Chbihi, M. Famiano, M.M. Bischak, and R.T.	Department of Physical Sciences	Nucl. Instrum. Methods A **837**, 28	2016	0168-9002 / 1872-9576	https://mjl.clarivate.com:/search-results?issn=0168-9002&hide_exact_match_fl=true&utm_source=mjl&utm_medium=share-by-link&utm_campaign=search-results-share-this-journal	https://ptu.ac.in/faculty/?fid=9
45	Fusion Enhancement at near and sub-barrier energies in 19O + 12C.	**Varinderjit Singh**, J. Vadas, T.K. Steinbach, B.B. Wiggins, S. Hudan, R. T. deSouza, Zidu Lin, C.J. Horowitz, I. T. Babv, S.A. Kuvin, Vandana	Department of Physical Sciences	Physics Letter B **765**, 99	2017	0217-9849 / 1793-6640	https://mjl.clarivate.com:/search-results?issn=0217-9849&hide_exact_match_fl=true&utm_source=mjl&utm_medium=share-by-link&utm_campaign=search-results-share-this-journal	https://ptu.ac.in/faculty/?fid=9
46	Experimental measurement of 12C + 16O fusion at stellar energies	X. Fang, W. P. Tan, M. Beard, G. Gilardy, H. Jung, Q. Liu, S. Lyons, D. Robertson, K. Setoodehnia, C. Seymour, E. Stech, B. Vande Kolk, M. Wiescher	Department of Physical Sciences	Phys. Rev. C **96**, 045804	2017	0556-2813 / 1089-490X	https://mjl.clarivate.com:/search-results?issn=0556-2813&hide_exact_match_fl=true&utm_source=mjl&utm_medium=share-by-link&utm_campaign=search-results-share-this-journal	https://ptu.ac.in/faculty/?fid=9
47	Development of a compact ExB micro-channel plate detector for beam imaging	B. B. Wiggins, **V. Singh**, J. Vadas, J. Huston, T. K. Steinbach, S. Hudan, R. T. deSouza,	Department of Physical Sciences	Nucl. Instr. Meth. in Phys. Res. A **866**, 202	2017	0168-9002 / 1872-9576	https://mjl.clarivate.com:/search-results?issn=0168-9002&hide_exact_match_fl=true&utm_source=mjl&utm_medium=share-by-link&utm_campaign=search-results-share-this-journal	https://ptu.ac.in/faculty/?fid=9
48	Fission time scale from pre-scission neutron and alpha multiplicities in the 16O + 194Pt reaction.	K. Kapoor, S. Verma, P. Sharma, R. Mahajan, N. Kaur, G. Kaur, B. R. Behera, K. P. Singh, A. Kumar, H. Singh, R. Dubey, N. Saneesh, A.	Department of Physical Sciences	Phys. Rev. C. **96**, 054605	2017	0556-2813 / 1089-490X	https://mjl.clarivate.com:/search-results?issn=0556-2813&hide_exact_match_fl=true&utm_source=mjl&utm_medium=share-by-link&utm_campaign=search-results-share-this-journal	https://ptu.ac.in/faculty/?fid=9
49	HYTAR: A HYbrid Telescope ARray detection system for heavy ion nuclear reactions around Coulomb barrier	Akhil Jhingan, Gurpreet Kaur, N. Saneesh, R. Ahuja, Tathagata Banerjee, Rakesh Dubey, **Varinderjit Singh**, Ruchi Mahajan, Meenu	Department of Physical Sciences	Nuclear Instruments and Methods in Physics Research A **903**, 326	2018	0168-9002 / 1872-9576	https://mjl.clarivate.com:/search-results?issn=0168-9002&hide_exact_match_fl=true&utm_source=mjl&utm_medium=share-by-link&utm_campaign=search-results-share-this-journal	https://ptu.ac.in/faculty/?fid=9
50	Probing the fusion of neutron-rich nuclei with re-accelerated radioactive beams	J. Vadas, **Varinderjit Singh,** B. B. Wiggins, J. Huston, S. Hudan, R. T. deSouza, Z. Lin, C. J. Horowitz, A. Chbihi, D. Ackermann, M. Famiano	Department of Physical Sciences	Physical Review C **97**, 031601	2018	0556-2813 / 1089-490X	https://mjl.clarivate.com:/search-results?issn=0556-2813&hide_exact_match_fl=true&utm_source=mjl&utm_medium=share-by-link&utm_campaign=search-results-share-this-journal	https://ptu.ac.in/faculty/?fid=9
51	Investigation of fusion enhancement for the neutron-rich mid-mass nuclei using dynamical cluster- decay model	Rupinder Kaur, Maninder Kaur, **Varinderjit Singh**, Sarbjeet Kaur, BirBikram Singh, and B. S. Sandhu	Department of Physical Sciences	Physical Review C **98**, 064612	2018	0556-2813 / 1089-490X	https://mjl.clarivate.com:/search-results?issn=0556-2813&hide_exact_match_fl=true&utm_source=mjl&utm_medium=share-by-link&utm_campaign=search-results-share-this-journal	https://ptu.ac.in/faculty/?fid=9
52	Dynamical aspects of $^{48}Ti+^{58}Fe$, $^{58}Ni \rightarrow ^{106}Cd^{*}, ^{106}Sn^{*}$ reactions at energies near the coulomb barrier	Rupinder Kaur, Maninder Kaur, **Varinderjit Singh**, Mandeep Kaur, BirBikram Singh, and B. S.	Department of Physical Sciences	Phys. Rev. C **101**, 044605	2020	0556-2813 / 1089-490X	https://mjl.clarivate.com:/search-results?issn=0556-2813&hide_exact_match_fl=true&utm_source=mjl&utm_medium=share-by-link&utm_campaign=search-results-share-this-journal	https://ptu.ac.in/faculty/?fid=9
53	Measurement of fission excitation function for $^{19}F+^{194,196,198}Pt$.	**Varinderjit Singh**, Bivash R. Behera, Maninder Kaur, Akhil Jhingan, Rupinder Kaur, Pullanhiotan Sugathan, Davinder Siwal, Savi Goyal, K. P. Singh	Department of Physical Sciences	Journal of Physics G: Nuclear and Particle Physics **48**, 075104	2021	0954-3899	https://mjl.clarivate.com:/search-results?issn=0954-3899&hide_exact_match_fl=true&utm_source=mjl&utm_medium=share-by-link&utm_campaign=search-results-share-this-journal	https://ptu.ac.in/faculty/?fid=9
54	Effect of increasing neutron-excess on the fusion cross-section in $^{12,13}C + ^{12}C$ at above barrier energies	R. T. deSouza, **Varinderjit Singh**, S. Hudan, Z. Lin and C. J. Horowitz	Department of Physical Sciences	Physics Letter B **814**, 136115	2021	0217-9849 / 1793-6640	https://mjl.clarivate.com:/search-results?issn=0217-9849&hide_exact_match_fl=true&utm_source=mjl&utm_medium=share-by-link&utm_campaign=search-results-share-this-journal	https://ptu.ac.in/faculty/?fid=9
55	Assessing the impact of valence sd neutrons and protons on fusion	**Varinderjit Singh**, J. Vadas, T.K. Steinbach, B.B. Wiggins, S. Hudan, and R.T. deSouza	Department of Physical Sciences	Phys. Rev. C 103, 064606	2021	0556-2813 / 1089-490X	https://mjl.clarivate.com:/search-results?issn=0556-2813&hide_exact_match_fl=true&utm_source=mjl&utm_medium=share-by-link&utm_campaign=search-results-share-this-journal	https://ptu.ac.in/faculty/?fid=9
56	MuSIC@Indiana: An effective tool for accurate measurement of fusion with low-intensity radioactive beams	J.E. Johnstone, Rohit Kumar, S. Hudan, **Varinderjit Singh**, R.T. deSouza, J. Allen, D.W. Bardayan, D. Blankstein, C. Boomershine, S.	Department of Physical Sciences	Nucl. Instrum. Methods A **1014**, 165697	2021	0168-9002 / 1872-9576	https://mjl.clarivate.com:/search-results?issn=0168-9002&hide_exact_match_fl=true&utm_source=mjl&utm_medium=share-by-link&utm_campaign=search-results-share-this-journal	https://ptu.ac.in/faculty/?fid=9
57	Gravitational form factors and angular momentum densities in light-front quark-diquark model	Narinder Kumar, Chandan Mondal, Neetika Sharma	Department of Physical Sciences	Scientific Research and Management **3**, 127 (2018).	2017	1434-601X	https://mjl.clarivate.com:/search-results?issn=1434-601X&hide_exact_match_fl=true&utm_source=mjl&utm_medium=share-by-link&utm_campaign=search-results-share-this-journal	https://ptu.ac.in/faculty/?fid=10

Head
Department of Physical Sciences
I.K. Gujral Punjab Technical University
Main Campus

58	Diffractive rho and phi vector meson production at HERA using a holographic light-front wavefunction	Mohammad Ahmady, Ruben Sandapen, and **Neetika Sharma**	Department of Physical Sciences	Phys. Rev. D **94**, 074018	2016	2470-0029	https://mjl.clarivate.com:/search-results?issn=1550-7998&hide_exact_match_fl=true&utm_source=mjl&utm_medium=share-by-link&utm_campaign=search-results-share-this-journal	https://ptu.ac.in/faculty/?fid=10
59	Momentum transfer dependence of generalized parton distributions	**Neetika Sharma**	Department of Physical Sciences	Eur. Phys. J. A **52**, 338	2016	1434-601X	https://mjl.clarivate.com:/search-results?issn=1434-6001&hide_exact_match_fl=true&utm_source=mjl&utm_medium=share-by-link&utm_campaign=search-results-share-this-journal	https://ptu.ac.in/faculty/?fid=10
60	Hard gluon evolution of nucleon Generalized Parton Distributions in the Light-front quark model	**Neetika Sharma**	Department of Physical Sciences	Eur. Phys. J. A **52**, 91	2016	1434-601X	https://mjl.clarivate.com:/search-results?issn=1434-6001&hide_exact_match_fl=true&utm_source=mjl&utm_medium=share-by-link&utm_campaign=search-results-share-this-journal	https://ptu.ac.in/faculty/?fid=10
61	Nucleon-generalized parton distributions in the Light-front quark model	**Neetika Sharma**	Department of Physical Sciences	Pramana, Journal of Physics **86**, 479	2016	0973-7111	https://mjl.clarivate.com:/search-results?issn=0304-4289&hide_exact_match_fl=true&utm_source=mjl&utm_medium=share-by-link&utm_campaign=search-results-share-this-journal	https://ptu.ac.in/faculty/?fid=10

Head
Department of Physical Sciences
I.K. Gujral Punjab Technical University
Main Campus